UNIVERSITY OF BIRMINGHAM

Project One: LIGAND BINDING AND STRUCTURAL STUDIES ON *MYCOBACTERIUM TUBERCULOSIS* DprE1, A NOVEL DRUG TARGET FOR TUBERCULOSIS THERAPY

and

Project Two: THE USEFULNESS OF ALGINATES IN THE TREATMENT OF COLORECTAL CANCER

by

MELANIE SCHNEIDER

A combined research thesis submitted to the University of Birmingham as part of the requirement for the degree of MASTER OF RESEARCH in Molecular and Cellular Biology.

College of Life and Environmental Sciences
School of Biosciences
University of Birmingham
September 2013

Summary

The following thesis is a combination of two individual research projects which were carried out by the author at the University of Birmingham as part of the requirement for the degree of Master of Research in Molecular and Cellular Biology.

The first part of this thesis focused on the ligand binding and structural properties of the *Mycobacterium tuberculosis* protein DprE1 which has recently been identified as a novel drug target for tuberculosis therapy. Project One aimed to investigate the mode of action and binding affinity of two promising DprE1 inhibitors, C12 and RKH06. Single ligand, competition and mutant DprE1 ligand binding experiments were performed to gain insight into the binding behaviour of the protein.

The second part of this thesis was a study into the usefulness of alginates in the prevention and treatment of colorectal cancer. Project Two aimed to investigate the *in vitro* effects of alginate-bound iron on cellular phenotype in comparison to iron only and to study a range of alginates for their iron binding potential and physiochemical properties. Results from this study identified several characteristics which seem to be important for a potential colonic iron chelator.

This thesis is dedicated to my wonderful family, partner and friends for their never-ending love and encouragement and for always being there for me. Without them I would not be where I am right now and knowing that they are just a phone call away has always been the greatest support.

Project One: LIGAND BINDING AND STRUCTURAL STUDIES ON *MYCOBACTERIUM TUBERCULOSIS* DprE1, A NOVEL DRUG TARGET FOR TUBERCULOSIS THERAPY

by

MELANIE SCHNEIDER

Supervisor – Dr Klaus Fütterer

College of Life and Environmental Sciences

School of Biosciences

University of Birmingham

March 2013

ABSTRACT

Despite well-established treatment plans being in place, tuberculosis, an infectious disease caused by the bacteria *Mycobacterium tuberculosis,* is still one of the leading causes of death worldwide. The rise of multidrug and extensively drug-resistant strains especially in the developing countries calls for new, more efficient and affordable antitubercular drugs. The *M. tuberculosis* protein DprE1 has recently been identified to be the target of several new drug compounds. In this study, two promising DprE1 inhibitors structurally different to representatives of the currently leading groups, benzothiazinones and dinitrobenzamides, were investigated. The ligands C12 and RKH06 were both identified in whole-cell assays to target DprE1. The aim of this study was to determine the mode of DprE1 ligand binding, in particular with RKH06. For this purpose, *M. tuberculosis* wild type DprE1 and two single amino acid change mutants DprE1 E294A and Y297A were overexpressed in *E. coli* and subsequently purified. The binding affinity of both ligands with wild type and mutant DprE1 was determined by measuring inherent tryptophan fluorescence. Single ligand, competition and mutant DprE1 ligand binding experiments were performed to gain further insight into the binding behaviour of the protein. The single ligand studies with the wild type showed a K_d of 7.4 µM for C12 and 15.2 µM for RKH06. The competition and mutant experiments suggested that both C12 and RKH06 bind in the active site of the protein next to the flavin adenine dinucleotide co-factor.

ACKNOWLEDGEMENTS

Great thanks goes to The Scripps Research Institute (Peter Schulz group) and the Albert Einstein College of Medicine (William R. Jacob group) for providing the ligands and therefore the basis of my study.

I would like to thank my project supervisor Dr Klaus Fütterer for giving me the opportunity to work as part of his research group and to acquire new skills, which will be invaluable for my future science career. I am grateful for the very useful advice and guidance he provided throughout this project.

I am especially grateful to Dr Rana Roy for his great support, guidance and patience throughout the whole project. Thank you for explaining so many things to me over and over again and for never sending me away. You were the greatest help I could have hoped for.

My appreciation also goes to Dr Sarah Batt for her advice and encouragement.

For boosting me morally and inspiring me to carry on despite the pressure we were both facing I thank my friend and lab partner Sarah Latchem. You were great fun to work with.

Melanie Schneider

TABLE OF CONTENTS

LIST OF ILLUSTRATIONS

LIST OF TABLES

LIST OF ABBREVIATIONS

AG	Arabinogalactan
B_{max}	Maximum binding capacity
BSA	Bovine serum albumin
BTZs	Benzothiazinones
CV	Column volumes
diH_2O	Distilled water
DMSO	Dimethyl sulfoxide
DNBs	Dinitrobenzamides
DPA	Decaprenylphosphoryl- β-D-arabinose
DPR	Decaprenylphosphoryl- β-D-ribose
DPX	Decaprenylphosphoryl-2-keto-β-D-erythro-pentofuranose
DR	Drug-resistant
E. coli	*Escherichia coli*
FAD	Flavin adenine dinucleotide
HCl	Hydrochloric acid
HIV	Human immunodeficiency virus
IPTG	Isopropyl-β-D-thiogalactopyranosid
K_d	Dissociation constant
LAM	Lipoarabinomannan
LB	Luria Bertani
mAGP	Mycolyl-arabinogalactan-peptidoglycan
MDR	Multidrug-resistant
MIC	Minimal inhibitory concentration
M. tuberculosis	*Mycobacterium tuberculosis*
O.C.	Overnight culture
NaOH	Sodium hydroxide
SDS	Sodium dodecyl sulphate
TB	Tuberculosis
TDR	Totally drug-resistant
Trp	Tryptophan
WHO	World Health Organization
XDR	Extensively drug-resistant

1. INTRODUCTION

1.1 Spread and impact of tuberculosis worldwide

Tuberculosis (TB) is a chronic infectious disease caused by the airborne pathogen *Mycobacterium tuberculosis* (*M. tuberculosis*) (Neres *et al.* 2012). According to the World Health Organization (WHO), in 86% of cases worldwide *M. tuberculosis* causes pulmonary TB, where the infection is localised in the lungs. The bacteria enter the body via the mouth or nose and move into the lungs where they infect alveolar macrophages, dendritic cells and pulmonary epithelial cells (Gupta *et al.* 2012). Nearly one third of the world's population is latently infected with TB. In 90% of all cases, *M. tuberculosis* persists in this dormant stage throughout an individual's lifetime without showing clinical symptoms. However, estimations show that the other 10% will develop active TB at some point (Christophe *et al.* 2009, Villemagne *et al*. 2012).

Despite well-established treatment plans being in place, TB is still the leading cause of death due to an infectious agent (Villemagne *et al.* 2012). According to the WHO, an estimated 8.7 million people were newly infected with TB in 2011, out of which 13% were also infected with the human immunodeficiency virus (HIV). In the same year, there was an estimated 1.4 million deaths caused by TB, overall affecting just under one million HIV-negative and nearly half a million HIV-positive individuals (WHO 2012).

The spread of this disease is promoted, especially in developing countries, due to poverty and homelessness, co-infection with HIV, and the rise of drug-resistant (DR) strains (Cole & Riccardi 2011, Neres *et al.* 2012).

Eighty per cent of people co-infected with HIV live in Africa, an area that accounts for 24% of TB cases worldwide and where infected individuals have a very low chance of being treated sufficiently (WHO 2012). However, not only the developing countries carry the burden of this disease. In our modern world, where fast transport and open borders have made long-distance travel and immigration effortless, even the industrialised countries are more and more at risk of the rapid spread of TB (Velayati *et al.* 2009, Cole & Riccardi 2011).

1.2 Current drugs and problems

The current multi-drug standard regimen for patients infected with drug-susceptible TB suggested by the WHO includes the use of the front-line drugs isoniazid, rifampicin, pyrazinamide and ethambutol for two months followed by four months of isoniazid and rifampicin (WHO 2010). This treatment plan has a success rate of nearly 90% in HIV-negative individuals. However, the outlook for those patients infected with DR-TB strains is far worse than for those with drug-susceptible TB (WHO 2012).

We distinguish between multidrug-resistant (MDR), extensively drug-resistant (XDR) and recently even so called “super-XDR strains” (Pasca *et al.* 2010, Cole & Riccardi 2011). MDR is defined as resistance against both front line drugs isoniazid and rifampicin. It is estimated that 3.7% of newly infected individuals and between 15% and 20% of patients, who have been previously treated for TB, carry MDR strains. Even though 60,000 cases of MDR-TB were reported to the authorities in 2011, this represents less than a fifth of the actual figure, estimated at around 310,000 cases of MDR-TB among all new infections.

For countries such as India and China, which account for a high percentage of TB cases worldwide, the estimated number of unreported MDR cases is especially high (WHO 2010, WHO 2012). The current treatment regimen for MDR-TB lasts at least twenty months and uses expensive but less efficient second-line drugs such as fluoroquinolone, aminoglycosides and ethionamide (Cole & Riccardi 2011). These drugs have higher toxicity, are associated with more serious side effects and the treatment has a cure rate below 75% (Lienhardt *et al.* 2012, WHO 2012).

With the treatment being very invasive, this can lead to treatment failure due to poor patient compliance (Field *et al.* 2012). This favours the development of further resistances and according to the WHO, XDR strains were reported in 84 countries in 2011 (Villemagne *et al.* 2012, WHO 2012). XDR strains are defined as MDR strains with additional resistance to fluoroquinolones and injectable antibiotics such as amikacin, kanamycin and capreomycin (Velayati *et al.* 2009, Field *et al.* 2012).

Even more worrying than the rise in XDR-TB cases, are the news about so-called "super-XDR" or totally drug-resistant (TDR) strains that have recently been reported in Iran and India. Velayati *et al.* (2009) and Udwadia *et al.* (2012) described the TDR strains isolated in their studies as MDR strains with resistance to all first and second-line drugs tested including fluoroquinolones, aminoglycosides, cyclic polypeptides, thioamides, serine analogues and salicylic acid derivatives.

Both studies attribute the development of TDR strains to the unknown medical history of their patients and therefore, possible previous treatments with second-line drugs for respiratory diseases other than TB (Velayati *et al*. 2009, Udwadia *et al.* 2012).

Looking at this data, it becomes obvious why there is an increasing need for new antitubercular drugs (Pasca *et al.* 2010). To be accepted into the WHO TB drug regime, new drugs will have to fulfil a list of desirable criteria. They need to be highly effective against drug-susceptible and DR strains, allow shorter and simpler treatment and have less host toxicity and therefore fewer side effects especially for the treatment of MDR-TB. Also, the development of several drugs with new targets and modes of action are desirable, as resistance-conferring mutations, which will occur inevitably, are more likely to incur a large cost-of-fitness that will curb the spread of a new DR strain.

Furthermore, to ease the burden on individuals co-infected with HIV, the drugs need to show reduced or no interaction between TB medication and antiretroviral therapy and they should be available at a low cost to be accessible for patients in the developing countries. Finally, the drugs should be effective against both growing and dormant TB bacilli, as antibiotics treatment using an inhibitor that prevents growth only tends to drive the infection into the latent state without full clearance. Latent TB is rarely treated, as there is only a 10% chance that the disease will become active. However, when treating the active disease, the outcome should be full clearance (Field *et al*. 2012, Lienhardt *et al.* 2012, WHO 2012).

Since rifampicin was first accepted in 1966 over 40 years ago, there have never been as many promising new drug candidates as there are at the moment (Cole & Riccardi 2011, Field *et al.* 2012). Eleven compounds, some targeting entirely new drug targets and some being repurposed tuberculosis drugs, are currently in different stages of clinical trials (Lienhardt *et al.* 2012). However, it is not known whether any of these inhibitors will ever be used in TB treatment. It is therefore crucial, to keep investing significant efforts in developing new drugs against TB.

1.3 The unique mycobacterial cell wall as drug target

1.3.1 Mycobacterial cell wall structure and synthesis

Mycobacteria, in comparison to gram-negative and gram-positive bacteria, have a unique hydrophobic cell wall structure. It forms the barrier between host and pathogen and its low permeability protects the bacteria against the host's immune response and makes it resistant to many antibiotics (Alderwick *et al.* 2007). Being the mycobacteria's strongest defence mechanism, it is not surprising that at least five out of the eleven compounds currently in clinical trials target the biosynthesis of cell wall components (Cole & Riccardi 2011).

As shown in figure 1, the mycobacterial cell wall can be divided into three major sections, the plasma membrane on the inside, the so-called mycolyl-arabinogalactan-peptidoglycan complex (mAGP) in the core, and a polysaccharide-rich capsule on the outside (Mikušová *et al.* 2005).

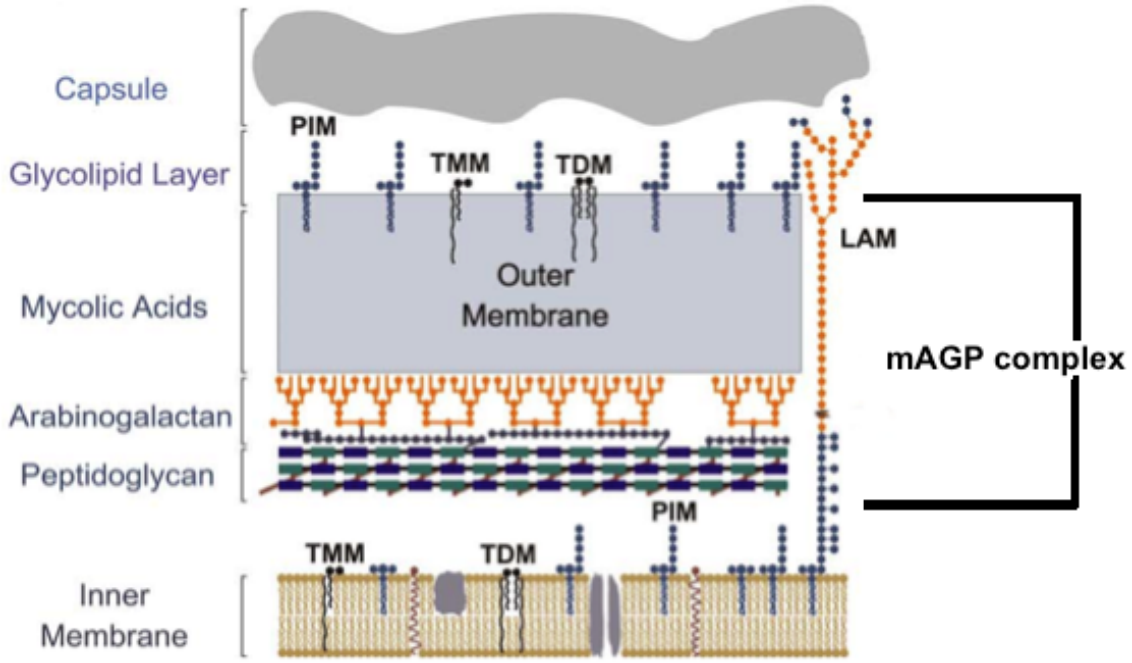

Fig. 1: Arrangement of the mycobacterial cell wall (figure modified from Crellin et al. 2011).

The complex biopolymer arabinogalactan (AG) is a major structural component of the mycobacterial cell wall. AG acts as a covalent linker between the cross-linked peptidoglycan and the outer layer of mycolic acids (Alderwick *et al.* 2011, Cole & Riccardi 2011). A great proportion of its chemical structure is made up of microbial arabinan (see figure 2).

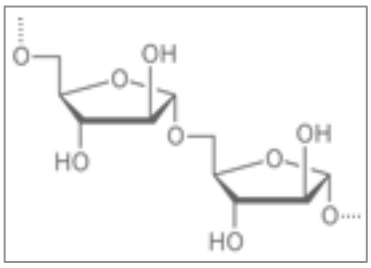

Fig. 2: Microbial cell wall arabinan - Building block for AG and LAM.

Overall, arabinan accounts for 18% of the mycobacterial cell wall and is the building block for another vital biopolymer, lipoarabinomannan (LAM) (Cole & Riccardi 2011, Crellin *et al.* 2011).

Besides its structural role (figure 1), LAM is an essential *M. tuberculosis* immunogen that is part of the cells protective mechanism against host toxins and allows interaction with the host cell (Alderwick *et al.* 2011). It has been found that the molecule decaprenylphosphoryl-β-D-arabinose (DPA) is the sole known precursor of mycobacterial cell wall arabinan and is therefore crucial for the synthesis of AG and LAM (Pasca *et al.* 2010, Neres *et al.* 2012). The conversion of decaprenylphosphoryl-β-D-ribose (DPR) to DPA is catalysed by the DprE1 catalytic subunit of the enzyme decaprenylphosphoryl-β-D-ribose-2'-epimerase together with its partner DprE2 (Pasca *et al.* 2010). The epimerase is encoded by the neighbouring genes *dprE1* (Rv3790) and *dprE2* (Rv3791), which have been found to be essential for the growth of *M. tuberculosis* and *Mycobacterium smegmatis* (Christophe *et al.* 2009, Neres *et al.* 2012).

The different steps of AG and LAM biosynthesis take place on both the cytoplasmic and the periplasmic side of the plasma membrane (Larrouy-Maumus *et al.* 2012). In the cytoplasm, DPR is oxidised by DprE1 to the intermediate decaprenylphosphoryl-2-keto-β-D-erythro-pentofuranose (DPX) as shown in figure 3. In the second step of the reaction, DPX is then reduced to DPA by DprE2 (Mikušová *et al.* 2005, Batt *et al.* 2012).

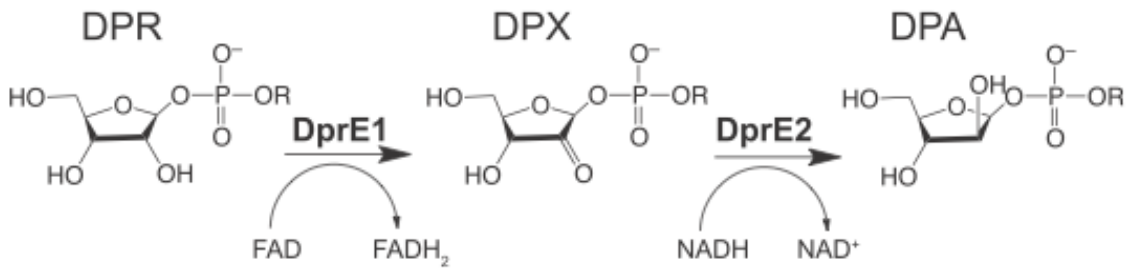

Fig. 3: Epimerization of DPR via DPX to DPA (Batt et al. 2012).

Recently, Larrouy-Maumus *et al.* (2012), suggested that the gene Rv3789 located next to the *dprE1* and *dprE2* genes, encodes a small multidrug resistance transporter that is thought to work as a DPA translocase thus moving it from the cytoplasm to the periplasm for further synthesis into AG and LAM.

1.3.2 DprE1 as TB drug target

Without DPA, a fully functional cell wall cannot be formed, making it essential for mycobacterial growth (Cole & Riccardi 2011, Crellin *et al.* 2011). It is therefore not surprising that recently several new drug compounds have been identified to target the turnover of DPR to DPA, specifically the reaction's catalysts DprE1 and DprE2. Even though neither of these proteins can catalyse the oxidation-reduction reaction of DPR to DPA individually, DprE1 has been found to be a more desirable drug target than the NADH-dependent reductase DprE2 (Mikušová *et al.* 2005, Makarov *et al.* 2009, Crellin *et al.* 2011, Batt *et al*. 2012).

DprE1 works as a decaprenylphosphoryl-β-D-ribose oxidoreductase with a flavin adenine dinucleotide (FAD) as redox-active component (Alderwick *et al.* 2011, Batt *et al.* 2012). The *dprE1* gene is highly conserved among mycobacteria supporting the statement that DprE1 is essential for mycobacterial survival (Neres *et al.* 2012). The 50 kDa protein has a two-domain structure with an FAD-binding domain and a substrate-binding domain. It has structural similarities with proteins from the vanillyl-alcohol oxidase family especially alditol oxidase (JCVI CMR a, Batt *et al.* 2012, Neres *et al.* 2012).

1.3.3 New TB drugs on the horizon

One promising group of nitro-aromatic compounds found to specifically target DprE1 are the so-called benzothiazinones (BTZs) (Neres *et al.* 2012, Villemagne *et al.* 2012). BTZs have been shown to have very high antimycobacterial activity against drug-susceptible and also MDR and XDR strains *in vitro*, *ex vivo* and in animal models of the disease with relatively low host toxicity (Makarov *et al.* 2009, Pasca *et al.* 2010). The compounds form a semimercaptal linkage with the Cys387 residue in the active site of DprE1, thus blocking any turnover of substrate. The leading compound in this group is BTZ043 (figure 4). It has nanomolar whole-cell activity with a minimal inhibitory concentration (MIC) of 1 ng/ml against *M. tuberculosis*. This is 20-fold less than the MIC of isoniazid and 1000-fold less than the MIC of ethambutol (Makarov *et al.* 2009, Neres *et al.* 2012). Also, in a study using 240 drug-susceptible and MDR strains from four European hospitals, no resistance against BTZ043 was found (Pasca *et al.* 2010). BTZ043 is currently in late pre-clinical development (Lienhardt *et al.* 2012).

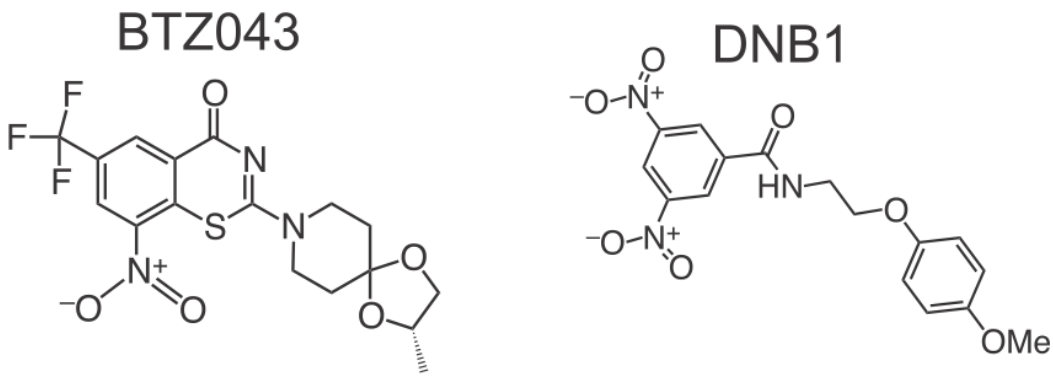

Fig. 4: Chemical structures of the compounds BTZ043 and DNB1 (Batt et al. 2012).

Other compound groups found to target DprE1 are the dinitrobenzamides (DNBs) and benzoquinoxalines. DNB1 (figure 4) has been proven to be effective against drug-susceptible and DR strains with an MIC of 0.072 mg/ml while the benzoquinoxaline compound VI-9376 has an MIC of 1 mg/ml (Cole & Riccardi 2011, Neres *et al.* 2012, Villemagne *et al.* 2012).

Giving the recent publications about several compounds successfully targeting DprE1, it is not surprising that is has been referred to as a 'magic' drug target (Manina *et al.* 2010). In order to satisfy the need for new antitubercular drugs, many research groups are using the data on hand to design new scaffolds similar or even unrelated to BTZs that also target DprE1. The knowledge about the active side of the protein and the mechanism of inhibition gives way to finding new inhibitors that may even be more potent and fulfil more of the WHO criteria for new drugs than the current compounds (Neres *et al.* 2012).

1.4 New ligands – C12 and RKH06

Two new ligands targeting DprE1, designed by The Scripps Research Institute (group leader Peter Schulz) and the Albert Einstein College of Medicine (group leader William R Jacobs's), were provided for this study. Besides genetic evidence proving their activity, the ligands C12 and RKH06 were both identified in whole-cell assays to target DprE1. They are structurally different from BTZs and DNBs and also employ a different mode of action than BTZs. The ligands have good potency and low host-toxicity and have been shown to be effective against MDR strains.

A potentially big advantage of C12 is that it appears to be effective against both active and latent TB, however in terms of potency, it is still distinctly weaker than BTZ043 (unpublished data P. Schulz group).

The K. Fütterer group co-crystallised DprE1 with the ligands and it was possible to obtain two separate inhibitor-bound crystal structures of the protein, one bound to C12 and a second one bound to RKH06. For simplicity's sake, both inhibitors are shown in figure 5 to demonstrate the non-overlapping binding sites of RKH06 and C12.

As shown in figure 5, C12 binds non-covalently in the protein's active side next to the FAD co-factor, thus inhibiting any turnover of substrate. RKH06 on the other hand appears to bind away from the flavin in a separate binding site. This is surprising for several reasons. Firstly, C12 and RKH06 share the same scaffold and therefore binding in the same site was expected. Also, given that FAD is the active component of DprE1, it is reasonable to expect that an inhibitor of this protein should bind next to the co-factor as it would then permanently blocks the active side for any substrate. Moreover, a resistance-conferring mutation at residue Tyr314 to cysteine (Y314C) was identified by the P. Schulz group. This residue is located right next to the flavin in the active site and the Y314C mutation would therefore likely affect binding. If RKH06 would bind where it is shown in figure 5, a mutation at this point would not be expected to have any effect, but would likely affect binding of C12 (unpublished data P. Schulz group).

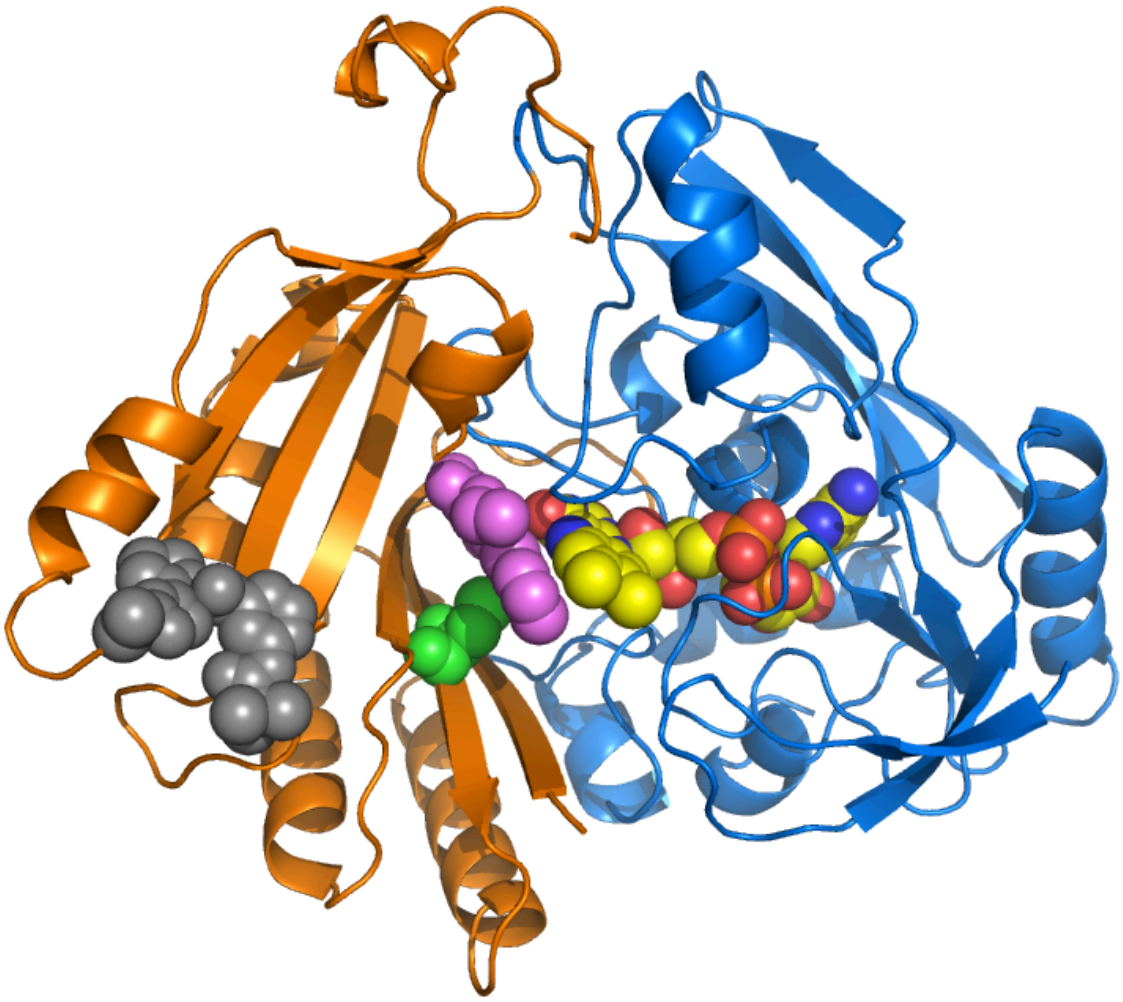

Fig. 5: Combination of two separate inhibitor-bound crystal structures of DprE1 bound to C12 (pink) and RKH06 (grey). The figure demonstrates the non-overlapping binding sites of both ligands. C12 binds in the active site next to the FAD co-factor (yellow) while RKH06 binds in an adjacent binding pocket. Cys387 is shown in green.

There are two possible explanations for the unexpected behaviour of RKH06. Either RKH06 is non-competitive and does not bind in the same site as the substrate. In this case the crystal structure shows a novel model of DprE1 inhibition. Or RKH06 binds in the active site as C12 and the crystal structure shows an experimental artefact.

1.5 Aims and objectives

The crystallographic evidence for binding of RKH06 contradicted the expectation raised by both the resistance mutation (Y314C) and also the C12-bound structure. However, in the development of any new drug compound, it is crucial to investigate and understand its mode of action in order to, for instance increase its affinity to the target, or to side step know resistance-conferring mechanisms. Therefore, to ascertain the mode of action of RKH06 in solution, the aim of this study was to determine whether RKH06 binds in the same site as C12 next to the flavin or whether it binds in the site suggested by the crystal structure.

To achieve this goal, sufficient amounts of wild type DprE1 were expressed and purified and its ligand binding affinity with C12 and RKH06 was assessed by measuring the protein's intrinsic tryptophan (Trp) fluorescence.

Single ligand experiments were performed to determine the dissociation constant (K_d) of both ligands. This was followed by competition experiments to assess the binding behaviour of each ligand in presence of the other ligand at its K_d.

To further support the findings from the ligand biding studies, selected single amino acid change mutants of wild type DprE1 were designed, expressed and purified. Their binding affinity with C12 and RKH06 was determined and the results were compared to draw a definite conclusion about the binding site of RKH06.

2. METHODS AND MATERIALS

The chemicals and other ingredients mentioned in this section were purchased from Sigma-Aldrich Company Ltd or Fisher Scientific UK Ltd unless stated otherwise. The recipes for all buffers / stocks / solutions mentioned in this section can be found in appendix 1.

2.1 SDS-PAGE protein gel protocol

2.1.1 Sample preparation

For samples containing cellular material, a 1 ml sample was taken and spun for three minutes at 14,000 RPM. The supernatant was discarded and the pellet was resuspended with 200 µl 1 X SDS buffer. For all clear samples, 15 µl of 4 X SDS buffer was mixed with 45 µl sample. The samples were boiled in a heat block at 100°C for five minutes.

2.1.2 SDS-PAGE gel

Using the Mini-PROTEAN Tetra handcast system (BIO-RAD), SDS-PAGE gels were prepared fresh. To cast a gel, all bottom gel ingredients were mixed according to table 1 and poured between the glass plates. To achieve an even surface, 2-buthanol was added drop-wise to cover the gel. After leaving the gel to set, the 2-buthanol was thoroughly washed off with deionised water (diH_2O). The top gel ingredients were mixed according to table 1 and poured onto the bottom gel. Immediately, a clean Mini-PROTEAN comb (10 or 15 wells) was pressed into the top gel and this was left to set.

The gel was transferred into a Mini-PROTEAN Tetra electrophoresis system filled with 1 X gel running buffer. After removing the comb, 10 µl Prestained Protein Marker, Broad Range (New England Biolabs) was added to the first well and 10 µl of each sample was added to the other wells. Gels were run at 200 V for 68 minutes using the Mini-PROTEAN Tetra electrophoresis system and a Power Pac 300 (BIO-RAD).

Table 1: Ingredients for SDS-PAGE gels

For two gels à 5 ml:	**10%**	**12%**	**Top gel**
diH_2O	4 ml	3.3 ml	2.7 ml
Gel buffer (I) or (II)	2.5 ml (I)	2.5 ml (I)	500 µl (II)
Polyacrylamide	3.3 ml	4 ml	670 µl
10% SDS	100 µl	100 µl	40 µl
10% ammonium persulfate	100 µl	100 µl	40 µl
Tetramethylethylenediamine	4 µl	4 µl	2 µl

(Polyacrylamide: ProtoGel - GENEFLOW)

2.1.3 Staining

For developing, the gels were placed in Coomassie Blue stain for one hour on a shaker. The stain was removed and the gels were placed in destain for 20 to 30 minutes. If necessary, the destain was changed after this time before examining the gels.

2.2 Protein overexpression protocol

The following protocol was carried out under sterile conditions. Benches and hands were cleaned using 70% ethanol and all equipment including pipette tips were sterilised with a Bunsen burner before use. The plasmid and *Escherichia coli* (*E. coli*) stocks mentioned here were provided by the G.S. Besra and K. Fütterer labs in Biosciences, University of Birmingham.

2.2.1 Luria Bertani (LB) agar plates

Unless the agar was used straight after autoclaving, it was completely liquefied in an microwave oven and then left to cool down to about 55°C before adding the appropriate antibiotics for a final concentration of 100 µg/ml ampicillin and spectinomycin and 25 µg/ml kanamycin. Also, 20% glucose was added for a final concentration of 1% (Suter-Crazzolara & Unsicker 1995). A thin layer of agar (about 10-15 ml per plate) was poured evenly into sterile Petri dishes and left to solidify.

2.2.2 Transformation

For transformation, 50 µl *E. coli* BL21 (DE3) competent cells was retrieved from the -80°C freezer and kept on ice at all times. The cells were thawed on ice for five minutes and were then transformed with 1 µl of either the Rv3790-pET28b or Rv3790-pCDF duet plasmid. The cells were co-transformed with 1 µl of the chaperone plasmid p*Trc*-60.2-GroES to aid DprE1 folding (Batt *et al.* 2012).

Table 2: Plasmids used for transformation and their antibiotic resistances

Name	**Encoding**	**Antibiotic resistance**
Rv3790-pET28b (N-terminal Hexa-HIS)	DprE1	kanamycin
Rv3790-pCDF duet (N-terminal HIS-tag)	DprE1	spectinomycin
Chaperone plasmid p*Trc*-60.2-GroES	*M. tuberculosis* Cpn60.2 and *E. coli* GroES	ampicillin

The mix was kept on ice for 20 minutes. The cells were heat shocked at 42°C for 90 seconds and then quickly placed on ice for three minutes. To this, 350 µl of LB medium was added and the cells were incubated for one hour at 37°C at 200 RPM.

Finally, 25 µl and 350 µl of culture were plated on LB agar supplemented with the appropriate antibiotics (see table 2) and 1% glucose. The plates were incubated overnight at 37°C.

In this study, to try and maximise the amount of protein expressed, transformations were done in different ratios as shown in table 3.

Table 3: Different transformation ratios used in this study

Rv3790	**Chaperone**	**Ratio**	**Host**
pet28b	p*Trc*-60.2-GroES	1:1	*E. coli* BL21 (DE3)
pCDF duet	p*Trc*-60.2-GroES	1:1, 3:1, 1:3	*E. coli* BL21 (DE3)

2.2.3 Overnight culture (O.C.)

For an O.C., 100 ml LB medium was supplemented with the appropriate antibiotics for a final concentration of 100 µg/ml ampicillin and spectinomycin and 50 µg/ml kanamycin. Also, 20% glucose was added for a final concentration of 1% (Suter-Crazzolara & Unsicker 1995). The medium was inoculated with one colony picked from the transformation plate with a sterile pipette tip and was incubated overnight at 37°C at 200 RPM.

2.2.4 Glycerol stock

To preserve transformations for future protein purifications, 500 µl O.C. and 500 µl 75% glycerol were mixed thoroughly in a sterile microcentrifuge tube and stored at -80°C.

2.2.5 Bulk culture

The pellets from two litres of bulk culture were used for purification. If Terrific Broth was used, 100 ml Terrific Broth salt were added to 900 ml medium before inoculation. Each litre of medium was inoculated with 10 ml O.C. and the culture was incubated at 37°C at 200 RPM. The growth was monitored by measuring the optical density in regular intervals until it reached a value between 0.4 and 0.6. Then, the incubator was cooled down to 16°C for one hour. A sample was taken and the protein expression was induced by adding isopropyl-β-D-thiogalactopyranosid (IPTG 1 M stock - BIOLINE) for a final concentration of 0.5 mM. The culture and sample were incubated at 16°C at 180 RPM for 12 to 16 hours.

2.3 Protein purification protocol

After removal from the 16°C incubator, all protein containing solutions (culture, crude and clear lysate etc.) were kept on ice and were centrifuged in pre-cooled 4°C rotors.

2.3.1 Cell pellet harvesting

A sample of induced cells was taken. To harvest the pellet, the bulk culture was transferred into centrifuge bottles and was spun for 10 minutes at 5000 RPM at 4°C. The pellets were transferred into 50 ml tubes and the bottles were rinsed with 15 ml 0.85% saline wash buffer. This was added to the tubes and the pellets were centrifuged for 10 minutes at 5000 RPM at 4°C. The saline was discarded and the pellets were either frozen at -80°C or resuspended with 30 ml buffer A 10 mM imidazole. A protease inhibitor cocktail tablet, complete EDTA-free (Roche) was added before sonication.

2.3.2 Sonication and collection of clear lysate

To lyse the cells, the resuspended pellet was sonicated on ice for a total time of 10 minutes à 20-second pulses and 40-seconds rest (Soniprep 150 MSE – Sonyo). After taking a sample, the crude lysate was transferred into centrifuge bottles and was spun for 35 minutes at 20,000 RPM at 4°C. The clear lysate was filtered through a 0.45 µm Acrodisc Syringe Filter (Pall Corporation) before taking a sample.

2.3.3 Hi-trap chromatography

A 1 ml Ni^{2+}-charged HisTrap HP column (GE Healthcare) was used together with a Minipuls 3 pump (Gilson) for the first purification step. The flow rate was set at 1 ml/minute and the column was equilibrated with 20 column volumes (CV) buffer A 10 mM imidazole. The filtered clear lysate was loaded onto the column and the flow through was collected. The column was washed with 10 CV buffer A 10 mM imidazole and the protein was eluted with a gradient of 10 mM, 20 mM, 40 mM, 60 mM, 80 mM, 100 mM, 200 mM and 300 mM imidazole using 10 CV each. The elutions were collected in individual tubes and kept at 4°C.

2.3.4 SDS-PAGE gel

A sample was taken from the flow through, wash and each elution step and was prepared as outlined in 2.1.1. The samples were run on an SDS-PAGE gel to identify the fractions containing pure protein.

2.3.5 Dialysis

A dialysis membrane (Size 8 Inf Dia 32/32", MWCO 12 – 14,000 Daltons) from Medicell International Ltd was used for dialysis. To remove contaminants, the membrane was boiled in 500 ml diH_2O supplemented with a pinch of EDTA and $NaHCO_3$ for 30 minutes on a hot plate. The membrane was rinsed with plenty of diH_2O and then placed in pre-chilled dialysis buffer. The membrane was closed with clips to form a bag before adding the protein. Fractions identified on the SDS-PAGE gels were dialysed overnight at 4°C. One litre buffer was prepared for each 10 ml fraction and it was changed for one hour in the morning.

2.3.6 Ion exchange chromatography

The dialysed sample was centrifuged for 10 minutes at 5000 RPM at 4°C and was then filtered through a 0.45 µm filter to remove any precipitate. A 1 ml HiTrap Q HP column (GE Healthcare) was used together with a Minipuls 3 pump (Gilson) for the second purification step. The flow rate was set at 1 ml/minute and the column was equilibrated with 20C V buffer B 10 mM NaCl. The dialysed protein was loaded onto the column and the flow through was collected. The column was washed with 10 CV buffer B 50 mM NaCl and the protein was eluted with a gradient of 50 mM, 100 mM, 120 mM, 140 mM, 160 mM, 180 mM, 200 mM and 1 M NaCl using 10 CV each. The flow through was collected in individual tubes and kept at 4°C. Fractions containing pure protein were identified on an SDS-PAGE gel and were dialysed overnight at 4°C. The buffer was changed for one hour in the morning.

2.4 Protein concentration

2.4.1 Calculation of protein concentration

The absorbance of the dialysed solution was determined with the NanoDrop 2000c Spectrophotometer (Thermo Scientific). Buffer B 10 mM NaCl was used as blank and the absorbance was measured at 280 nm. Using the following equation, the protein concentration was determined (Rv3790 DNA sequence – see appendix 2):

- Extinction coefficient Rv3790 (ε): 63370 $M^{-1}C^{-1}$ (Swiss Institute of Bioinformatics a)
- Molecular weight Rv3790: 50163 g/mol (JCVI CMR a)
- e.g.: A_{280} = 0.2; volume = 50 ml

Formula: $A_{280} = \varepsilon \times C \times L$ → $0.2 \times 63370\ M^{-1}C^{-1} \times C \times 1cm$

$$C = \frac{0.2}{63370\ M^{-1}C^{-1} \times 1\ cm} \rightarrow C = 1.42 \times 10^{-5}\ M\ (14.2\ \mu M)$$

1.42×10^{-5} M x 50163 g/mol = 0.712 mg/ml
0.712 mg/ml x 50 ml = 35.62 mg protein overall

2.4.2 Concentrating of protein

After determining the initial concentration, an Amicon Ultra centrifugal filter Ultracel 10K (Merck Millipore) was used to concentrate the protein. The filter was washed with 4 ml diH_2O and 4 ml buffer B 10 mM NaCl (5 minutes, 7000xg, 4°C). Then the protein solution was loaded into the filter and spun for 25 minutes at 7000xg and 4°C. The concentrated protein in the filter was removed and collected before adding fresh solution. After centrifuging all dialysed protein, the absorbance was measured with the NanoDrop. Using the average of three readings, the concentration was calculated.

If necessary, the protein was then further concentrated to reach the desired final concentration. Due to degradation over time, the protein concentration was checked regularly to assure accuracy for any protein measurements.

2.4.3 Determination of sample purity

To check the purity and state of the protein, a SDS-PAGE gel was run with samples of concentrated protein and 1:10, 1:20 and 1:50 dilutions.

2.5 Ligand binding with wild type DprE1

2.5.1 Measurement parameters

For the ligand binding studies, a Perkin Elmer Luminescence Spectrometer LS 50B (Software: Perkin Elmer FLWinLab, Version 4.00.03) and a Fluorimeter Quartz Cell Type 3 (3-5.45) with a FCA adaptor (Starna) were used.

The measurement parameters were as follows:

- Scan speed: 120 nm/min
- No temperature control of the cuvette
- Ambient temperature: around 21°C
- No constant stirring

2.5.2 Buffer

Buffer B 10 mM NaCl was used for the ligand binding measurements. To decrease any background noise, five different batches of glycerol were tested for their fluorescence caused by contamination. The one with the lowest intrinsic fluorescence was subsequently used to make up buffer B 10 mM NaCl for measurements.

2.5.3 Emission and excitation scan

To determine the maximum emission of DprE1, an emission scan from 300 nm to 450 nm with a fixed excitation wavelength of 280 nm was performed. The fluorescence maximum was recorded at 337 nm.

To determine the maximum excitation, an excitation scan from 210 nm to 310 nm with a fixed emission wavelength of 337 nm was performed. The fluorescence maximum was recorded at 282 nm and therefore the excitation was fixed at 280 nm for further set ups.

2.5.4 Slit width

To optimise the measurements, slit widths of 3.0, 3.5, 3.7, 3.8, 3.9, 4.0, and 4.5 mm were tested. A slit width of 3.9 mm gave the smoothest curve with Trp fluorescence in the detectable range.

All initial tests were performed with a final concentration of 0.46 µM wild type DprE1 in 600 µl of buffer (initial volume).

2.5.5 Bovine serum albumin (BSA) test measurement

To check the accuracy of the machine, detect any measuring errors and to determine the impact of photobleaching on the protein, a test measurement using 0.5 µM BSA was performed. Readings were taken in 5-minute intervals for 30 minutes. This showed that the impact of photobleaching could be reduced significantly by blocking out the light in between readings. Therefore, this was done for all other experiments.

2.5.6 Protein and ligand preparation

All ligands for this project were provided by The Scripps Research Institute and the Albert Einstein College of Medicine. Ligand C12 (molecular weight: 375.42 g/mol) and RKH06 (molecular weight: 418.47 g/mol) were made up to 20 µM and 500 µM working stocks in 100% dimethyl sulfoxide (DMSO). Experiments using 20 µM stocks were unsuccessful due to the DMSO concentration becoming too high and affecting the protein's behaviour. They are therefore not further elaborated here (see appendix 4 – 5.4.4).

To obtain a high enough fluorescence signal from DprE1 on its own, an initial concentration of 2 µM was chosen. The initial volume of buffer and protein together was 600 µl.

Calculation to determine protein concentration and addition:
Example:

$$\frac{2\ \mu M \times 600\ \mu l}{55\ \mu M\ (\text{conc. DprE1})} = 21.82\ \mu l$$

$$\frac{21.82\ \mu l \times 55\ \mu M}{600\ \mu l} = 2.0\ \mu M$$

→ Add 21.82 µl concentrated DprE1 to 578.18 µl buffer
→ Protein concentration in the cuvette: 2.0 µM

Calculation to determine ligand concentration and addition:
For a ration of 1:4 protein to ligand:

$$2\ \mu M \times 0.25 = 0.5\ \mu M$$

$$\frac{0.5\ \mu M \times 600\ \mu l}{500\ \mu M} = 0.6\ \mu l$$

→ Add 0.6 µl of 500 µM ligand stock for a concentration of 0.5 µM.

Table 4: Wild type DprE1 and ligand concentrations / additions used for binding studies

Measurement	Buffer (µl)	Protein stock conc. (µM)	Protein conc. (µM) / addition (µl)	Ligand conc. (µM) / addition (µl)
Buffer	583.7	74	2.01 / 16.3	0.5 / 0.6
DMSO	583.7	74	2.01 / 16.3	0.5 / 0.6
Single ligand	574	47	2.04 / 26	0.51 / 0.61
Competition	573.2	45	2.01 / 26.8	0.5 / 0.6
Control –RKH06	597.6	509	2.04 / 2.4	0.51 / 0.61
Control – C12	597.3	450	2.0 / 2.67	0.5 / 0.6

2.5.7 Buffer and DMSO control measurements

To determine the effect of buffer and DMSO additions on the protein fluorescence, control measurements were performed. To be able to compare the results with the ligand titrations, DMSO and buffer were added in the same quantities as the ligands would be added and 'ligand concentration' was used as a unit for buffer or DMSO concentration. This refers to the volume of buffer or DMSO added to achieve a particular ligand concentration.

The appropriate amount of buffer (table 4) was added to the cuvette and a measurement was taken immediately. Wild type DprE1 was added according to table 4 and the fluorescence was measured immediately (DprE1_0). Then the light was blocked out in front of the cuvette to reduce photobleaching. Further readings were taken after two and four minutes (DprE1_2 and DprE1_4) and the light was blocked out in between readings. The light was always blocked out after taking a measurement and before each addition of buffer or DMSO. The appropriate amount of buffer or DMSO (table 4) was added. Using a 200 µl pipette the solution was mixed thoroughly by pipetting up and down a few times.

This was done immediately after the addition, after one minute and after two minutes before taking the reading. Measurements were taken two minutes after each addition. One experiments was carried out for the buffer and two replicates were carried out for DMSO. Table 5 shows how the measurements were recorded.

Table 5: Data recording table for buffer and DMSO measurements

Description	**Concentration (µM)**	**Individual addition (µl)**	**Total addition (µl)**	**Arbitrary units**
Buffer only	-	-	-	32
DprE1_0	-	-	-	923
DprE1_2	-	-	-	915
DprE1_4	-	-	-	908
DprE1 with buffer / DMSO only	0.5	0.6	0.6	899
---"------"------"---	4.5	4.8	5.49	876

2.5.8 Single ligand experiments

The protocol for measuring DprE1 with a single ligand was the same as described under 2.5.7, however, instead of adding buffer or DMSO after measurement DprE1_4, either C12 or RKH06 was added. For the initial experiments, three replicates were carried out for both ligands with the wild type. To confirm these results, two independent control measurements were performed for each ligand with a new batch of protein. Table 6 shows how the readings were recorded for further analysis.

2.5.9 Competition experiments

The buffer and DprE1 only measurements were undertaken in the same way as described under 2.5.7. To study the effects of one ligand on the other, a certain amount of ligand A (C12 – 7.5 µM, RKH06 – 15 µM) was added to the cuvette.

This was the only addition of ligand A and therefore the concentration of ligand A stayed constant throughout the experiment. Ligand B was then titrated into this solution as described before under 2.5.7. Three replicates were carried out with C12 being ligand A and RKH06 being ligand B. Two replicates were carried out with RKH06 being ligand A and C12 being ligand B. Table 7 shows how the readings were recorded for further analysis.

Table 6: Data recording table for single ligand experiments

Description	**Concentration (µM)**	**Individual addition (µl)**	**Total addition (µl)**	**Arbitrary units**
Buffer only	-	-	-	32
DprE1_0	-	-	-	923
DprE1_2	-	-	-	915
DprE1_4	-	-	-	908
DprE1 with ligand	0.51	0.61	0.6	900
---"------"------"------"---	4.58	4.88	5.4	450

Table 7: Data recording table for competition experiments

Description	**Concentration (µM)**	**Individual addition (µl)**	**Total addition (µl)**	**Arbitrary units**
Buffer only	-	-	-	32
DprE1_0	-	-	-	923
DprE1_2	-	-	-	915
DprE1_4	-	-	-	908
DprE1 with ligand A	-	-	-	520
DprE1 with ligands A & B	0.5	0.6	0.6	450
---"------"------"---	4.5	4.8	5.4	375

2.6 Evaluation of ligand binding data

The data for each experiment was recorded as shown in tables 5, 6 and 7. Using Microsoft Excel for Mac 2011, the data was analysed and recorded as saturation binding curves based on the fluorescence quenching caused by ligand binding. To determine the maximum binding capacity (B_{max}) and dissociation constant (K_d), the saturation binding data were fitted to a single site binding model, described by the equation $\Delta F = B_{max}\,[L]/(K_d + [L])$, where [L] = ligand concentration. The data fitting was done using the Microsoft Excel Solver function. The graphs show volume corrected and normalised data in order to allow comparison between measurements on a scale from 1 to 100 independent from B_{max}.

2.7 DprE1 mutant design

Three mutants of wild type DprE1 were designed using the Stratagene QuikChange Site-Directed Mutagenesis protocol (Stratagene 2006).

2.7.1 Primer design

Three primers were designed to cause single amino acid changes in the Rv3790 DNA sequence (see appendix 2) according to the mutagenesis protocol guidelines. Table 8 shows the original and primer sequences which were synthesised by Eurofins MWG Operon.

Table 8: Original Rv3790 and mutated primer sequence

Name	Original sequence	Mutated sequence
3790_R242A_F	gcgctcccccgaagctgggc**cgc**gcggcg gtatcgcgtggccg	gcgctcccccgaagctgggc**gcc**gcggcg gtatcgcgtggccg (43)
3790_R242A_R	cggccacgcgataccgccgcgcggcccag cttcgggggagcgc	cggccacgcgataccgccgcggcgcccag cttcgggggagcgc
3790_E294A_F	ccttcggcccgatcggc**gaa**ctgtggtacc gcaaatc	ccttcggcccgatcggc**gca**ctgtggtacc gcaaatc (37)
3790_E294A_R	gatttgcggtaccacagttcgccgatcggg ccgaagg	gatttgcggtaccacagtgcgccgatcggg ccgaagg
3790_Y297A_F	ggcccgatcggcgaactgtgg**tac**cgcaa atccggcacctatc	ggcccgatcggcgaactgtgg**gcc**cgcaa atccggcacctatc (43)
3790_Y297A_R	gataggtgccggatttgcggtaccacagtt cgccgatcgggcc	gataggtgccggatttgcgggcccacagtt cgccgatcgggcc

2.7.2 Extraction of plasmid DNA

E. coli Top10 competent cells were transformed with 1 µl Rv3790-pET28b or Rv3790-pCDF duet (see 2.2.2) and two 5 ml O.C.s for each plasmid were made (see 2.2.3). The plasmid DNA was extracted following the QIAprep Miniprep protocol (QIAGEN 2006). Therefore, the O.C.s were centrifuged for 10 minutes at 5000 RPM at 4°C. The pellet was resuspended with 250 µl buffer P1 and transferred into a microcentrifuge tube. Buffer P2 (250 µl) was added and the solution was mixed thoroughly by inverting the tube several times. Buffer N3 (350 µl) was added and the solution was mixed immediately by inverting the tube several times. This was centrifuged for 10 minutes at 14,000 RPM. The supernatant was transferred into a QIAprep spin column and this was centrifuged for 60 seconds. After discarding the flow through, 500 µl buffer PB was added and the column was centrifuged for 60 seconds. After discarding the flow through, 750 µl buffer PE was added and the column was centrifuged for 60 seconds. After discarding the flow through, the column was centrifuged for another minute.

To elute the plasmid DNA the column was placed in a clean microcentrifuge tube before adding 50 µl buffer EB (heated to 70°C). This was left to stand for 60 seconds before centrifuging for 60 seconds at 14,000 RPM.

2.7.3 PCR and transformation

The mutagenesis protocol required 50 ng plasmid template and 125 ng of each oligonucleotide primer. Therefore, the plasmid DNA concentration was determined by measuring the absorbance at 260 nm using the NanoDrop 2000c Spectrophotometer (Thermo Scientific). The primer concentration was calculated using the manufacturers table (Eurofins MWG Operon – see appendix 3). According to that, the composition of the PCR sample reaction was determined as shown in table 9.

Table 9: PCR sample reaction

Mutation	**pET28b (51 ng/µl)**			**pCDF duet (52.8 ng/µl)**		
	R242A	E294A	Y297A	R242A	E294A	Y297A
Reaction buffer	5 µl	5 µl	5 µl	5 µl	5 µl	5 µl
Plasmid	3 µl	3 µl	3 µl	1 µl	1 µl	1 µl
Primer_F	1 µl	1.1 µl	1 µl	1 µl	1.1 µl	1 µl
Primer_R	1 µl	1.1 µl	1 µl	1 µl	1.1 µl	1 µl
dNTP	1 µl	1 µl	1 µl	1 µl	1 µl	1 µl
DMSO	2.5 µl	2.5 µl	2.5 µl	2.5 µl	2.5 µl	2.5 µl
H_2O	35.5 µl	35.3 µl	35.5 µl	37.5 µl	37.3 µl	37.5 µl
Pfu Turbo C_x Polymerase	1 µl	1 µl	1 µl	1 µl	1 µl	1 µl

(Pfu Turbo C_x (2.5 U/µl) – Agilent Technologies, dNTP – New England Biolabs)

Regarding the Pfu Turbo enzyme properties (Agilent Technologies 2011) and the size of the plasmids (GSL Biotech LLC. a & b, JCVI CMR a), the extension time was calculated as follows (table 10):

Pfu Turbo C_x - Extension time: 1 min/kb for targets >1 kb
2 min/kb for 6-10 kb genomic template
Extension temp.: 72°C

pET28b 5368bp + Rv3790 1386bp = 6754 bp / 6.7 kb → 13 min 24 sec
pCDF duet 3781bp + Rv3790 1386bp = 5167 bp / 5.1 kb → 5 min 06 sec

Table 10: PCR cycling parameters

Segment	Cycle	Temperature	Time	
			pET28b	**pCDF duet**
1	1	95°C	1 min	1 min
2	16	95°C	30 sec	30 sec
3	16	72°C	13 min 24 sec	5 min 6 sec

After temperature cycling, the reactions were cooled down to 37°C before adding 1 µl of *Dpn* I restriction enzyme (Agilent Technologies). The reactions were incubated at 37°C for one hour to digest the parental supercoiled plasmid DNA. *E. coli* Top10 competent cells were transformed with the PCR products (see 2.2.2).

2.7.4 Small-scale expression series

The plasmid DNA from four colonies from each transformation plate was extracted following the QIAprep Miniprep protocol (see 2.7.2). The obtained plasmids were transformed into *E. coli* BL21 (DE3) competent cells together with the chaperone p*Trc*-60.2-GroES plasmid (see 2.2.2).

O.C.s were prepared straight from the transformation without plating first (see 2.2.3). The O.C.s that grew successfully were used to inoculate 10 ml Terrific Broth bulk cultures (see 2.2.5). To check the expression of each mutant before sequencing, samples of cells before and after induction with IPTG were run on an SDS-PAGE gel (see 2.1).

2.7.5 Sequencing

As all bulk cultures showed expression in equal quantities, following plasmids were sent for sequencing: Rv3790-pET28b R242A and E294A and Rv3790-pCDF duet R242A, E294A and Y297A (Eurofins MWG Operon).

The mutations were successful in all sequenced plasmids. The Rv3790-pCDF duet E294A and Y297A sequenced plasmids were transformed into *E. coli* BL21 (DE3) competent cells together with the chaperone p*Trc*-60.2-GroES plasmid. The mutated proteins were overexpressed and purified as for wild type DprE1 (see 2.2-2.4).

2.8 Ligand binding with DprE1 mutants E294A and Y297A

Using the protocol described under 2.5.8, ligand binding was tested for both mutants with C12 and RKH06. Table 11 shows the values for protein and ligand concentration and addition calculated for these measurements (formula under 2.5.6.). The data was recorded as shown in table 6 and evaluated as described under 2.6.

Table 11: Mutant DprE1 and ligand concentrations / additions used for binding studies

Measurement	**Buffer (µl)**	**Protein stock conc. (µM)**	**Protein conc. (µM) / addition (µl)**	**Ligand conc. (µM) / addition (µl)**
DprE1 mutant E294A – RKH06	550	24	2.0 / 50	0.5 / 0.6
DprE1 mutant E294A – C12	540	20	2.0 / 60	0.5 / 0.6
DprE1 mutant Y297A – RKH06	565.7	35	2.0 / 34.3	0.5 / 0.6
DprE1 mutant Y297A – C12	565.7	35	2.0 / 34.3	0.5 / 0.6

3. RESULTS

3.1 Unsuccessful expression of wild type DprE1

Chaperone-assisted expression of DprE1 using the plasmids Rv3790-pET28b and p*Trc*-60.2-GroES grown in LB medium produced only insoluble protein. The protein obtained from transformations with Rv3790-pCDF and p*Trc*-60.2-GroES grown in LB medium was soluble, however, it did not incorporate / had lost the FAD co-factor in the process. Therefore, these results are not presented in the following (see appendix 4).

3.2 Expression of wild type DprE1 using ratio transformation

As a measure to try and increase the amount of purified protein, and to see how the chaperone affects DprE1 expression, Rv3790-pCDF duet and p*Trc*-60.2-GroES were transformed in *E. coli* BL21 (DE3) competent cells in 3:1 and 1:3 ratios. These transformations were grown in LB medium and the protein expression was induced by adding IPTG for a final concentration of 0.2 mM. It was observed that the 1:3 (more chaperone) culture grew slower than the 3:1 (more Rv3790) culture and both grew slower than previous 1:1 cultures. As shown in figure 6, more DprE1 was expressed in the 3:1 culture, however some protein was lost in the crude lysate, which is a sign for insolubility. Even though less protein was expressed in the 1:3 culture, none was lost in the crude lysate. Both ratio transformations produced more protein than the 1:1 transformation. Also, the chaperone was expressed in much higher quantities than DprE1 in both ratio transformations and it was expressed stronger than in the 1:1 transformation. Even though the ratio transformations produced a small amount of soluble protein, this was not pursued further due to time constraints.

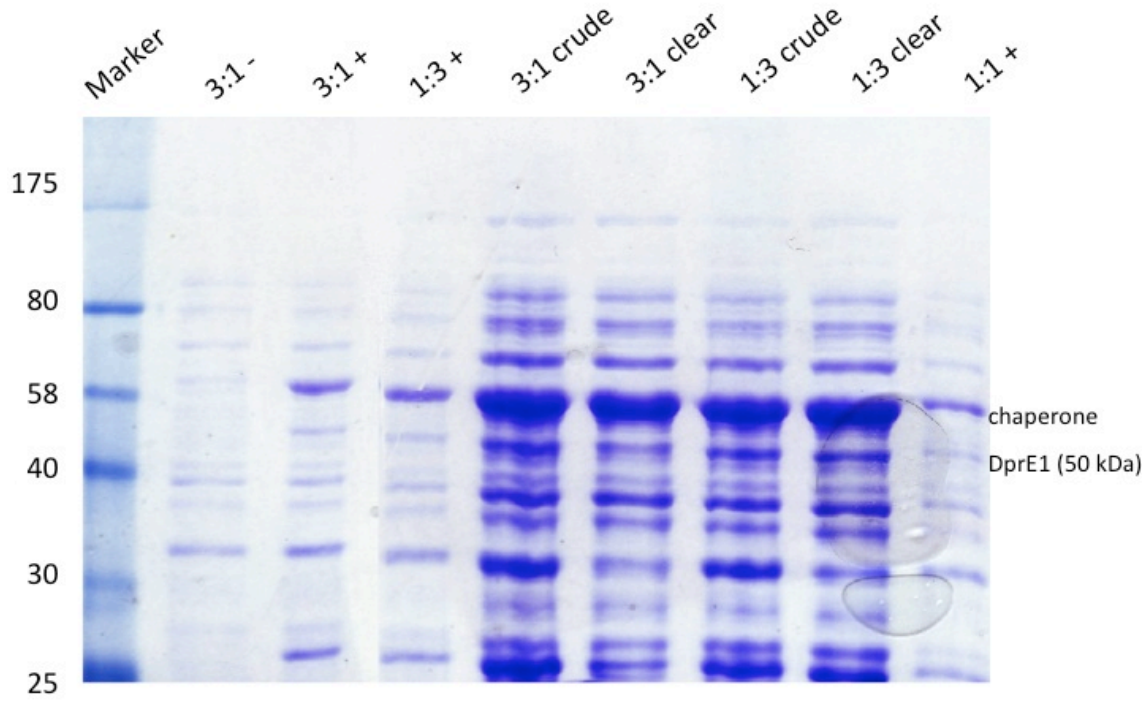

Fig. 6: Coomassie-stained SDS-PAGE gel showing the outcome of the ratio transformations (3:1 – more Rv3790; 1:3 – more chaperone). From left to right the gel shows the molecular marker, cells before IPTG induction (-), cells after IPTG induction (+), crude lysate, clear lysate, and cells after IPTG induction from a 1:1 transformation as reference. Molecular masses are given in units of kDa.

3.3 Successful expression and purification of wild type DprE1

Transformations using Rv3790-pCDF duet together with the chaperone p*Trc*-60.2-GroES grown in Terrific Broth were always successful and produced reasonable quantities of soluble DprE1.

The gel in figure 7 shows samples taken throughout the expression and HisTrap chromatography purification process of wild type DprE1. DprE1 and the chaperone Cpn60.2 were both strongly expressed after IPTG induction and carried through the crude into the clear lysate. The chaperone was mostly retained in the flow through and was fully removed in the 10 mM elution. DprE1 was present in the 60 mM elution, however this fraction was not dialysed due to contamination.

Pure DprE1 was identified the 80 mM and 100 mM elutions, which were dialysed together for further purification.

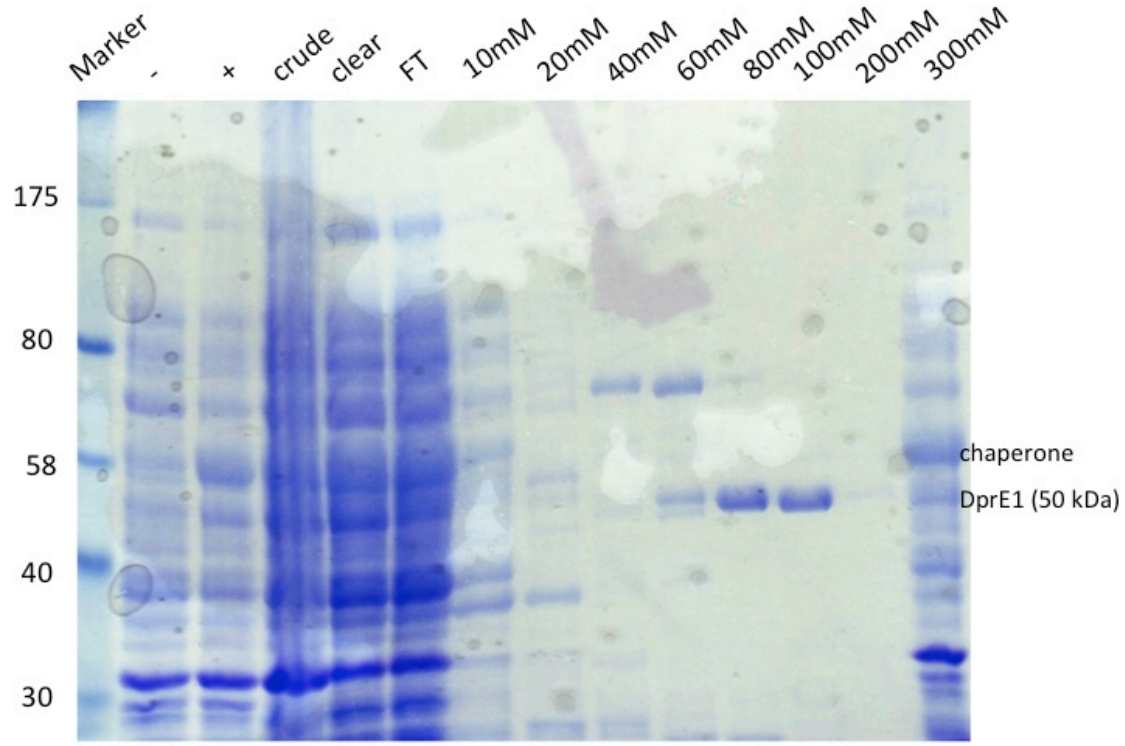

Fig. 7: Coomassie-stained SDS-PAGE gel showing samples taken throughout the expression and HisTrap chromatography purification process of wild type DprE1. From left to right the gel shows the molecular marker, cells before IPTG induction (-), cells after IPTG induction (+), crude lysate, clear lysate, HisTrap column flow through (FT) and elutions with imidazole concentrations given in mM. Molecular masses are given in units of kDa.

The gel in figure 8 shows the ion exchange chromatography elutions. No impurities were detected on the gel and purified DprE1 was present in the 140 mM, 160 mM, 180 mM, 200 mM and 1 M elutions, which were dialysed together.

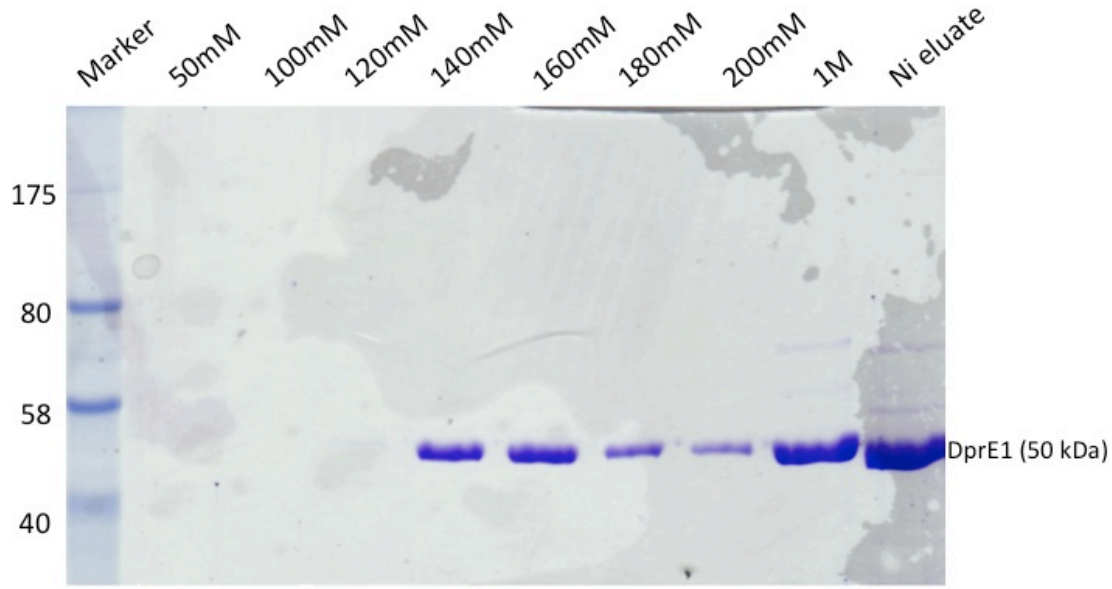

Fig. 8: Coomassie-stained SDS-PAGE gel showing elution samples taken throughout the ion exchange chromatography purification process of wild type DprE1. NaCl concentrations are given in mM and the HisTrap column (Ni) eluate was used as reference. Molecular masses are given in units of kDa.

To check the purity and state of the protein after concentrating with a 10 kDa cut-off filter, concentrated DprE1 and 1:10, 1:20 and 1:50 dilutions were run on a SDS-PAGE gel. As shown in figure 9 the protein was in a good condition with hardly any contamination. For the purpose of this study, a purity of 95% and a concentration of around 50 µM was acceptable.

Yellow coloration of the concentrated solution meant that the FAD co-factor was incorporated in the protein and in the oxidised state. This was used as an indicator for proper folding and activity of the protein (Batt *et al.* 2012, Neres *et al*. 2012).

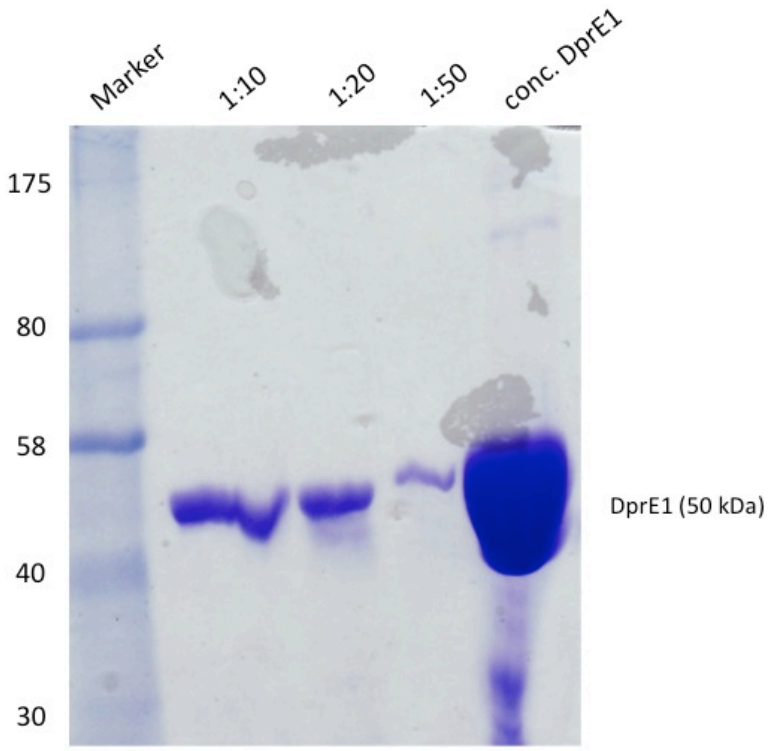

Fig. 9: Coomassie-stained SDS-PAGE gel showing samples of concentrated wild type DprE1 and dilutions after concentration. Molecular masses are given in units of kDa.

3.4 Ligand binding studies with wild type DprE1

Given that the structure of DprE1 has been known (figure 5), it was reasonable to expect that an inhibitor of this enzyme should bind in the binding pocket next to the flavin. However, it is conceivable that an inhibitor is uncompetitive or non-competitive, in other words does not bind in the same site as the substrate. This means that the RKH06 complex structure could either show a novel model of DprE1-inhibition or an experimental artefact. Therefore, the aim of this project was to ascertain the mode of action of the DprE1 inhibitor RKH06.

To determine the binding affinity of wild type DprE1 with C12 and RKH06, the change in intrinsic Trp fluorescence was measured. Firstly, to rule out any effects of buffer and DMSO on the protein fluorescence, control measurements were performed.

This was followed by single ligand experiments to determine the K_d of both ligands. Then, to either support or disprove the crystallographic evidence, competition experiments with both ligands were performed. Finally, to confirm the results of the initial single ligand measurements, control measurements using protein from a different transformation were taken. Measurements with a third ligand (327-4) were also performed. As they were not relevant for the aim of this study, the results are not shown here (see appendix 5).

The saturation binding curves presented in the following show volume corrected and normalised data in order to allow comparison between individual experiments on a scale from 1 to 100 independent from B_{max}. The binding curves represent the mean value obtained for each experiment.

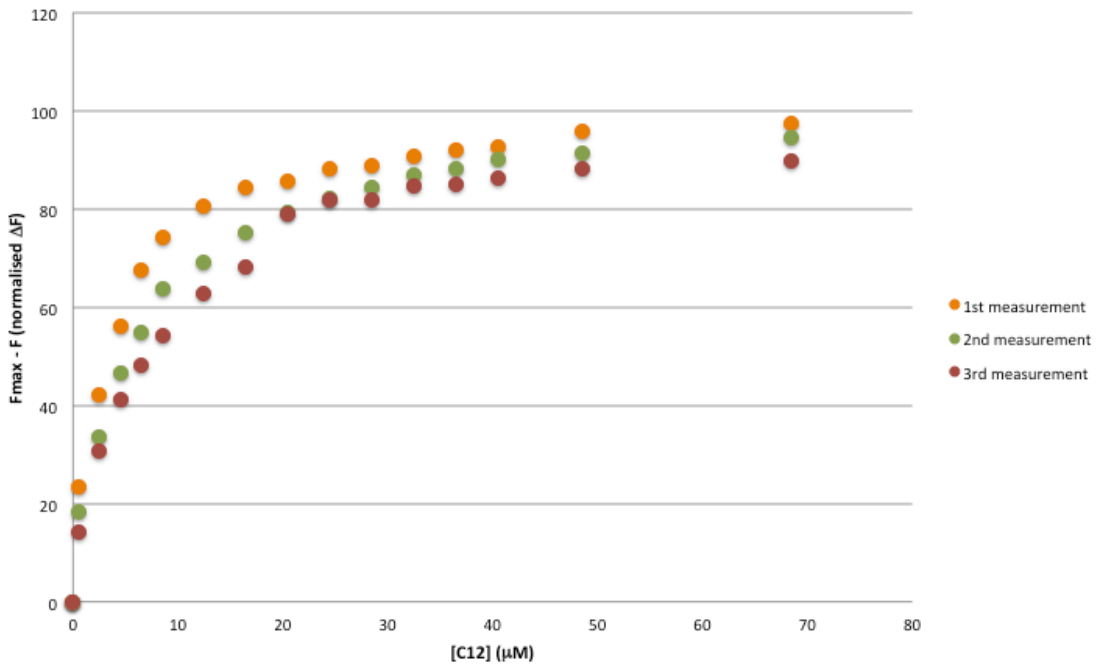

Fig. 10: Example graph showing the saturation binding curves of DprE1 with ligand from three replicates within one experiment.

Figure 10 shows the three replicates within one experiment (experiment with the most variation in this study). This demonstrates the variation of replicates and shows that the average binding curve is a good representative of the individual replicates.

3.4.1 Buffer and DMSO control measurements

To determine the effect of buffer and/or DMSO additions on the Trp fluorescence spectra, two control measurements were performed. Buffer and DMSO were added until a final volume of 178.2 µM was reached. Figure 11 illustrates that upon increasing DMSO above a certain threshold concentration, the trace of the fluorescence spectrum changes significantly from the shape expected for Trp fluorescence. The effects were seen at a total volume of 82.2 µM (equal to ligand volume of 68.5 µM) which corresponds to a DMSO concentration of 0.12%.

As shown in figure 12, there was a linear decrease in fluorescence for both buffer and DMSO up to a concentration equivalent to 68.5 µM of ligand. After that, the fluorescence reaches a plateau for buffer and decreases linearly for DMSO. This indicates that DMSO induces changes that may make the protein non-functional. Hence, if a ligand is dissolved in DMSO, ligand binding by way of Trp fluorescence can only be measured as long as the Trp spectrum does not indicate deviations from the expected spectrum (figure 11). To minimise the impact of these non-specific changes on the Trp fluorescence, the following binding studies were carried out to a maximum ligand concentration of 72 µM.

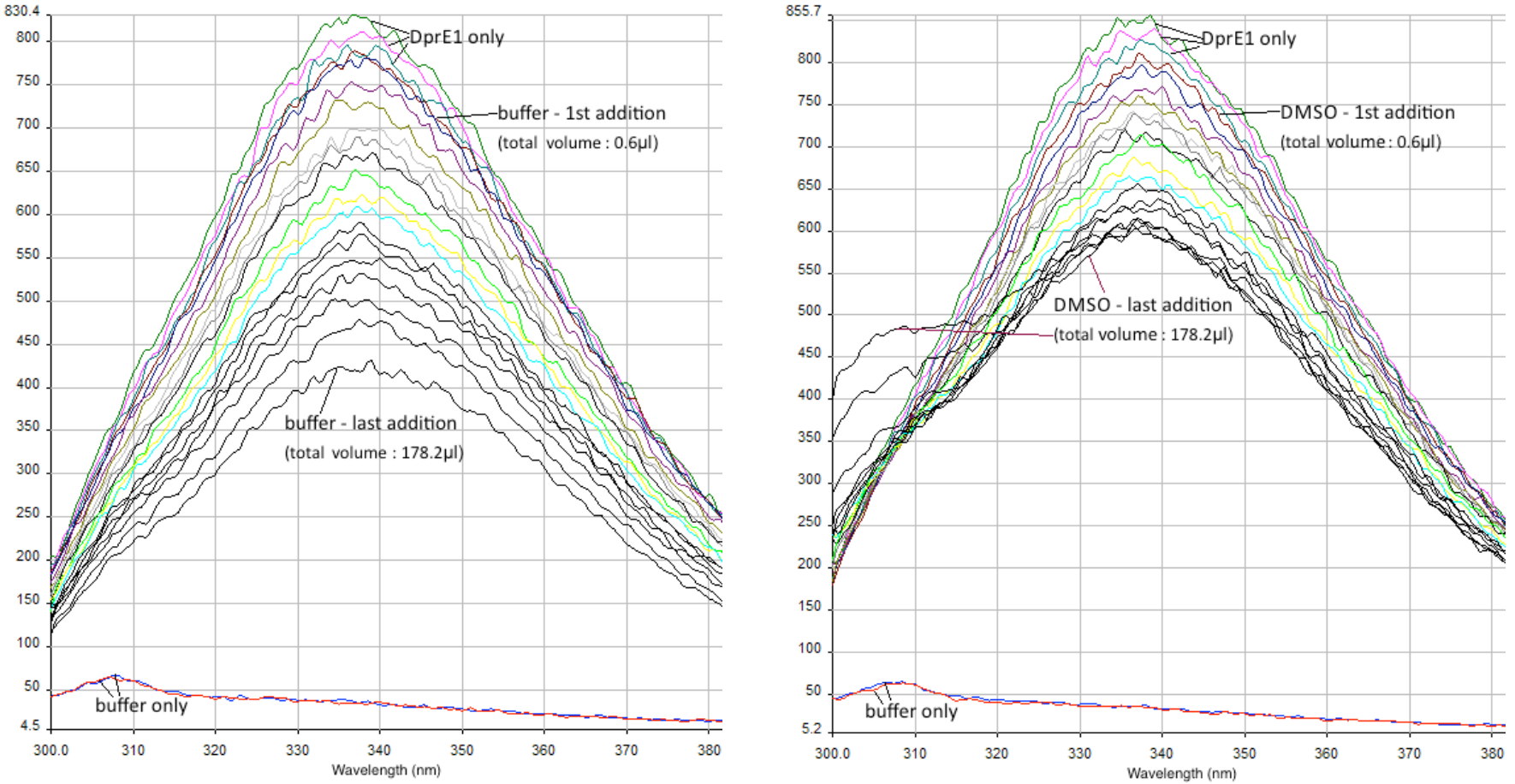

Fig. 11: Fluorescence spectrum of control measurements showing wild type DprE1 with (left) buffer and (right) DMSO.

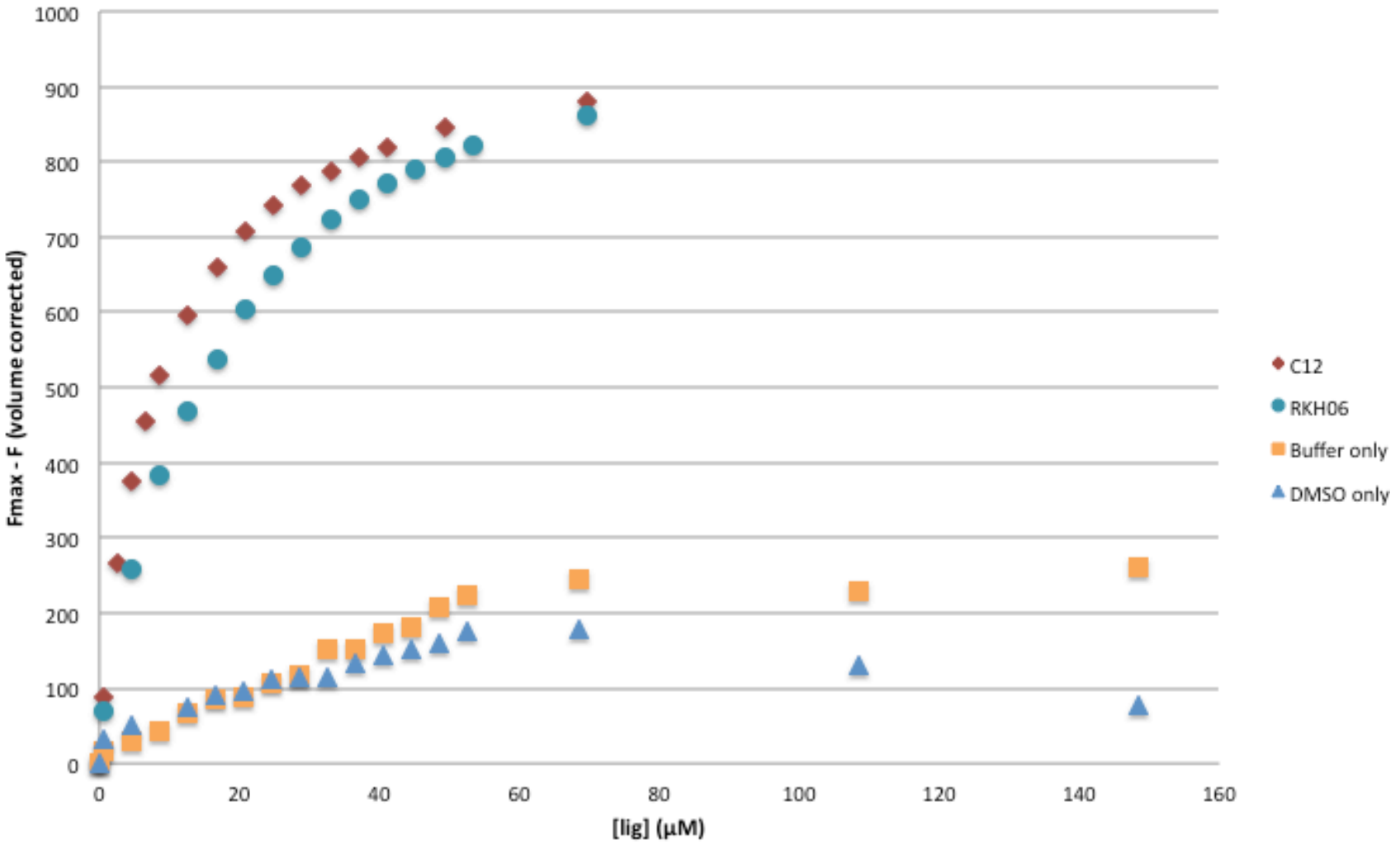

Fig. 12: Saturation binding curves of wild type DprE1 with C12 and RKH06 and control measurements with buffer and DMSO.

3.4.2 Single ligand experiments

To determine the K_d and B_{max} of C12 and RKH06, single ligand experiments were performed. Therefore, the ligands were gradually added to DprE1 starting at 0.51 µM up to a final concentration of 69.64 µM.

Figure 13 shows two example fluorimeter spectra of one C12 and RKH06 measurement illustrating the fluorescence quenching cause by ligand addition. Figure 15 shows the DprE1 saturation binding curves with both ligands. C12 had a mean K_d of 7.41 µM and a mean B_{max} of 965.5 while RKH06 had a mean K_d of 15.19 µM and a mean B_{max} of 1053.6 (table 12).

3.4.3 Competition experiments

To determine whether the ligands are binding in different sites or compete for the same binding site, competition experiments with wild type DprE1 and both ligands were performed. The expectation for this was that if RKH06 binds in the site shown in the crystal structure then the K_d of both ligands would not be affected, as there would be no competition for the binding sites. However, if RKH06 binds in the same site as C12 then the K_d of both ligands would increase significantly, suggesting competition for one site.

Therefore, one ligand was added to DprE1 at its (K_d, 7.5 µM for C12; 15 µM for RKH06), and the other ligand was then titrated into this from 0.5 µM to a final concentration of 68.5 µM as for the single ligand measurements.

Figure 14 shows two example fluorimeter spectra of one competition experiment measurement where C12 was titrated onto 15 µM RKH06 and RKH06 was titrated onto 7.5 µM C12. Figure 15 shows a comparison graph between the DprE1 saturation binding curves of the single ligand and competition experiments. There is a visible shift of the curves to the right indicating an increase in K_d for both conditions. The K_d of C12 increased to 13.73 µM and the K_d of RKH06 increased to 24.28 µM.

Table 12 shows the protein stock concentration, the mean K_d and mean B_{max} obtained for each condition. To be able to monitor any effects of degradation on the ligand binding affinity, the protein age was recorded from the day of HisTrap purification. The wild type DprE1 described in this table came from the same transformation and the same batch of bulk cultures.

Table 12: Protein stock concentration, mean K_d, mean B_{max} and protein age for all experiments

Set up	**Stock conc. (µM)**	**Mean K_d (µM)**	**Mean B_{max}**	**Protein age (days)**
Wild type – buffer	74	-		7
Wild type – DMSO	74	-		7
Wild type – RKH06	47	15.19	1053.6	17
Wild type – C12	47	7.41	965.5	18
Wild type – RKH06 with 7.5 µM C12	45	24.28	635.6	19
Wild type – C12 with 15 µM RKH06	45	13.73	381.7	20
Mutant Y297A – RKH06	35	8.63	660.4	6
Mutant Y297A – C12	35	4.89	657.8	7
Mutant E294A – RKH06	24	10.60	702.0	8
Mutant E294A – C12	20	5.93	758.2	11

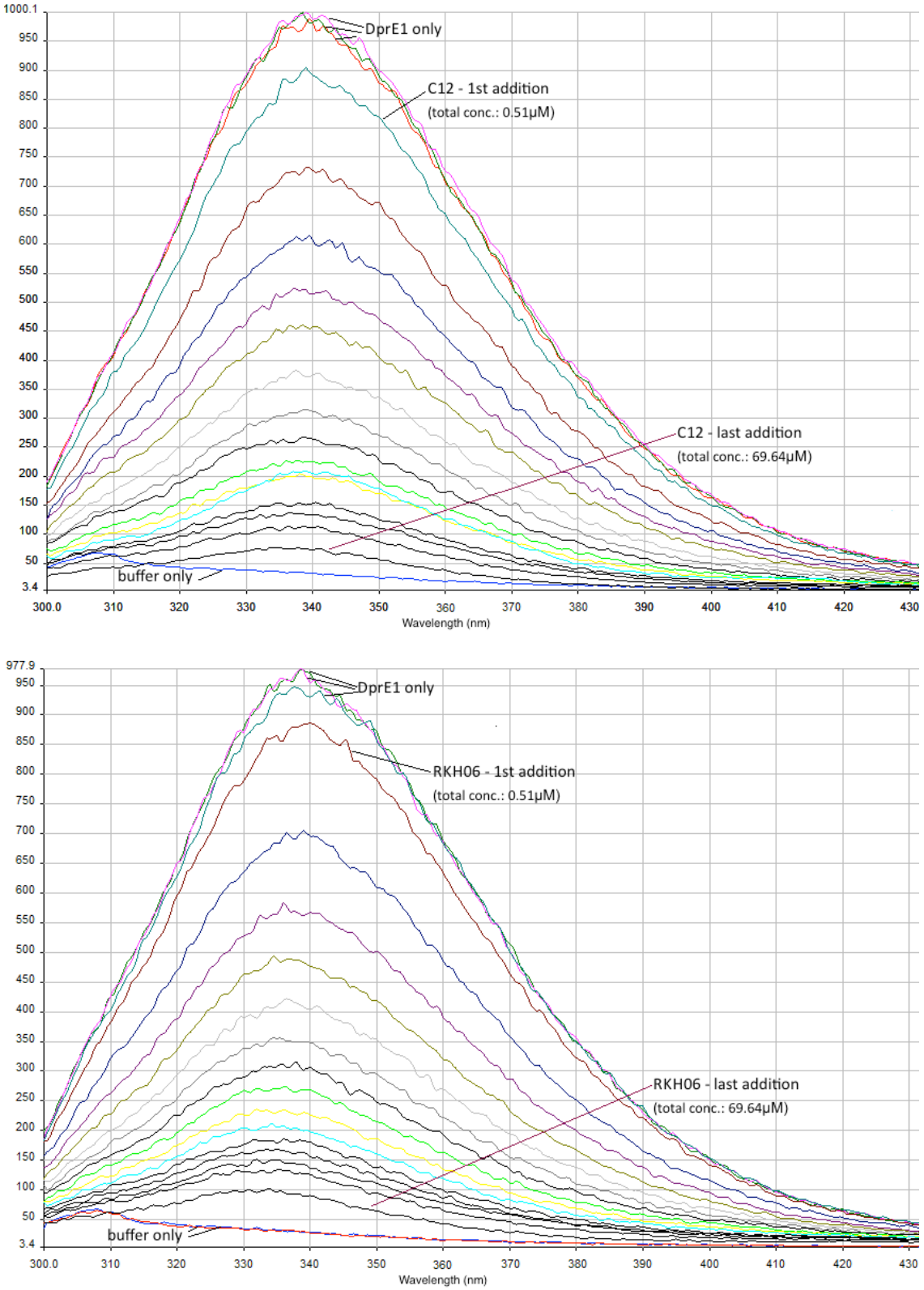

Fig. 13: Fluorescence spectrum example of single ligand binding experiments showing wild type DprE1 with (top) C12 and (bottom) RKH06.

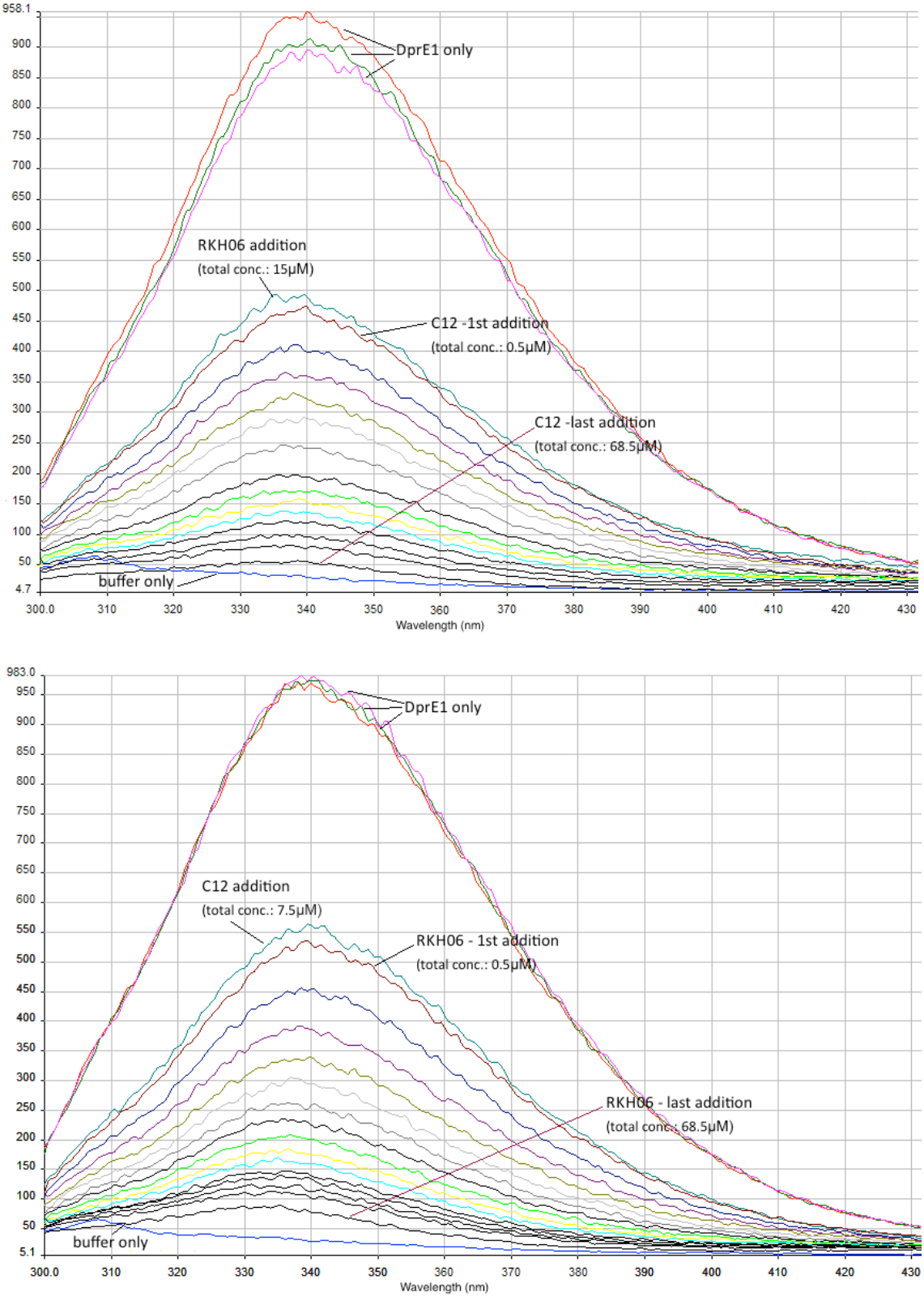

Fig. 14: Fluorescence spectrum example of competition experiments showing wild type DprE1 with (top) C12 and 15 µM RKH06 and (bottom) with RKH06 and 7.5 µM C12.

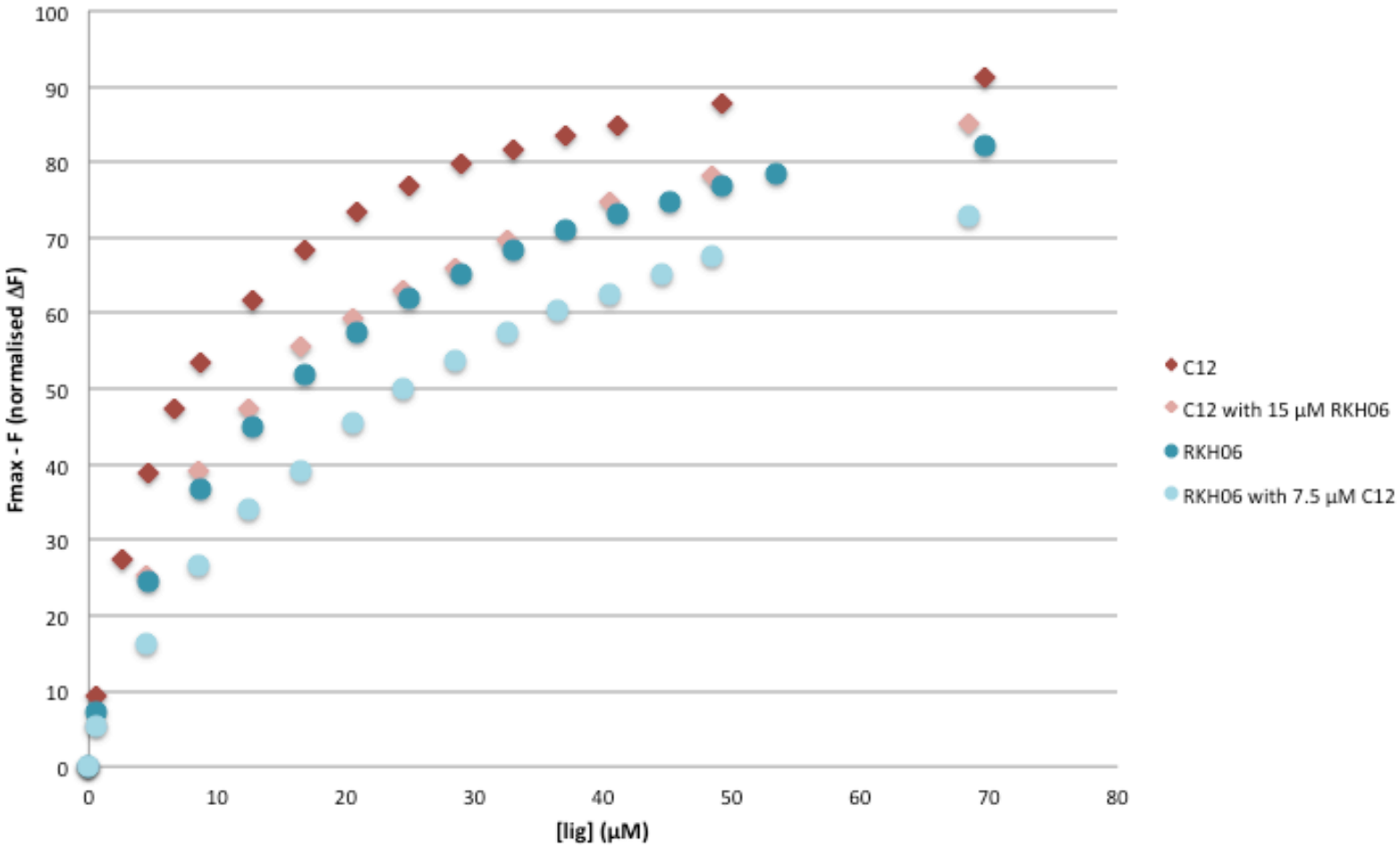

Fig. 15: Saturation binding curves of single ligand experiments showing wild type DprE1 with C12 and RKH06 and saturation binding curves of competition experiments showing wild type DprE1 with C12 and 15 µM RKH06 and with RKH06 and 7.5 µM C12. Data represents the mean of two / three independent measurements.

3.4.4 Wild type DprE1 control measurements

To confirm the results of the initial single ligand measurements, two control measurements for each ligand were performed with DprE1 from a different transformation. The measurements were all done on different days.

Table 13 shows the protein stock concentration and the K_d for each wild type DprE1 control measurement with C12 and RKH06. To be able to monitor any effects of degradation on the ligand binding affinity, the protein age was recorded from the day of HisTrap purification. As the measurements were taken with several days gap between them, no mean K_d was calculated. The protein stock used for these set ups came from a different transformation and bulk culture batch than the stocks used in previous measurements. It had a very high initial concentration of 599 µM and the first control measurement was only performed after the protein was 15 days old. Two independent measurements were taken for each ligand on different days.

Table 13: Information on stock concentration, K_d and protein age for the wild type DprE1 control measurements

Set up	**Stock conc. (µM)**	**K_d (µM)**	**Protein age**
Wild type – C12 control one	599	8.7338	15 days
Wild type – RKH06 control one	509	32.2064	23 days
Wild type – C12 control two	450	20.9345	28 days
Wild type – RKH06 control two	450	31.1532	28 days

Figure 16 shows the wild type DprE1 saturation binding curves with C12 and RKH06.

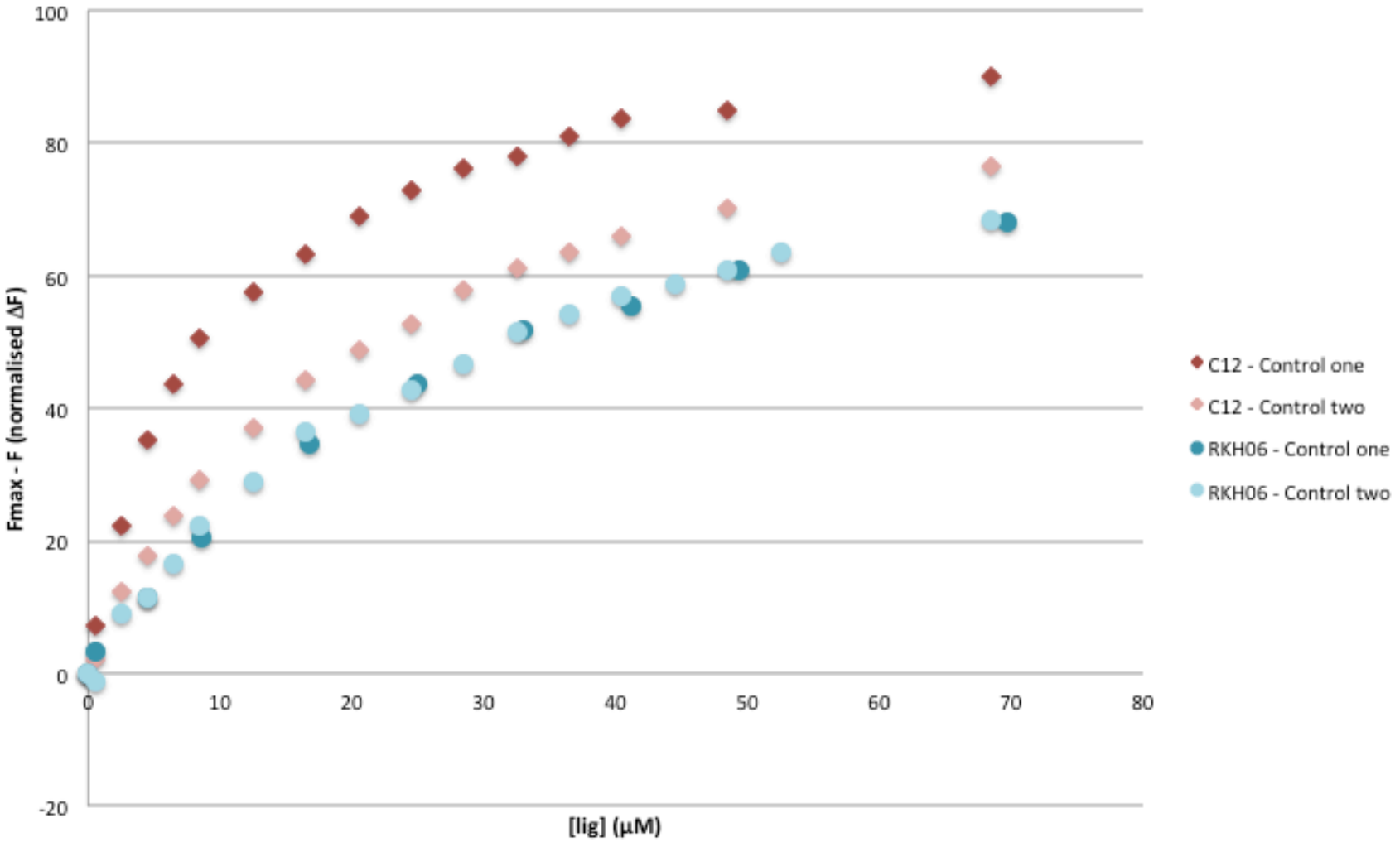

Fig. 16: Saturation binding curves of control measurements showing wild type DprE1 with C12 and RKH06.

3.5 Expression and purification of mutant DprE1

To confirm or disprove the results of the competition experiments, three single amino acid change mutants of the RKH06 binding site shown in the crystallographic evidence (figure 5) were designed in both Rv3790-pET28b and Rv-3790-pCDF duet. These mutations 'cut-back' side chains that form close contacts with the inhibitor in the binding site (figure 17).

Out of time constraints, only the Rv3790-pCDF duet mutants E294A and Y297A were chosen for further ligand binding studies. Both DprE1 mutants were successfully expressed and purified and produced adequate quantities of pure soluble protein.

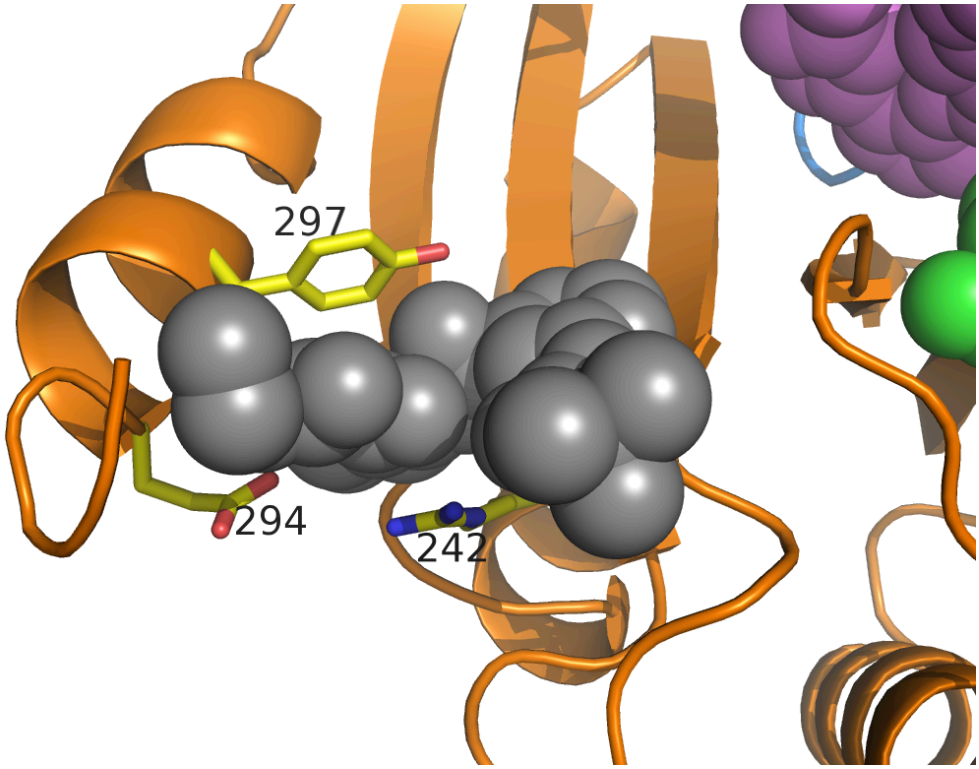

Fig. 17: Sites of mutation for single amino acid change DprE1 mutants E294A and Y297A. Mutations 'cut-back' side chains that form close contacts with the inhibitor in the binding site.

3.5.1 E294A mutant DprE1

The gel in figure 18 shows samples taken throughout the expression and HisTrap chromatography purification process of E294A mutant DprE1. E294A mutant DprE1 was expressed after IPTG induction and carried through the crude into the clear lysate. Protein was present in the 20 mM, 100 mM and 200 mM elutions, however these fractions were not dialysed due to contamination. Pure E294A mutant DprE1 was identified the 40 mM, 60 mM and 80 mM elutions, which were dialysed together for further purification.

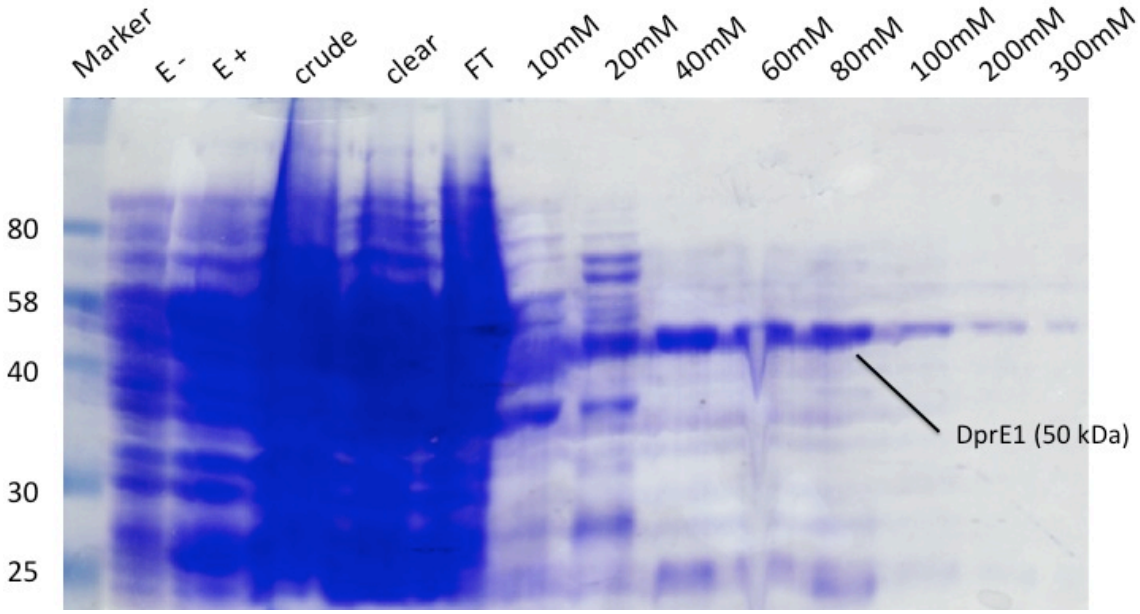

Fig. 18: Coomassie-stained SDS-PAGE gel showing samples taken throughout the expression and HisTrap chromatography purification process of recombinant E294A mutant DprE1. From left to right the gel shows the molecular marker, cells before IPTG induction (-), cells after IPTG induction (+), crude lysate, clear lysate, HisTrap column flow through (FT) and elutions with imidazole concentrations given in mM. Molecular masses are given in units of kDa.

The gel in figure 19 shows the ion exchange chromatography elutions with NaCl concentrations given in mM and the HisTrap (Ni) eluate used as reference. Also, as there was precipitate in the dialysis bag, samples were taken before and after spinning down the solution. The band on the gel was much thinner after centrifuging, indicating that some of the protein had precipitated and was lost in the pellet.

E294A mutant DprE1 was present in the 140 mM to 1 M elutions. However, pure protein without contaminations was only present in the 160 mM, 180 mM and 200 mM elutions, which were dialysed together.

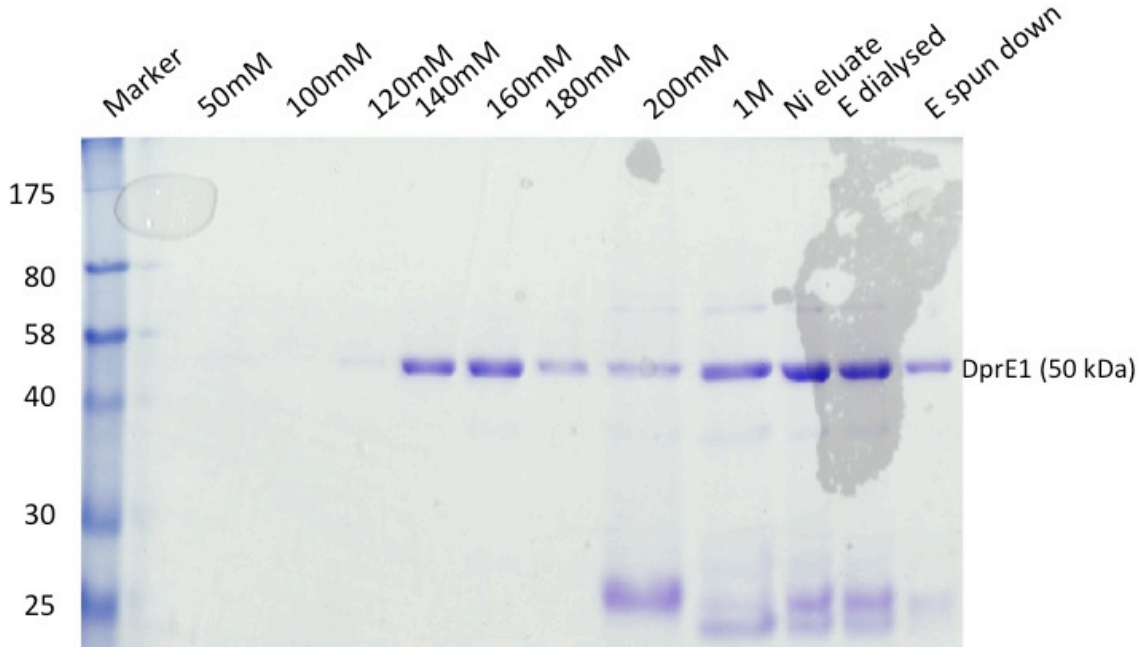

Fig. 19: Coomassie-stained SDS-PAGE gel showing elution samples taken throughout the ion exchange chromatography purification process of E294A mutant DprE1. NaCl concentrations are given in mM and the HisTrap column (Ni) eluate was used as reference. Samples of dialysed protein before and after spinning down any precipitate are also shown. Molecular masses are given in units of kDa.

3.5.2 Y297A mutant DprE1

The gel in figure 20 shows samples taken throughout the expression and HisTrap chromatography purification process of Y297A mutant DprE1. Y297A mutant DprE1 was expressed after IPTG induction and carried through the crude into the clear lysate. The chaperone was very strongly expressed after IPTG induction but was completely removed after the 10 mM elution. Protein was present in the 20 mM elution, however this fraction was not dialysed due to contamination. Pure Y297A mutant DprE1 was identified the 40 mM, 60 mM and 80 mM elutions, which were dialysed together for further purification.

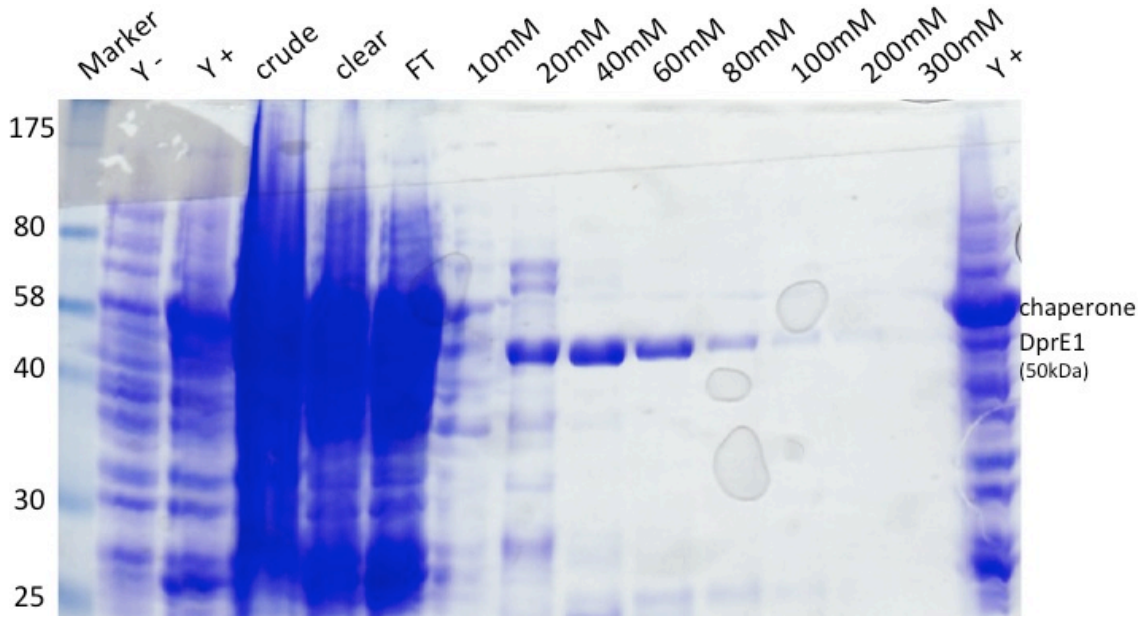

Fig. 20: Coomassie-stained SDS-PAGE gel showing samples taken throughout the expression and HisTrap chromatography purification process of recombinant Y297A mutant DprE1. From left to right the gel shows the molecular marker, cells before IPTG induction (-), cells after IPTG induction (+), crude lysate, clear lysate, HisTrap column flow through (FT) and elutions with imidazole concentrations given in mM. Molecular masses are given in units of kDa.

The gel in figure 21 shows the ion exchange chromatography elutions with NaCl concentrations given in mM and the HisTrap (Ni) eluate used as reference. Also, as there was precipitate in the dialysis bag, samples were taken before and after spinning down the solution. The band on the gel was the same after centrifuging and therefore no protein was lost due precipitation.

No impurities were visible on the gel and pure Y297A mutant DprE1 was present in the 140 mM, 160 mM and 180 mM elutions, which were dialysed together.

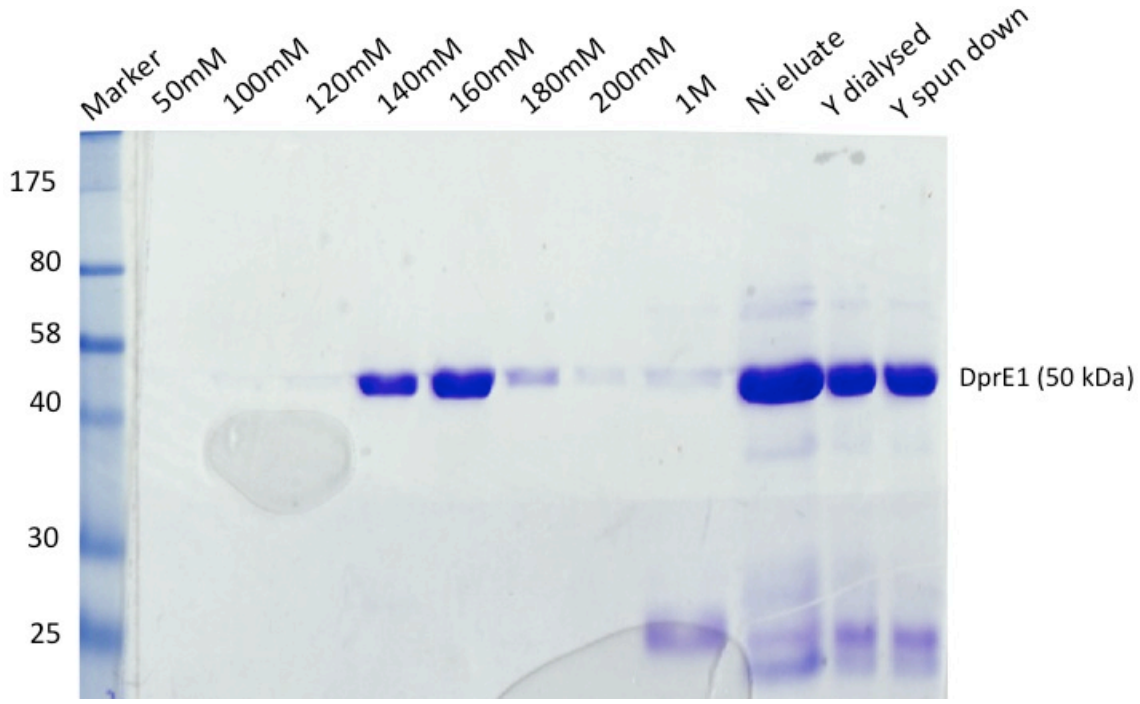

Fig. 21: Coomassie-stained SDS-PAGE gel showing elution samples taken throughout the ion exchange chromatography purification process of Y297A mutant DprE1. NaCl concentrations are given in mM and the HisTrap column (Ni) eluate was used as reference. Samples of dialysed protein before and after spinning down any precipitate are also shown. Molecular masses are given in units of kDa.

3.5.3 Purity of concentrated mutated DprE1

To check the purity and state of the mutated proteins after concentrating with a 10 kDa cut-off filter, concentrated E294A and Y297A mutant DprE1 and 1:10, 1:20 and 1:50 dilutions were run on a gel (figure 22). Even though there was some degradation visible in the concentrated protein lanes, this was pure enough for ligand binding studies.

It was not possible to concentrate the mutated proteins to 50 µM as the wild type. The protein solutions started to become gloopy after concentration and had to be diluted with buffer B 10 mM NaCl. Both mutants showed the characteristic yellow colouring (Batt *et al.* 2012).

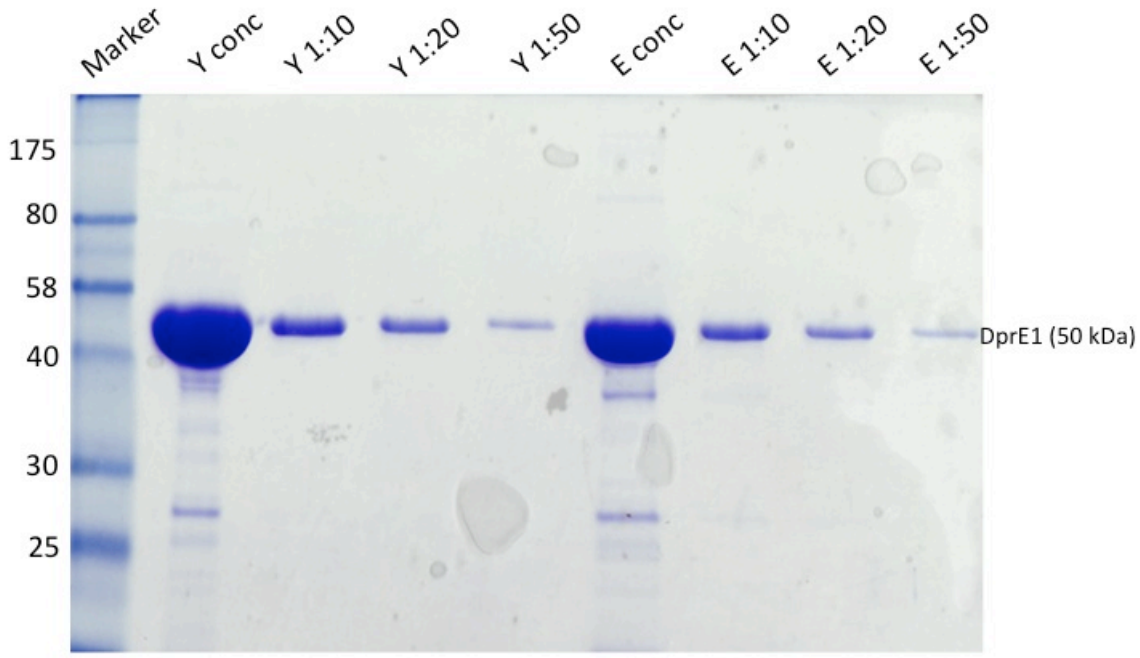

Fig. 22: Coomassie-stained SDS-PAGE gel showing concentrated E294A and Y297A mutant DprE1 and dilutions after concentration.

3.6 Ligand binding studies with mutant DprE1

Both mutant proteins expressed well and were purified to similar levels as wild type DprE1. Therefore, single ligand measurements were carried out with both E294A and Y297A mutant DprE1 to determine the K_d of each individual ligand.

Given the crystallographic evidence (figure 5), the hypothesis for the mutant binding studies was that if RKH06 binds in the site shown in the crystal structure then the K_d would increase, as binding with this site is more difficult. However, if RKH06 binds in the same site as C12 then the K_d would be unaffected by the mutation.

The saturation binding curves presented in the following show volume corrected and normalised data in order to allow comparison between individual experiments on a scale from 1 to 100 independent from B_{max}. The binding curves represent the mean value obtained for each experiment.

As for the wild type DprE1 experiments, the ligands were gradually added to the protein starting at 0.5 µM up to a final concentration of 68.5 µM.

Figure 23 shows two example fluorimeter spectra of both E294A and Y297A mutant DprE1 with C12. Figure 24 shows both DprE1 mutants with RKH06. Figure 25 shows the saturation binding curves of both DprE1 mutants with C12 and RKH06. C12 had a K_d of 5.93 µM with E294A and a K_d of 4.89 µM with Y297A while RKH06 had a K_d of 10.60 µM with E294A and a K_d of 8.63 µM with Y297A.

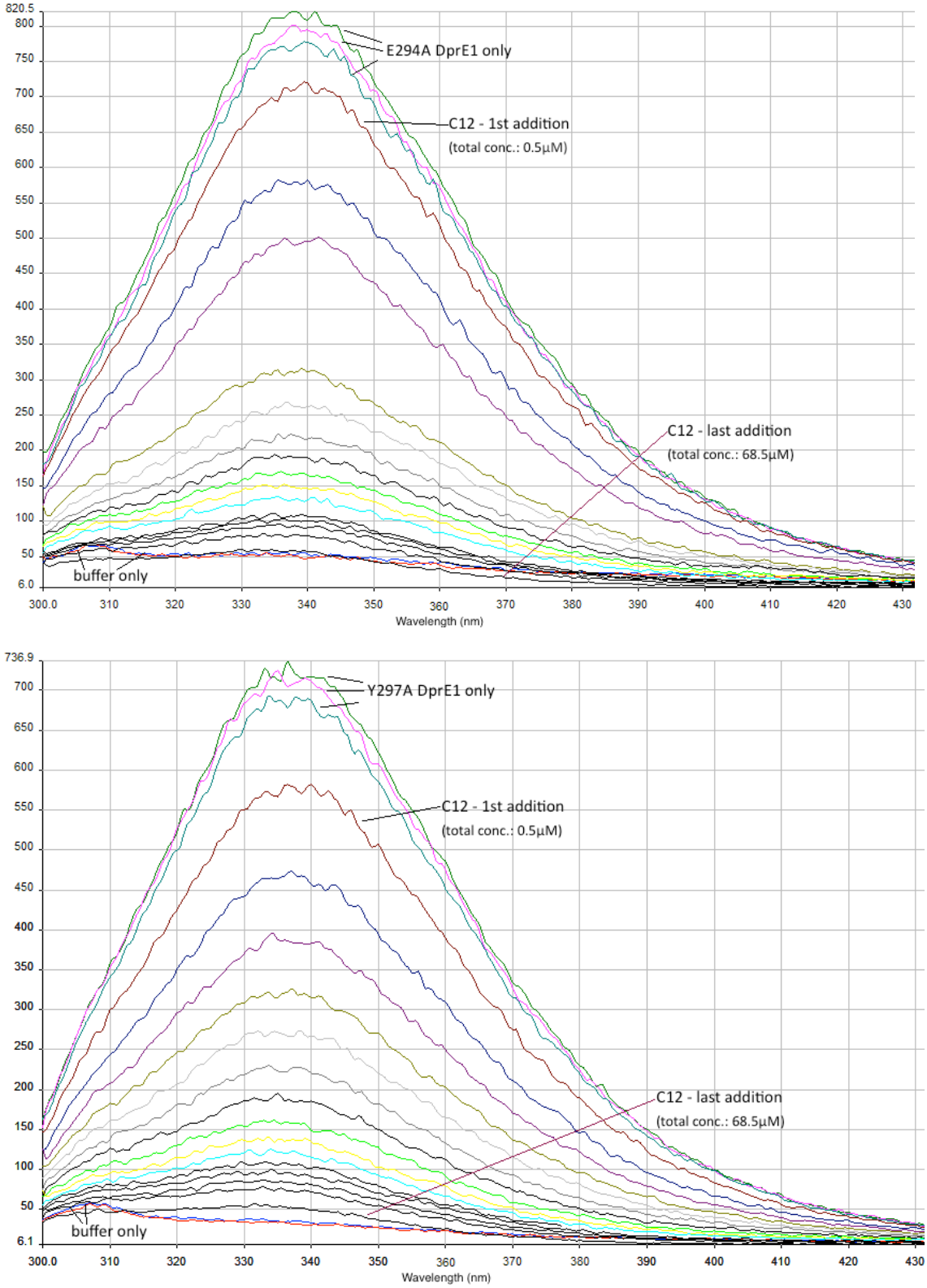

Fig. 23: Fluorescence spectrum example of single ligand experiments showing (top) E294A mutant DprE1 and (bottom) Y297A mutant DprE1 with C12.

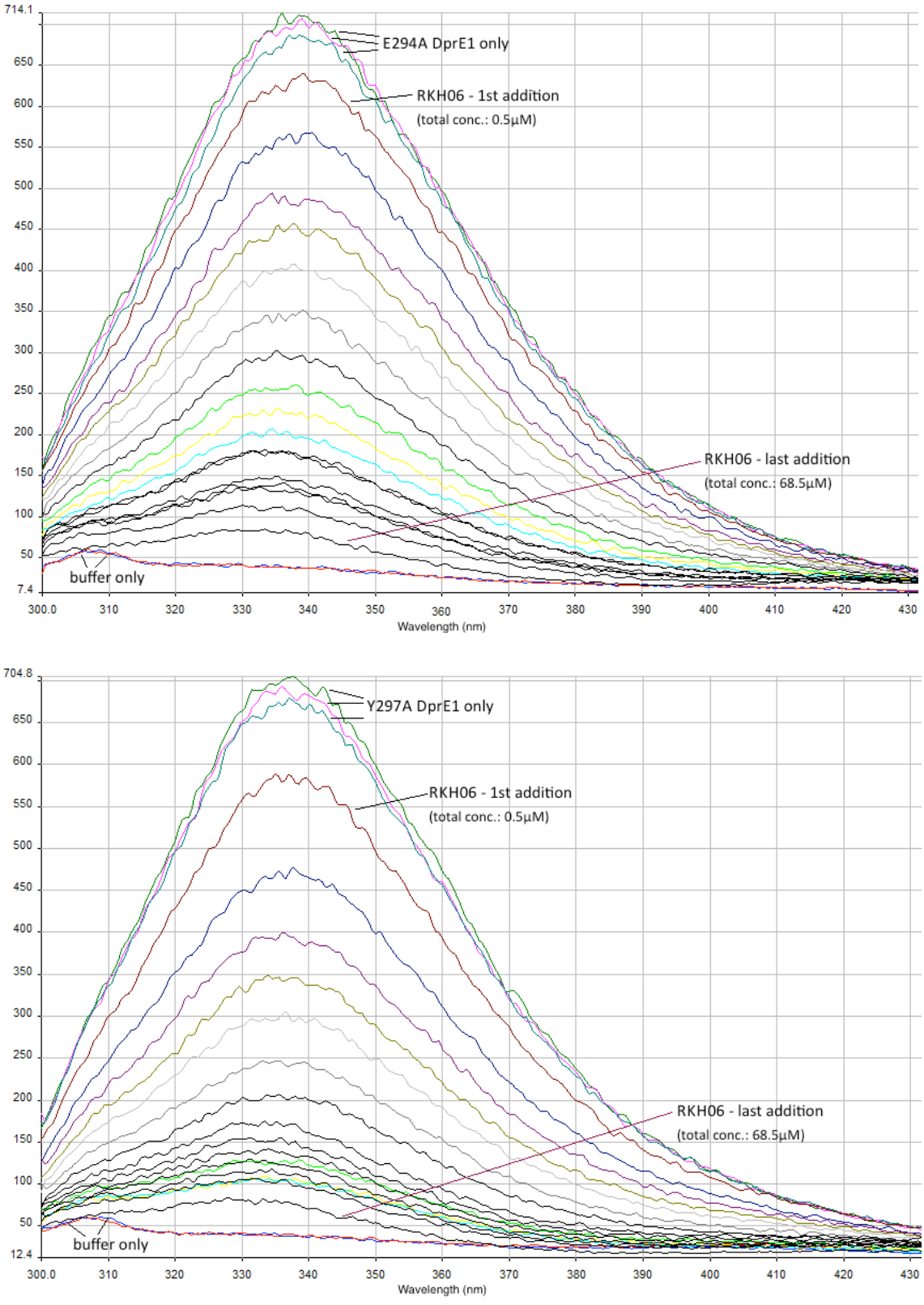

Fig. 24: Fluorescence spectrum example of single ligand experiments showing (top) E294A mutant DprE1 and (bottom) Y297A mutant DprE1 with RKH06.

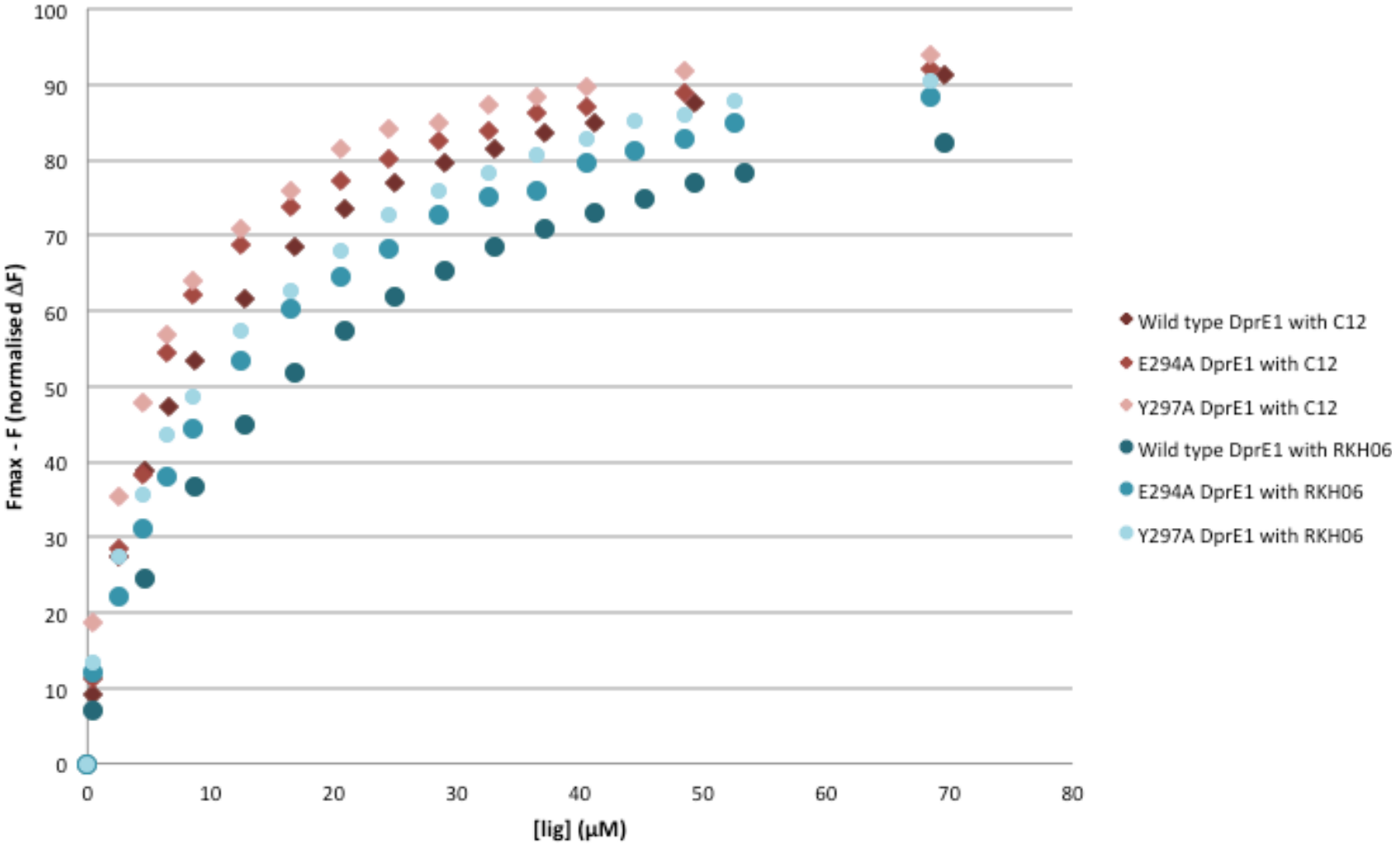

Fig. 25: Saturation binding curves of single ligand experiments showing E294A and Y297A mutant DprE1 with C12 and RKH06. Data represents the mean of three independent measurements.

4. DISCUSSION

The crystallographic evidence obtained for the binding of DprE1 with the inhibitor RKH06 (figure 5) contradicted the expectation raised by both the resistance mutation (Y314C) and the C12-bound structure.

X-ray crystallography, the technique which allows the construction of protein structures, relies on the principle of crystal lattice formation from highly concentrated protein. However, a crystal lattice does not represent the physiological state of the protein and can cause changes in the proteins properties. In order to form a crystal, there has to be sufficient contact between the molecules. The tight interaction between the molecules due to the pressure in the lattice can induce conformational changes, which in turn can alter the binding affinity of the protein. Even very small conformational changes can have great impact on the binding affinity. Furthermore, the protein concentration in a crystal is very high with values around 12.5 µM whereas the physiological protein concentration in cells is about three times lower. This high concentration of protein can also cause changes in binding behaviour. Therefore, it can happen that the evidence provided by X-ray crystallography does not capture the binding behaviour that the protein would show *in vivo* or in solution.

At a minimum, the ligand-bound crystal structure indicates that DprE1 offers an alternative binding site for RKH06 even though this may not be the physiologically relevant binding site.

Therefore, to ascertain the mode of action of RKH06 in solution, the aim of this study was to determine whether RKH06 in fact binds in the same site as C12 next to the FAD co-factor or whether it binds in the site suggested by the crystal structure.

In order to determine the binding affinity of DprE1, the quenching in intrinsic Trp fluorescence following the addition of ligand was measured. This is a common, quick and reliable method to determine the relationship between a protein and a ligand of interest (Bisswanger 2008). According to the spectroscopic data, the maximum binding capacity (B_{max}) and dissociation constant (K_d) were calculated for each measurement. The B_{max} value represents the maximum binding capacity of the protein in solution and is an arbitrary value depending on the instrument and unit used for measuring the fluorescence. The K_d value is used to determine the binding affinity and represents the ligand concentration at which half of the maximum binding sites are occupied. It is given in M (Lambert 2004).

To determine any background noise or effect on the Trp fluorescence before undertaking any binding studies, control measurements with DprE1 and buffer / DMSO were performed. As shown in figure 11, gradual decrease in fluorescence with each buffer / DMSO addition was observed. This can be explained by the fact that with each addition the volume in the cuvette expands which causes a decrease in protein concentration. This effect was accounted for in the determination of B_{max} and K_d by calculating the correction factor to then obtain F_{max} volume corrected.

Looking at figure 12, the curves for both buffer and DMSO show a linear increase up to an equivalent ligand concentration of 68.5 µM. Given that the fluorescence of both was so low, no effect on the protein was suspected. However, after the 68.5 µM addition it seems that the effect of buffer and DMSO becomes unpredictable. This is especially noticeable in the fluorescence spectrum example for DMSO (figure 11). The last three additions equivalent to 68.5 µM, 108.5 µM and 148.5 µM ligand concentration caused a fluorescence peak at about 305 nm, which was not the Trp fluorescence. Due to these changes in the curve, and to avoid any effects on the protein fluorescence, the binding studies were only carried out to a maximum ligand concentration of 72 µM.

To determine the K_d and B_{max} of C12 and RKH06, single ligand experiments were performed. As shown in table 12, the mean K_d of C12 was 7.41 µM and the mean B_{max} was 956.5. In comparison to that, the mean K_d of RKH06 was 15.19 µM and the mean B_{max} was 1053.6. The K_d of RKH06 was about 2.05 times higher than that of C12 and there was a difference of 7.78 µM between these values. This means that C12 has a higher binding affinity and binds tighter to the protein than RKH06 (Lambert 2004). Looking at figure 15, this also explains the obvious difference between the saturation binding curves, with the C12 curves being shifted to the left and upwards, representing a lower K_d.

To confirm the results of the initial single ligand experiments, two control measurements for each ligand were performed with DprE1 from a different transformation. The control measurements for C12 were performed when the protein was 15 and 28 days old. The K_d for first measurement was 8.73 µM and the K_d for second measurement was 20.93 µM. The K_d of the second measurement was more than two times higher which looking at figure 16 is shown by a drastic shift of the curve. Comparing the two measurements, the K_d of the second measurement was more than twice as high as for the first measurement with a difference of 12.20 µM between the two values. The K_d of the first C12 control measurement was only slightly higher than the original wild type DprE1 measurement with only 1.32 µM difference. However, the K_d of the second measurement was significantly higher with a difference of 13.52 µM. In comparison to the initial wild type DprE1 measurements, the K_d was more than double with a difference of about 17 µM between the two values.

The control measurements for RKH06 were performed 23 and 28 days after HisTrap purification. The K_d for first measurement was 32.20 µM and the K_d for the second measurement was 31.15 µM. The K_d values were very similar and the curves overlap in all data points.

These findings suggest very strongly that age had an impact on the wild type DprE1 control measurements. After 15 days the protein seems to still behave normal as the K_d for the first C12 measurements agrees with the previous values.

However, after 23 days when the first RKH06 measurement was taken, it seems that the protein had lost some of its binding capacity and the K_d increased by about two fold. It might also be that the high protein concentration (table 13) could have had an impact on the pace of the degradation process and therefore the binding affinity. The high concentration achieved in the purification was very surprising and different to the other stocks which came from the same bulk culture batch.

To determine whether the ligands are binding in different sites or compete for the same binding site, competition experiments with wild type DprE1 and both ligands were performed. Therefore, one ligand was added to DprE1 at its K_d, 7.5 µM for C12 and 15 µM for RKH06, and the other ligand was then titrated in as for the single ligand measurements. The expectation for this was that if RKH06 binds in the site shown in the crystal structure then the K_d of both ligands would not be affected, as there would be no competition for the binding sites. However, if RKH06 binds in the same site as C12 then the K_d of both ligands would increase significantly, suggesting competition for one site.

The mean K_d of C12 with 15 µM RKH06 was 13.73 µM and the mean B_{max} was 381.7. The K_d was about 1.85 times higher than that of C12 on its own and there was a difference of 6.32 µM between these values. Looking at figure 15, there is an obvious difference between the saturation curves with the competition experiment curves being shifted to the right and downwards, indicating a higher K_d.

The mean K_d of RKH06 with 7.5 µM C12 was 24.28 µM and the mean B_{max} was 635.60. The K_d was about 1.6 times higher than that of RKH06 on its own and there was a difference of 9.08 µM between these values. This explains the obvious difference between the saturation curves shown in figure 15, with the competition experiment curves being shifted to the right and downwards indicating a higher K_d.

Looking at the data from both competition experiments, the K_d values for both ligands were nearly two times higher than for the single ligand measurements. These findings suggest that the ligands have to compete for one binding site. With the first ligand being present in the solution at its K_d, significantly more of the second ligand was needed to outcompete the other. This indicates that RKH06 indeed binds in the same site as C12 as expected.

Given that the competition experiments did not confirm the crystallographic evidence, further studies were needed to obtain more information on the protein's binding behaviour. Therefore, two single amino acid change DprE1 E294A and Y297A mutants were designed and successfully purified. These mutations 'cut-back' side chains that form close contacts with the RKH06 in the binding site (see figure 17). The expectation was that if RKH06 binds in the site shown in the crystal structure (figure 5), then the K_d would increase, as binding to that site would be weaker due to fewer binding points. However, if RKH06 binds in the same site as C12, then the K_d would stay the same and would not be affected by the mutation.

The mean K_d of DprE1 mutant E294A with C12 was 5.93 µM and the mean B_{max} was 758.2. In comparison to that, the mean K_d of wild type DprE1 with C12 was about 1.25 times higher and there was difference of 1.47 µM between the values. Looking at figure 25, there is no obvious difference between the saturation binding curves with overlap in some data points, and the K_d values are very similar.

The mean K_d of DprE1 mutant Y297A with C12 was 4.89 µM and the mean B_{max} was 657.8. Compared to that, the mean K_d of wild type DprE1 with C12 was about 1.51 times higher and there was a difference of 2.52 µM between the values. This is illustrated by the small shift in the saturation binding curves (figure 25).

Looking at the binding affinity of the DprE1 mutants with C12 in comparison to wild type DprE1, there is no great difference in K_d. Even though the wild type DprE1 K_d value was higher than that of the two DprE1 mutants, the difference appears not to be significant.

The mean K_d of DprE1 mutant E294A with RKH06 was 10.60 µM and the mean B_{max} was 702.0. In comparison to that, the mean K_d of wild type DprE1 with RKH06 was about 1.43 times higher and there was a difference of 4.59 µM between the two values. Even though the wild type DprE1 K_d value was higher than that of the DprE1 E294A mutant, the values are still similar and there is only a small difference between the saturation binding curves (figure 25).

The mean K_d of mutant Y297A with RKH06 was 8.63 µM and the mean B_{max} was 660.4. Compared to that, the mean K_d of wild type DprE1 with RKH06 was about 1.76 times higher and there was a difference of 6.56 µM between the two values. This explains the obvious shift of the mutant binding curve compared to the wild type as shown in figure 25. Similar to the K_d values of the competition experiments, the K_d for the Y297A mutant decreased by nearly two fold. There was a very definite shift in curve also comparable to the competition experiments. This significant change in K_d was not expected. On the contrary, the hypothesis for this experiment expected either an increase in K_d if RKH06 binds in the site shown in the crystal structure or no change in K_d if it binds in the same site as C12.

A possible explanation is that single amino acid changes can have an impact on the structure and therefore the behaviour of the protein, which may not be obvious or predictable from looking at the DNA sequence. Generally, 50% to 80% of residues can be mutated without having an impact on the protein structure. However, some changes can have a great effect on the protein's conformation (Schaefer & Rost 2012). Looking at the structure of DprE1, the active site is covered by a disordered loop which is thought to open up to allow the substrate DPR to enter (Neres *et al.* 2012). Given the fact that single amino acid mutations, especially those that effect binding sites and disordered residues, can have an unexpected effect on the proteins conformation it might be that the Y297A mutation resulted in a conformational change that caused the loop to open up thus allowing easier access to the active side (Bhardwaj & Gerstein 2009, Schaefer & Rost 2012).

This would explain why the K_d decreased so significantly for mutant Y297A with RKH06, however, this does not explain with the small change in K_d for mutant Y297A with C12.

There was no great difference between the K_d values for wild type DprE1 single ligand measurements and the K_d values for mutant E294A with both ligands and Y297A with C12. As explained above, the change in K_d could be due to the effect of the single amino acid mutation on the protein but this cannot be said with certainty. Nevertheless, as the K_d value did not increase, these findings suggest that RKH06 binding is not affected by the mutation of the side chains in the binding site shown in the crystal structure.

Together with the results from the competition experiments, this supports the opinion that RKH06 and C12 in fact bind in the same site next to FAD co-factor.

The methods used to measure the ligand binding affinity of DprE1 had several limitations. Firstly, the machine used for the measurements was a Perkin Elmer Luminescence Spectrometer LS 50B with a 10W lamp. The machine represents the protein fluorescence on an arbitrary scale from 0 to 1000 with no units. The problem with arbitrary scales is that they are not comparable. Therefore, the B_{max} values measured in this study cannot be compared with results from a machine that uses a different scale. It would be better to use a more sensitive machine that gives readings in comparable units, for example a photon counter.

Furthermore, the machine provided no constant stirring. It was tried to overcome this problem by mixing the solution manually with a pipette. However, a constant stirrer would provide a more homogenous solution for more accurate results.

Also, there was no constant temperature in the machine and the ambient temperature was fairly constant between 21°C and 22°C. However, given that protein should be kept at 4°C the ambient temperature might have had an impact on the binding affinity.

Finally, in some of the initial ligand binding studies protein up to an age of 20 days was used. Given the impact age had on the wild type DprE1 control measurements, it is difficult to say at which point the protein affinity changes significantly. Ideally fresh protein should be used for the measurements.

It might be useful to prepare fresh protein five days after the HisTrap purification. As three replication measurements take up one day, it would then be possible to measure both ligands with the same batch of protein.

To ensure a constant protein concentration for all measurements, any precipitation was removed by centrifugation in regular intervals and the accurate protein concentration was determined. Even though, all efforts were made to keep the measurements consistent, measuring or pipetting errors may have occurred which cannot be accounted for.

To support the results presented in this study, all ligand measurements should be repeated several times to obtain publishable data. For any repeat measurements, a different machine for example a photon counter with constant stirring and controlled temperature should be used. Using a more sensitive machine would also allow to use lower concentrations of protein. In some cases it can happen that the protein concentration if too high has a decreasing impact on the fluorescence (Bisswanger 2008). Therefore, it might be interesting to repeat the measurements with different protein concentrations for example starting at 0.2 µM and then gradually going up to 2 µM. Then it would be possible to see whether the K_d stays the same for all protein concentration or whether it is affected by it. Providing constant stirring and controlled temperature would eliminate any effects on the protein that might have been overlooked in this study.

Also, to validate the results of the competition experiments, dose-dependant titrations for both ligands are necessary. Taking the competition experiment with RKH06 and 7.5 µM C12 as an example, C12 would be added to DprE1 at a quarter of its K_d (1.87 µM), at half of its K_d (3.75 µM), at three-quarter of its K_d (5.52 µM), at double of its K_d (15 µM) and maybe even at triple of its K_d (22.5 µM). This is done to study if the effect on the other ligand, in this example RKH06, is linear and therefore dependant on the other ligand or not.

Finally, it might be interesting to look into the results of the ratio transformation to see whether it is possible to achieve higher quantities of DprE1. The 1:3 transformation with more chaperone p*Trc*-60.2-GroES than Rv3790-pCDF duet gave promising results even though it was grown in LB medium. Growing this transformation in Terrific Broth might result in a greater yield of DprE1.

The aim of this study was to determine the binding site of the DprE1 ligand RKH06. The crystal structure of DprE1 with the ligands C12 and RKH06 suggested a separate binding site for RKH06 away from the FAD co-factor. However, looking at the results from the competition experiment with wild type DprE1 and the single ligand measurements with mutant E294A and Y297A, it has been determined that the crystallographic evidence does not represent the physiological binding behaviour of DprE1. In fact, the results suggest that RKH06 and C12 compete for a site when titrated together and therefore bind in the same site. This was supported by the mutant measurements, as no increase in RKH06 K_d was determined. Even though, the study had some limitations, the results provide an accurate picture of the binding behaviour of DprE1 in solution.

5. APPENDICES

5.1 Appendix 1 - Recipes for Section 2

Growth media and additions

LB agar

For 500 ml LB agar, 5 g tryptone, 2.5 g yeast extract and 5 g NaCl were dissolved in 400 ml diH_2O. The pH was adjusted to 7.5 with sodium hydroxide (NaOH) and 15 g agar was added. The solution was made up to a final volume of 500 ml.

LB medium

For one litre, 10 g tryptone, 5 g yeast extract and 10 g NaCl were dissolved in 800 ml diH_2O. The pH was adjusted to 7.5 with NaOH and the medium was made up to a final volume of one litre.

Terrific Broth medium

For the Terrific Broth, 12 g tryptone, 24 g yeast extract and 4 ml glycerol were dissolved in 800 ml diH_2O. This was adjusted to a final volume of 900 ml. For the Terrific Broth salt, 136.09 g (0.17 M) KH_2PO_4 and 62.7 g (0.72 M) K_2HPO_4 were dissolved in 400 ml diH_2O. This was adjusted to a final volume of 500 ml.

All growth media were autoclaved for 15 minutes at 121°C immediately after preparation and stored at room temperature.

20% glucose

For a 20% stock, 1 g glucose was dissolved in 5 ml diH_2O and filter sterilised with a 0.2 µm Acrodisc Syringe Filter (Pall Corporation). This stock was prepared fresh every time.

Antibiotic stocks

For 100 mg/ml ampicillin and spectinomycin stocks and for a 25 mg/ml kanamycin stock, the required amount of antibiotic powder was dissolved in diH_2O before filter sterilising with a 0.2 µm filter. The stocks were stored in 1 ml aliquots at -20°C.

Buffers

0.85% (w/v) saline wash buffer

For 100 ml, 0.85g NaCl were dissolved in 100ml diH_2O. The solution was filter sterilised with a 0.2 µm filter and stored at 4°C.

Dialysis buffer

For one litre, 2.42 g (20 mM) Tris, 0.58 g (10 mM) NaCl and 100 ml (10% v/v) glycerol were dissolved in 900 ml diH_2O. The pH was adjusted to 8.5 with hydrochloric acid (HCl) and the buffer was made up to a final volume of one litre. This buffer was made fresh for each dialysis and was kept at 4°C before use.

Buffer A - for HisTrap column

For 50 ml buffer A, 0.345 g (50 mM) NaH_2PO_4 and 0.877 g (300 mM) NaCl were dissolved in 40 ml diH_2O and imidazole was added according to table 14. The pH was adjusted to 8 and the buffer was made up to a final volume of 50 ml. All buffers were filter sterilised with a 0.2 µm filter and stored at 4°C.

Buffer B - for HiTrap Q HP column

For 50 ml buffer B, 0.121 g (20 mM) Tris and 5 ml (10% v/v) glycerol were dissolved in 40 ml diH_2O and NaCl was added according to table 14 The pH was adjusted to 8.5 with HCl and the buffer was made up to a final volume of 50 ml. All buffers were filter sterilised with a 0.2 µm filter and stored at 4°C.

Table 14: Imidazole concentrations for buffer A; NaCl concentrations for buffer B

Final concentration	**Buffer A Imidazole addition**	**Buffer B NaCl addition**
10 mM	0.034 g	0.029 g
20 mM	0.068 g	-
40 mM	0.136 g	-
50 mM	0.17 g	0.146 g
60 mM	0.204 g	-
80 mM	0.272 g	-
100 mM	0.34 g	0.292 g
120 mM	-	0.35 g
140 mM	-	0.41 g
160 mM	-	0.467 g
180 mM	-	0.525 g
200 mM	0.68 g	0.584g
300 mM	1.02 g	-
1 M	-	2.92 g

4 X SDS-PAGE sample loading buffer

For a 4 X stock, 3.2 ml 1 M Tris-HCl (pH 6.8), 5.3 ml 75 % glycerol, 0.008 g bromophenol blue and 0.8 g sodium dodecyl sulphate (SDS) were mixed and the solution was made up to 10 ml with diH_2O. This stock was stored at room temperature. For a 4 X working solution, 950 µl of 4 X stock was mixed with 50 µl (500 mM) β-mercaptoethanol. For a 1 X working solution, 250 µl of 4 X stock was mixed with 50 µl (500 mM) β-mercaptoethanol and 700 µl diH_2O. These working solutions were stored at 4°C. In case the solution changed from blue to orange or yellow, a drop of 5 M NaOH was added to adjust the pH.

10 X gel running buffer

For one litre, 30 g (248 mM) Trisma Base, 144 g (1.92 M) glycine and 10 g (1% w/v) SDS were dissolved in 900 ml diH_2O. The pH was adjusted to 8.3 and the buffer was made up to a final volume of one litre. For running SDS-PAGE gels, the buffer was diluted to 1X.

Gel buffer (I) – 1.5 M Tris-HCl

Gel buffer (I) was prepared by dissolving 118.2 g Tris in 400 ml diH_2O. The pH was adjusted to 8.8 with HCl and the buffer was made up to a final volume of 500 ml before filtering and degasing.

Gel buffer (II) – 1 M Tris-HCl

Gel buffer (II) was prepared by dissolving 78.8 g Tris in 400 ml diH_2O. The pH was adjusted to 6.8 with HCl and the buffer was made up to a final volume of 500 ml before filtering and degasing. All gel related buffers were stored at room temperature.

Staining solutions

Coomassie Blue R-250 Stain

The stain was prepared by dissolving 1.5 g Coomassie Brilliant Blue R250 in 450 ml methanol before slowly adding 100 ml acetic acid and 450 ml diH_2O.

Destain

Destain was prepared by mixing 300 ml methanol with 100 ml acetic acid and 600 ml diH_2O.

Both solutions were stored at room temperature.

5.2 Appendix 2 - Rv3790 DNA Protein sequence

```
atgttgagcgtgggagctaccactaccgccacccggctgaccgggtggggccgcacagcg
M  L  S  V  G  A  T  T  T  A  T  R  L  T  G  W  G  R  T  A
ccgtcggtggcgaatgtgcttcgcaccccagatgccgagatgatcgtcaaggcggtggct
P  S  V  A  N  V  L  R  T  P  D  A  E  M  I  V  K  A  V  A
cgggtcgccgagtcgggggggcggccggggtgctatcgcgcgcgggctgggccgctcctat
R  V  A  E  S  G  G  G  R  G  A  I  A  R  G  L  G  R  S  Y
ggggacaacgcccaaaacggcggtgggttggtgatcgacatgacgccgctgaacactatc
G  D  N  A  Q  N  G  G  G  L  V  I  D  M  T  P  L  N  T  I
cactccattgacgccgacaccaagctggtcgacatcgacgccggggtcaacctcgaccaa
H  S  I  D  A  D  T  K  L  V  D  I  D  A  G  V  N  L  D  Q
ctgatgaaagccgccctgccgttcgggctgtgggtcccggtgctgccgggaacccggcag
L  M  K  A  A  L  P  F  G  L  W  V  P  V  L  P  G  T  R  Q
gtcaccgtcggcggggcgatcgcctgcgatatccacggcaagaaccatcacagcgctggc
V  T  V  G  G  A  I  A  C  D  I  H  G  K  N  H  H  S  A  G
agcttcggtaaccacgtgcgcagcatggacctgctgaccgccgacggcgagatccgtcat
S  F  G  N  H  V  R  S  M  D  L  L  T  A  D  G  E  I  R  H
ctcactccgaccggcgaggacgccgaactgttctgggccaccgtcgggggcaacggtctc
L  T  P  T  G  E  D  A  E  L  F  W  A  T  V  G  G  N  G  L
accggcatcatcatgcgggccaccatcgagatgacgcccacttcgacggcgtacttcatc
T  G  I  I  M  R  A  T  I  E  M  T  P  T  S  T  A  Y  F  I
gccgacggcgacgtcaccgccagcctcgacgagaccatcgccctgcacagcgacggcagc
A  D  G  D  V  T  A  S  L  D  E  T  I  A  L  H  S  D  G  S
gaagcgcgctacacctattccagtgcctggttcgacgcgatcagcgctcccccgaagctg
E  A  R  Y  T  Y  S  S  A  W  F  D  A  I  S  A  P  P  K  L
ggccgcgcggcggtatcgcgtggccgcctggccaccgtcgagcaattgcctgcgaaactg
G  R  A  A  V  S  R  G  R  L  A  T  V  E  Q  L  P  A  K  L
cggagcgaacctttgaaattcgatgcgccacagctacttacgttgcccgacgtgtttccc
R  S  E  P  L  K  F  D  A  P  Q  L  L  T  L  P  D  V  F  P
aacgggctggccaacaaatatacttcggcccgatcggcgaactgtggtaccgcaaatcc
N  G  L  A  N  K  Y  T  F  G  P  I  G  E  L  W  Y  R  K  S
ggcacctatcgcggcaaggtccagaacctcacgcagttctaccatccgctggacatgttc
G  T  Y  R  G  K  V  Q  N  L  T  Q  F  Y  H  P  L  D  M  F
ggcgaatggaaccgcgcctacggcccagcgggcttcctgcaatatcagttcgtgatcccc
G  E  W  N  R  A  Y  G  P  A  G  F  L  Q  Y  Q  F  V  I  P
acagaggcggttgatgagttcaagaagatcatcggcgttattcaagcctcgggtcactac
T  E  A  V  D  E  F  K  K  I  I  G  V  I  Q  A  S  G  H  Y
tcgtttctcaacgtgttcaagctgttcggcccccgcaaccaggcgccgctcagcttcccc
S  F  L  N  V  F  K  L  F  G  P  R  N  Q  A  P  L  S  F  P
atcccgggctggaacatctgcgtcgacttccccatcaaggacgggctggggaagttcgtc
I  P  G  W  N  I  C  V  D  F  P  I  K  D  G  L  G  K  F  V
agcgaactcgaccgccgggtactggaattcggcggccggctctacaccgccaaagactcc
S  E  L  D  R  R  V  L  E  F  G  G  R  L  Y  T  A  K  D  S
cgtaccaccgccgaaacctttcatgccatgtatccgcgcgtcgacgaatggatctccgtg
R  T  T  A  E  T  F  H  A  M  Y  P  R  V  D  E  W  I  S  V
cgccgcaaggtcgatccgctgcgcgtattcgcctccgacatggcccgacgcttggagctg
R  R  K  V  D  P  L  R  V  F  A  S  D  M  A  R  R  L  E  L
ctgtag
L  -
```

(JCVI CMR b, Swiss Institute of Bioinformatics b)

5.3 Appendix 3 - Eurofins primers

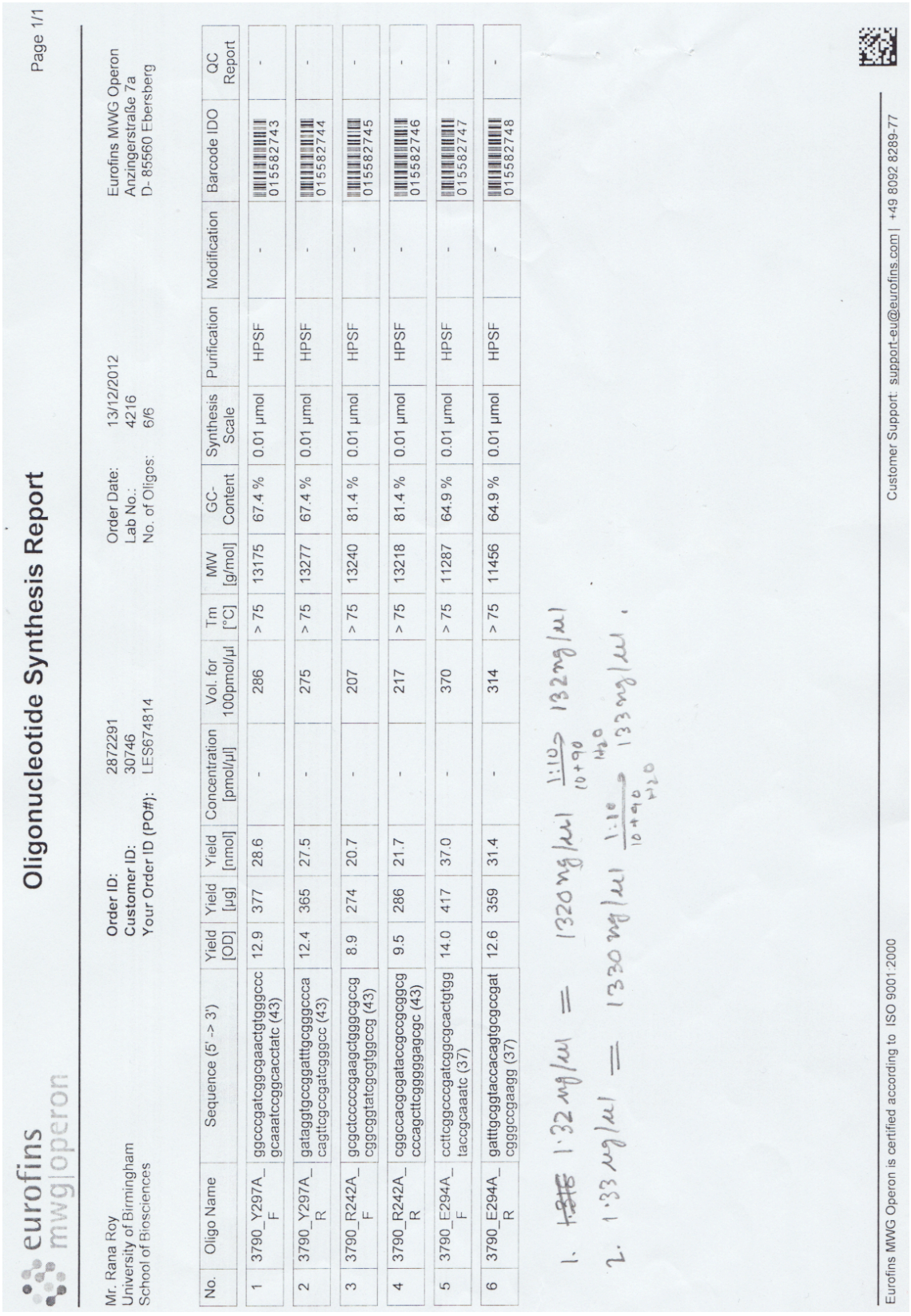

eurofins | mwg|operon

Oligonucleotide Synthesis Report

Page 1/1

Mr. Rana Roy
University of Birmingham
School of Biosciences

Order ID: 2872291
Customer ID: 30746
Your Order ID (PO#): LES674814

Order Date: 13/12/2012
Lab No.: 4216
No. of Oligos: 6/6

Eurofins MWG Operon
Anzingerstraße 7a
D- 85560 Ebersberg

No.	Oligo Name	Sequence (5' -> 3')	Yield [OD]	Yield [µg]	Yield [nmol]	Concentration [pmol/µl]	Vol. for 100pmol/µl	Tm [°C]	MW [g/mol]	GC-Content	Synthesis Scale	Purification	Modification	Barcode IDO	QC Report
1	3790_Y297A_F	ggcccgatcggcgaactgtgggcccgcaaatccggcacctatc (43)	12.9	377	28.6	-	286	> 75	13175	67.4 %	0.01 µmol	HPSF	-	015582743	-
2	3790_Y297A_R	gataggtgccggatttgcgggccacagttcgccgatcgggcc (43)	12.4	365	27.5	-	275	> 75	13277	67.4 %	0.01 µmol	HPSF	-	015582744	-
3	3790_R242A_F	gcgctcccccgaagctgggcgccgcggcggtatcgcgtggccg (43)	8.9	274	20.7	-	207	> 75	13240	81.4 %	0.01 µmol	HPSF	-	015582745	-
4	3790_R242A_R	cggccacgcgataccgccgcggcgcccagcttcgggggagcgc (43)	9.5	286	21.7	-	217	> 75	13218	81.4 %	0.01 µmol	HPSF	-	015582746	-
5	3790_E294A_F	ccttcggcccgatcggcgcactgtggtaccgcaaatc (37)	14.0	417	37.0	-	370	> 75	11287	64.9 %	0.01 µmol	HPSF	-	015582747	-
6	3790_E294A_R	gatttgcggtaccacagtgcgccgatcgggccgaagg (37)	12.6	359	31.4	-	314	> 75	11456	64.9 %	0.01 µmol	HPSF	-	015582748	-

1. ~~1.818~~ 1.32 mg/µl = 1320 mg/µl $\xrightarrow{1:10}$ 132 mg/µl (10+90 H2O)
2. 1.33 mg/µl = 1330 mg/µl $\xrightarrow{1:10}$ 133 mg/µl (10+90 H2O)

Eurofins MWG Operon is certified according to ISO 9001:2000

Customer Support: support-eu@eurofins.com | +49 8092 8289-77

5.4 Appendix 4 – Unsuccessful methods and results

5.4.1 Rv3790-pET28b in LB medium

Attempts to express and purify soluble and active DprE1 when using Rv3790-pET28b and p*Trc*-60.2-GroES grown in LB medium were unsuccessful. Besides fresh transformations, different glycerol stocks were tried. Also, final IPTG concentrations of 0.2 mM, 0.3 mM and 0.5 mM were tested to increase expression. The problem was, that even though the protein was expressed, it was always insoluble and was nearly completely lost after spinning down the crude lysate.

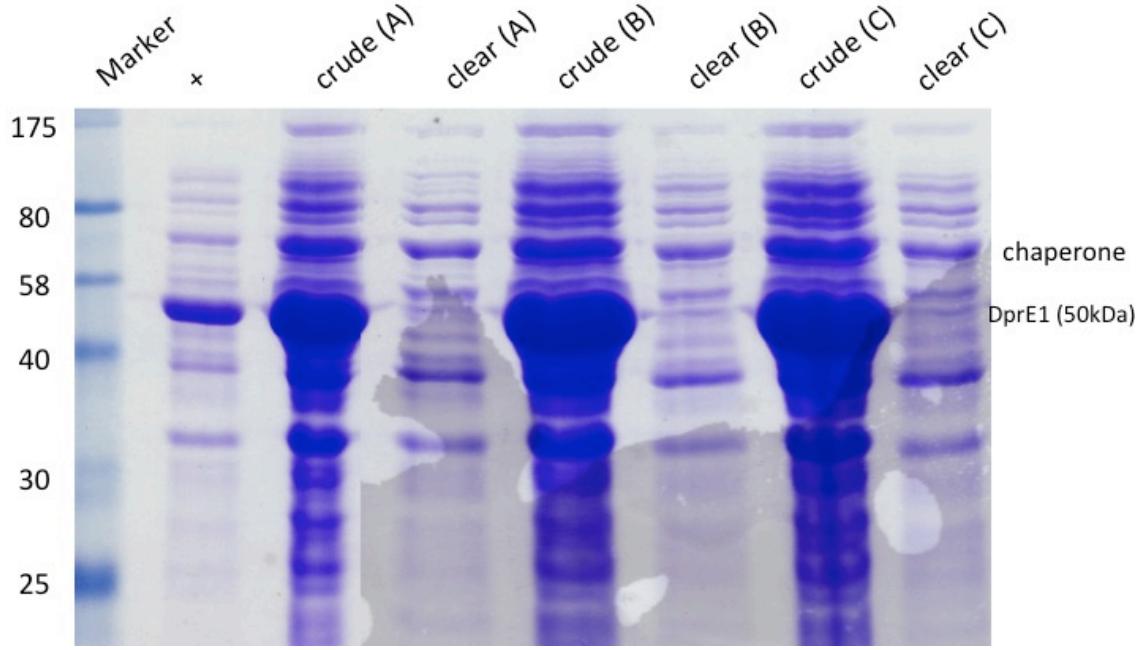

Fig. 26: Coomassie-stained SDS-PAGE gel showing samples of clear and crude lysates from three different glycerol stocks and a sample of cells after induction with IPTG (+) as reference.

As shown in figure 26, all three glycerol stocks produced a reasonable amount of protein which is seen as a thick band in the crude lysate. However, nearly all of the protein was lost after spinning down the pellet and only a faint band remained on the gel.

5.4.2 Rv3790-pCDF duet in LB medium

Transformations with Rv3790-pCDF and p*Trc*-60.2-GroES grown in LB medium produced small amounts of soluble but defective protein. After the two purification steps the fractions containing protein showed no characteristic yellow coloration. This indicates that the protein had not taken up or lost the FAD co-factor at some point during the process. Nevertheless, the protein was concentrated to 0.9 mg/ml but still no coloration could be seen. A sample of the concentrated protein was run on an SDS-PAGE gel together with concentrated DprE1 to check whether the solution actually contained DprE1.

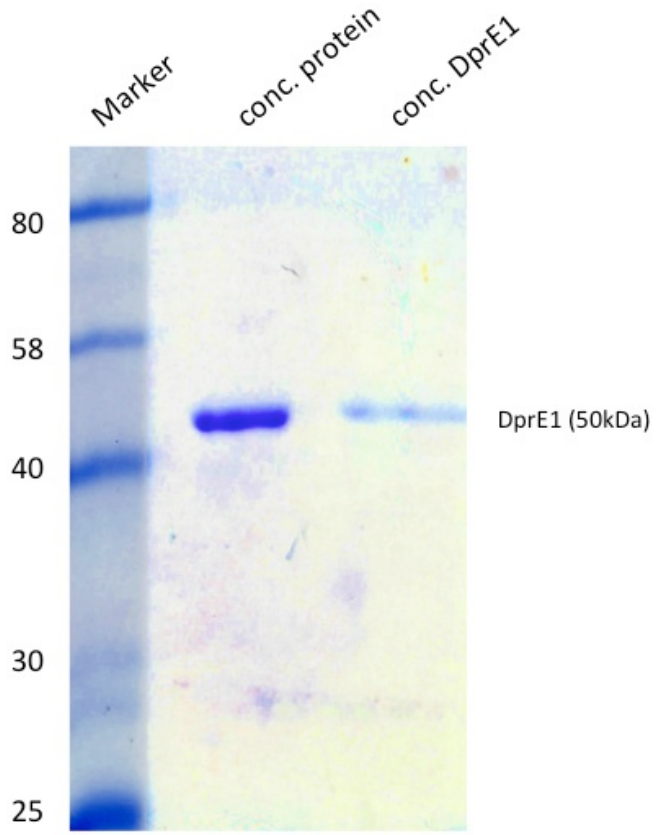

Fig. 27: Coomassie-stained SDS-PAGE gel showing a sample of the concentrated protein and concentrated DprE1.

Figure 27 shows that both bands are on the same level, which means that the concentrated protein was actually DprE1. However, the loss of the FAD co-factor could mean that the protein was not properly folded and therefore it was not useful for further experiments.

5.4.3 Rv3790-pCDF duet with FAD addition

To make the protein viable and take up the FAD co-factor, FAD was added to the cells to a final concentration of 0.5 mM before lysing. The thought was that if FAD was not provided in the growth medium it could then be taken up when added to the solution to fully develop DprE1. However, this was unsuccessful and the FAD washed off in the 10 mM imidazole elution on the HisTrap column. Again this suggested that the protein was not properly folded and did not take up the FAD. Therefore, the growth medium was changed from LB medium to Terrific Broth, as this is a richer medium and might contain ingredients that support the folding of the protein. This change was successful and provided sufficient amounts of protein as presented in the result section.

5.4.4 Ligand binding studies using 20 µM ligand DMSO stock

During the initial measurements for the ligand binding studies, 0.46 µM DprE1 and a 20 µM ligand DMSO stock were used. As shown in figure 28, the problem with the 20 µM stock was the increasing fluorescence peak at 305 nm with every addition, which did not originate from the proteins intrinsic Trp fluorescence. At a final concentration of 6.9 µM the peak completely overshadowed the protein fluorescence and made the result invalid, as the effect of this peak on the results could not be estimated. The ligands were made up in a fresh 500 µM ligand DMSO stock. Measurements using this stock and 2 µM DprE1 did not cause any problems and therefore this ligand stock was used for the measurements as presented in the result section.

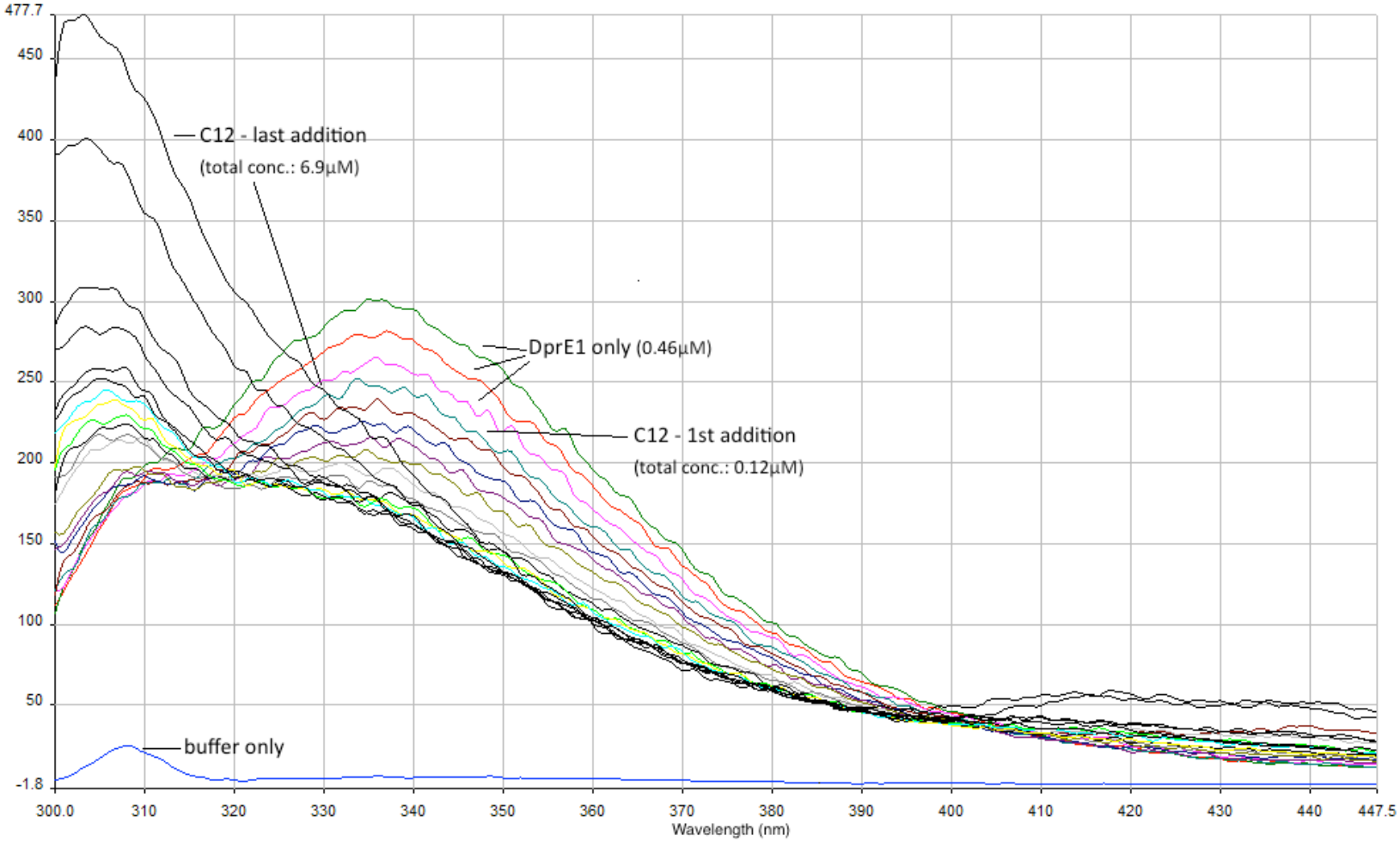

Fig. 28: Fluorescence spectrum example for 0.46 µM wild type DprE1 with 20 µM C12 ligand stock.

5.5 Appendix 5 – Wild type DprE1 with 327-4

The measurements for wild type DprE1 with 327-4 were carried out as described under 2.5.8 and the data was evaluated as shown under 2.6. The results are presented here as they were not relevant to the conclusions drawn in the discussion.

Figure 29 (top) shows an example fluorimeter graph of a 327-4 measurement. 327-4 was gradually added from 0.5 µM up to a concentration of 280.5 µM. Two independent measurements were taken when the protein was eight days old. Figure 29 (bottom) shows the DprE1 saturation curves with 327-4. The curves describe the same shape but there is a wide gap between them. The first measurement curve is shifted upwards and to the left representing a lower K_d.

Table 15: K_d and B_{max} for wild type DprE1 with 327-4

	K_d (µM)	**B_{max}**
Measurement 1	13.58	657.2
Measurement 2	31.76	650.9
Mean	22.67	654.0
Standard deviation	12.85	4.4

The great variation between the two curves is also represented in the high K_d standard deviation (table 15). The K_d of the second measurement is more than two times higher than that of the first measurement. A third measurement to draw a conclusion as to which value was an accurate representation of the K_d of 327-4 was not performed due to lack of protein. Therefore, no comment on the actual K_d value can be made.

One problem with this ligand was that it needed to be titrated to a very high final concentration of 280.5 µM to reach saturation. However, the control measurements with DMSO and buffer showed that after a ligand concentration of 68.5 µM the effect on the protein becomes unpredictable and therefore only values up to 72 µM were regarded in the analysis.

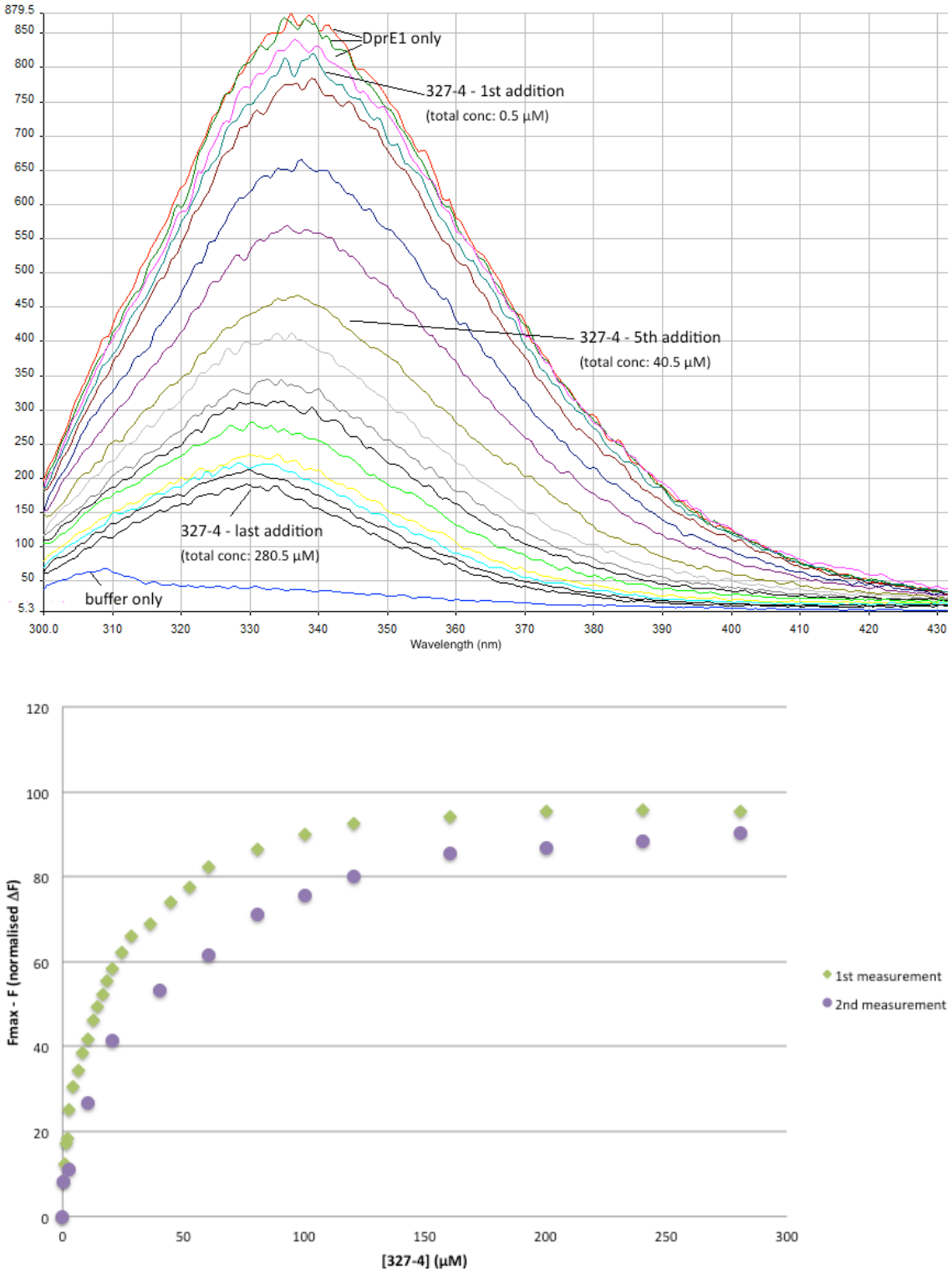

Fig. 29: Fluorescence spectrum example for wild type DprE1 with 327-4 (top) and saturation binding curves of wild type DprE1 with 327-4 (bottom).

6. REFERENCES

Agilent Technologies. (2011) *PfuTurbo C_x Hotstart DNA Polymerase - Instruction Manual.* [Online]. Available from: http://www.genomics.agilent.com/files/Manual/600410.pdf [Accessed on 8th January 2013].

Alderwick, L.J., Birch, H.L., Mishra, A.K., Eggeling, L. and Besra, G.S. (2007) Structure, function and biosynthesis of the *Mycobacterium tuberculosis* cell wall: arabinogalactan and lipoarabinomannan assembly with a view to discovering new drug targets. *Biochemical Society Transactions*. 35 (5), 1325-1328.

Alderwick, L.J., Lloyd, G.S., Lloyd, A.J., Lovering, A.L., Eggeling, L. and Besra, G.S. (2011) Biochemical characterization of the *Mycobacterium tuberculosis* phosphoribosyl-1-pyrophosphate synthetase. *Glycobiology*. 21 (4), 410-425.

Batt, S.M., Jabeen, T., Bhowruth, V., Quill, L., Lund, P.A., Eggeling, L., Alderwick, L.J., Fütterer, K. and Besra, G.S. (2012) Structural basis of inhibition of *Mycobacterium tuberculosis* DprE1 by benzothiazinone inhibitors. *Proceedings of the National Academy of Sciences USA*. 109 (28), 11354-11259.

Bhardwaj, N. and Gerstein, M. (2009) Relating protein conformational changes to packing efficiency and disorder. *Protein Science*. 18, 1230-1240.

Bisswanger H. (2008) *Enzyme Kinetics – Principles and Methods*. 2nd edition. Weinheim, WILEY-VCH Verlag GmbH & Co KGaA.

Christophe, T., Jackson, M., Jeon, H.K., Fenistein, D., Contreras-Dominguez, M., Kim, J., Genovesio, A., Carralo, J.P, Ewann, F., Kim, E.H., Lee, S.Y., Kang, S., Seo, M.J., Park, E.J., Skovierová, H., Pham, H., Riccardi, G., Nam, J.Y., Marsollier, L., Kempf, M., Joly-Guillou, M.L., Oh, T., Shin, W.K., No, Z., Nehrbass, U., Brosch, R., Cole S.T. and Brodin, P. (2009) High Content Screening Identifies Decaprenyl-Phosphoribose 2' Epimerase as a Target for Intracellular Antimycobacterial Inhibitors. *PLoS Pathogens*. 5 (10), 1-10.

Cole, S.T. and Riccardi, G. (2011) New tuberculosis drugs on the horizon. *Current Opinion in Microbiology.* 14, 570–576.

Crellin, P.K., Brammananth, R. and Coppel, R.L. (2011) Decaprenylphosphoryl-β-D-Ribose 2'-Epimerase, the Target of Benzothiazinones and Dinitrobenzamides, Is an Essential Enzyme in *Mycobacterium smegmatis*. *PLoS ONE*. 6 (2), 1-8.

Field, S.K., Fisher, D., Jarand, J.M. and Cowie R.L. (2012) New treatment options for multidrug-resistant tuberculosis. *Therapeutic Advances in Respiratory Disease.* 6 (5), 255-268.

GSL Biotech LLC. (no date - a) *Snap Gene – Plasmid Files pCDFDuet-1.* [Online]. Available from: http://www.snapgene.com/resources/plasmid_files/pet_and_duet_vectors_(novagen)/pCDFDuet-1/ [Accessed on 8th January 2013].

GSL Biotech LLC. (no date - b) *Snap Gene – Plasmid Files pET-28b(+).* [Online]. Available from: http://www.snapgene.com/resources/plasmid_files/pet_and_duet_vectors_(novagen)/pCDFDuet-1/ [Accessed on 8th January 2013].

Gupta, A., Kaul, A., Tsolaki, A.G., Kishore, U., and Bhakta, S. (2012) *Mycobacterium tuberculosis*: Immune evasion, latency and reactivation. *Immunobiology.* 217, 363-374.

JCVI CMR. (no date - a) *Primary Annotation Display: Rv3790.* [Online]. Available from: http://cmr.jcvi.org/cgi-bin/CMR/shared/GenePage.cgi?locus=NTL02MT03782 [Accessed on 29th October 2012].

JCVI CMR. (no date - b) *Primary Annotation Sequence Display: Rv3790.* [Online]. Available from: http://cmr.jcvi.org/cgi-bin/CMR/shared/GenePage.cgi?locus=NTL02MT03782 [Accessed on 29th October 2012].

Lambert, D.G. (2004) Drugs and receptors. *Continuing Education in Anaesthesia, Critical Care & Pain*. 4 (6), 181-184.

Larrouy-Maumus, G., Skovierová, H., Dhouib, R., Angala, S.K., Zuberogoitia, S., Pham, H., Villela, A.D., Mikusová, K., Noguera, A., Gilleron, M., Valentínová, L., Korduláková, J., Brennan, P.J., Puzo, G., Nigou, J. and Jackson, M. (2012) A Small Multidrug Resistance-like Transporter Involved in the Arabinosylation of Arabinogalactan and Lipoarabinomannan in Mycobacteria. *The Journal of Biological Chemistry*. 287 (47), 39933–39941.

Lienhardt, C., Raviglione, M., Spigelman, M., Hafner, R., Jaramillo, E., Hoelscher, M., Zumla, A. and Gheuens, J. (2012) New Drugs for the Treatment of Tuberculosis: Needs, Challenges, Promise, and Prospects for the Future. *The Journal of Infectious Diseases*. 205 (Suppl 2), 241-249.

Manina, G., Pasca, M.R., Buroni, S., De Rossi, E. and Riccardi, G. (2010) Decaprenylphosphoryl-β-D-ribose 2'-epimerase from *Mycobacterium tuberculosis* is a magic drug target. *Current Medicinal Chemistry.* 17, 3099-3108.

Makarov, V., Manina, G., Mikušová, K. Möllman, U., Ryabova, O., Saint-Joanis, B., Dhar, N., Pasca, M.R., Buroni, S., Lucarelli, A.P., Milano, A., De Rossi, E., Belanova, M., Bobovska, A., Dianiskova, P., Kordulakova, J., Sala, C., Fullam, E., Schneider, P., McKinney, J.D., Brodin, P., Christophe, T., Waddell, S., Butcher, P., Albrethsen, J., Rosenkrands, I., Brosch, R., Nandi, V., Bharath, S., Gaonkar, S., Shandil, R.K., Balasubramanian, V., Balganesh, T., Tyagi, S., Grosset, J., Riccardi, G. and Cole, S.T. (2009) Benzothiazinones kill *Mycobacterium tuberculosis* by blocking arabinan synthesis. *Science.* 324, 801-804.

Mikušová, K., Huang, H., Yagi, T., Holsters, M., Vereecke, D., D'Haeze, W., Scherman, M.S., Brennan, P.J., McNeil, M.R. and Crick, D.C. (2005) Decaprenylphosphoryl Arabinofuranose, the Donor of the D-Arabinofuranosyl Residues of Mycobacterial Arabinan, Is Formed via a Two-Step Epimerization of Decaprenylphosphoryl Ribose. *Journal of Bacteriology*. 187 (23), 8020–8025.

Neres, J., Pojer, F., Molteni, E., Chiarelli, L.R., Dhar, N., Boy-Röttger, S., Buroni, S., Fullam, E., Degiacomi, G., Lucarelli, A.P., Read, R.J., Zanoni, G., Edmondson, D.E., De Rossi, E., Pasca, M.R., McKinney, J.D., Dyson, P.J., Riccardi, G., Mattevi, A., Cole, S.T. and Binda, C. (2012) Structural Basis for Benzothiazinone-Mediated Killing of *Mycobacterium tuberculosis*. *Science Translational Medicine*. 4 (150ra121), 1-11.

Pasca, M.R., Degiacomi, G., de Jesus Lopes Ribeiro, A.L., Zara, F., De Mori, P., Heym, B., Mirrione, M., Brerra, R., Pagani, L., Pucillo, L., Troupioti, P., Makarov, V., Cole, S.T. and Riccardi, G. (2010) Clinical Isolates of *Mycobacterium tuberculosis* in Four European Hospitals Are Uniformly Susceptible to Benzothiazinones. *Antimicrobial Agents and Chemotherapy*. 54 (4), 1616-1618.

QIAGEN. (2006) *QIAprep Miniprep Handbook Second Edition 12/2006.* [Online]. Available from: http://kirschner.med.harvard.edu/files/protocols/QIAGEN_QIAprep MiniprepKit_EN.pdf [Accessed on 16th October 2012].

Schaefer, C. and Rost, B. (2012) Predict impact of single amino acid change upon protein structure. *BMC Genomics*. 13 (Suppl 4): S4, 1-10.

Stratagene. (2006) *QuikChange Site-Directed Mutagenesis Kit – Instruction Manual.* [Online]. Available from: http://www.tufts.edu/~mcourt01/Documents/Stratagene %20Quikchange%20mutagenesis.pdf [Accessed on 7th December 2012].

Suter-Crazzolara, C. and Unsicker, K. (1995) Improved expression of toxic proteins in *E.coli*. BioTechniques. 19, 202-204.

Swiss Institute of Bioinformatics (SIB). (no date - a) *ProtParam tool.* [Online]. Available from: http://web.expasy.org/protparam/ [Accessed on 29th October 2012].

Swiss Institute of Bioinformatics (SIB). (no date - b) *Translate tool.* [Online]. Available from: http://web.expasy.org/translate/ [Accessed on 29th October 2012].

Udwadia, Z.F, Amale, R.A., Ajbani, K.K and Rodrigues, C. (2012) Totally drug-resistant tuberculosis in India. *Clinical Infectious Diseases*. 54, 579-581.

Velayati, A.A, Masjed, M.R, Farnia, P., Tabarsi, P., Ghanavi, J., ZiaZarifi, A.H. and Hoffner, S.E. (2009) Emergence of new forms of totally drug-resistant tuberculosis bacilli: super extensively drug-resistant tuberculosis or totally drug-resistant strains in Iran. *Chest.* 136(2), 420-425.

Villemagne, B., Crauste, C., Flipo, M., Baulard, A.R., Déprez, B. & Willand, N. (2012) Tuberculosis: The drug development pipeline at a glance. *European Journal of Medicinal Chemistry.* 51, 1-16.

World Health Organization. (2010) *Treatment of tuberculosis: guidelines – 4th edition.* [Online]. Available from: http://whqlibdoc.who.int/publications/2010/9789241547833_eng.pdf [Accessed on 22nd January 2013].

World Health Organization (2012) *Global Tuberculosis Report 2012.* [Online]. Available from: http://www.who.int/tb/publications/global_report/gtbr12_main.pdf [Accessed on 22nd January 2013].

Project Two: THE USEFULNESS OF ALGINATES IN THE TREATMENT OF COLORECTAL CANCER

by

MELANIE SCHNEIDER

Supervisor – Dr Chris Tselepis

College of Medical and Dental Sciences

School of Cancer Sciences

University of Birmingham

July 2013

ABSTRACT

There is overwhelming evidence from epidemiological, cellular and animal studies associating high iron levels with the development of colorectal cancer. Recent studies have specifically linked excess, unabsorbed dietary iron in the colonic lumen with colorectal carcinogenesis and a therapy based on the chelation of this pool of iron was suggested. A range of naturally occurring, non-absorbable and non-fermentable biopolymers, namely alginates, were identified as ideal candidates to study their iron chelating properties. However, previous cellular data in the group indicated that the alginate Manucol DH augmented total cellular iron levels within an *in vitro* setting, a confounding and somewhat surprising effect of a supposed iron chelator. What remains unknown is whether alginate-bound iron within cells is inert or whether it can exert phenotypical changes similar to iron alone. Therefore, this study aimed to identify any phenotypic changes associated with iron delivery using iron only and iron co-incubated with Manucol DH at equal total cellular iron concentrations. Following this, the range of alginate types was broadened to study their iron binding potential and physiochemical properties. Results from this study show that Manucol LD, a small, low molecular weight alginate with low guluronic acid content was the strongest iron binder, decreasing both cell viability and ferritin expression *in vitro*. These properties identified for Manucol LD seem to play an important underlying role in the alginate's iron binding potential and therefore could point the way for a future colonic luminal iron chelator in the prevention and treatment of colorectal cancer.

ACKNOWLEDGEMENTS

First and foremost, I would like to thank my project supervisor Dr Chris Tselepis for giving me the opportunity to work as part of his research group. It has allowed me to acquire new skills and to gain faith in my abilities, which will be invaluable for my future science career. I really appreciate the advice and guidance he provided throughout this project.

I am especially grateful to Richard Horniblow who was my tutor for this project. Thank you for being such a great mentor and friend, for being so patient with me and for never getting tired of me asking you for help. I now know that science is so much more exciting when you have a little fun. You really are the best!

Finally, I would like to thank the other members of the Tselepis group, especially Dr Dan Stones and Matt Bedford, for their advice and encouragement. I had such a great time with you guys.

For boosting me morally and inspiring me to carry on despite the pressure we were all facing, I thank my course mates. You all have become such good friends and I feel so lucky to have met you all.

Melanie Schneider

TABLE OF CONTENTS

LIST OF ILLUSTRATIONS

LIST OF TABLES

LIST OF ABBREVIATIONS

ACF	Aberrant crypt foci
APC	Adenomatous polyposis coli
BSA	Bovine serum albumin
CK1α	Casein kinase 1 α
diH_2O	Deionised water
DCYTB	Duodenal cytochrome b
DMEM	Dulbecco's Modified Eagle Medium
DMSO	Dimethyl sulfoxide
DMT1	Divalent metal transporter 1
Dsh	Dishevelled
EDTA	Ethylenediaminetetraacetic acid
FAC	Ferric ammonium citrate
FAP	Familial adenomatous polyposis
FCS	Fetal calf serum
Fe	Iron / Ferrous sulphate heptahydrate
Ferrozine	3-(2-Pyridyl)-5,6-diphenyl-1,2,4-triazine-4',4''-disulfonic acid sodium salt
G	α-L-guluronic acid
GSK3β	Glycogen synthase kinase 3β
HCl	Hydrochloric acid
HNPCC	Hereditary non polyposis colorectal cancer
IMS	Industrial methylated spirits
Keltone	Keltone HVCR KTHVCR
M	β-D-mannuronic acid
Man DH	Manucol DH
Man LD	Manucol LD
Man GHB	Manugel GHB
MeOH	Methanol
MTT	3-(4,5-dimethylthiazol-2-yl)-2,5-diphenyltetrazolium bromide
MW	Molecular weight

NaCl	Sodium chloride
NaOH	Sodium hydroxide
Na-Asc	Sodium L-ascorbate
NM	Non-modifiable
PBS	Phosphate buffered saline
LFR	Protanal LFR 5/60
RF 6650	Protanal RF 6650
PSA	Phenol-sulphuric acid
PVDF	Hydrophobic polyvinylidene difluoride
ROS	Reactive oxygen species
SDS	Sodium dodecyl sulphate
TBST	Tris buffered saline with Tween 20
TCA	Trichloroacetic acid solution
TCF	T cell factor
TfR1	Transferrin receptor 1
WHO	World Health Organisation

1. INTRODUCTION

1.1 Colorectal cancer

1.1.1 Incidence, symptoms and diagnosis

The term colorectal cancer refers to cancers of the large intestine which is made up of the colon, rectum and anus. Worldwide, this is the third most common cancer in men and second in women with an estimated 1.2 million cases in 2008. Furthermore, colorectal cancer accounted for eight per cent of all cancer deaths in the same year, with about 608,700 victims (American Cancer Society 2011b). In the UK, being ranked third in cancer incidence after lung and breast, it is stated that more than 41,000 people are diagnosed with bowel cancer every year (Cancer Research UK).

Colorectal cancer commonly presents with bleeding from the rectum or blood in stools and new onset of diarrhoea / looser stool or bowel obstruction for an extended period of time. Further symptoms include weight loss, abdominal discomfort and cramping pains, tiredness and breathlessness due to anaemia (Cancer Research UK, American Cancer Society 2011a).

As part of the NHS bowel cancer screening programme, a guaiac-based faecal occult blood test has been introduced to detect early stage occurrences of colorectal cancer. If any abnormalities are found in the stool sample, a thorough exam of the bowel by (flexible) sigmoidoscopy or colonoscopy becomes necessary. If a tumour is found during the bowel examination, a tissue biopsy is taken.

In combination with results from imaging techniques, such as CT or MRI scans, this is used for appropriate cancer staging (Cancer Research UK, American Cancer Society 2011a).

1.1.2 TNM staging

The large intestine can be divided into five sections, the ascending colon, transverse colon, descending colon, sigmoid colon and rectum. Cancer can develop in any of these sections. The intestinal wall is made up of several layers of tissue as shown in figure 30. Cancer development starts in the intestinal lining and progresses through the muscle layer into the outer lining. It is estimated that colorectal cancers can take between five to ten years to develop (Cancer Research UK).

To determine the size and spread of a tumour, the TNM (Tumour, Node, Metastasis) colorectal cancer staging system is commonly used. As shown in figure 30, the T stage describes the size of the primary lesion, with T1 meaning tumour growth is localised to the intestinal inner lining, through to T4 where the tumour has broken through the outer lining and grown into surrounding parts of the bowel and other organs nearby (Cancer Research UK, American Cancer Society 2009). The N stage describes whether the cancer has spread into regional lymph nodes, with N0 meaning no spread, through to N2 were metastases are present in four or more regional lymph nodes. Finally, the M stage describes the spread of the cancer throughout the body, with M0 meaning that there is no distant metastasis and M1 representing metastasis (Cancer Research UK, American Cancer Society 2009).

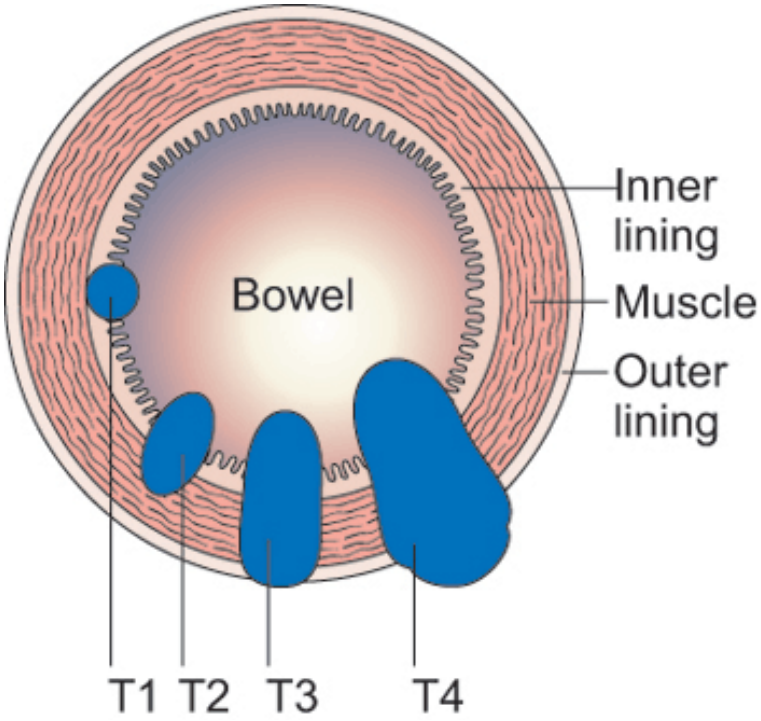

Fig. 30: T stages of bowel cancer (Cancer Research UK).

Depending on the stage at which the cancer is diagnosed, the five-year relative survival rate varies greatly. Patients who are treated at an early stage have a survival rate of around 90% whereas patients with later stage tumours have a greatly decreased chance of survival (Gunderson *et al*. 2010, American Cancer Society 2011b).

1.1.3 Development

Colorectal cancer development follows a stepwise progression through the so-called 'mucosa-adenoma-carcinoma' pathway caused by an accumulation of mutations in protooncogenes and important tumour suppressor genes. The inactivation of the adenomatous polyposis coli (APC) gene located on chromosome 5 is the most common genetic alteration in sporadic colorectal cancer and has been found to be mutated in over 80% of adenomas and carcinomas (Bienz & Clevers 2000, Rodriguez-Bigas *et al.* 2003, Chua *et al*. 2010).

APC plays an important role in the canonical Wnt/β-catenin signalling pathway which has been found to drive colorectal carcinogenesis. As shown in figure 31, in the absence of Wnt ligand, the scaffold protein Axin binds to the tumour suppressor APC, glycogen synthase kinase 3β (GSK3β), casein kinase 1 α (CK1α) and free cytoplasmic β-catenin. In this multi-protein destruction complex, β-catenin is phosphorylated by the kinases leading to ubiquitination and subsequent degradation by the proteasome. In the nucleus, the transcription of Wnt target genes is repressed by the binding of Groucho to T cell factor (TCF) (Bienz & Clevers 2000).

When Wnt ligand binds to Frizzled, a family of Wnt transmembrane receptors, and coreceptor LRP-5/6, the cytoplasmic protein Dishevelled (Dsh) causes Axin to bind to the Frizzled/LRP complex leading to inhibition of the protein. The inactivation of the Axin/GSK3β/CK1α/APC multi-protein destruction complex leads to the stabilisation of β-catenin, allowing it to translocate into the nucleus. Here, β-catenin replaces Groucho and binds to TCF, activating the transcription of Wnt target genes (Bienz & Clevers 2000).

APC acts as negative regulator of the Wnt signalling pathway due to its role in the destabilisation of free β-catenin. In colorectal cancer, the mutation and therefore inactivation of the APC gene leads to an accumulation of β-catenin within the cell which in turn causes the β-catenin/TCF mediated activation of oncogenes (Bienz & Clevers 2000).

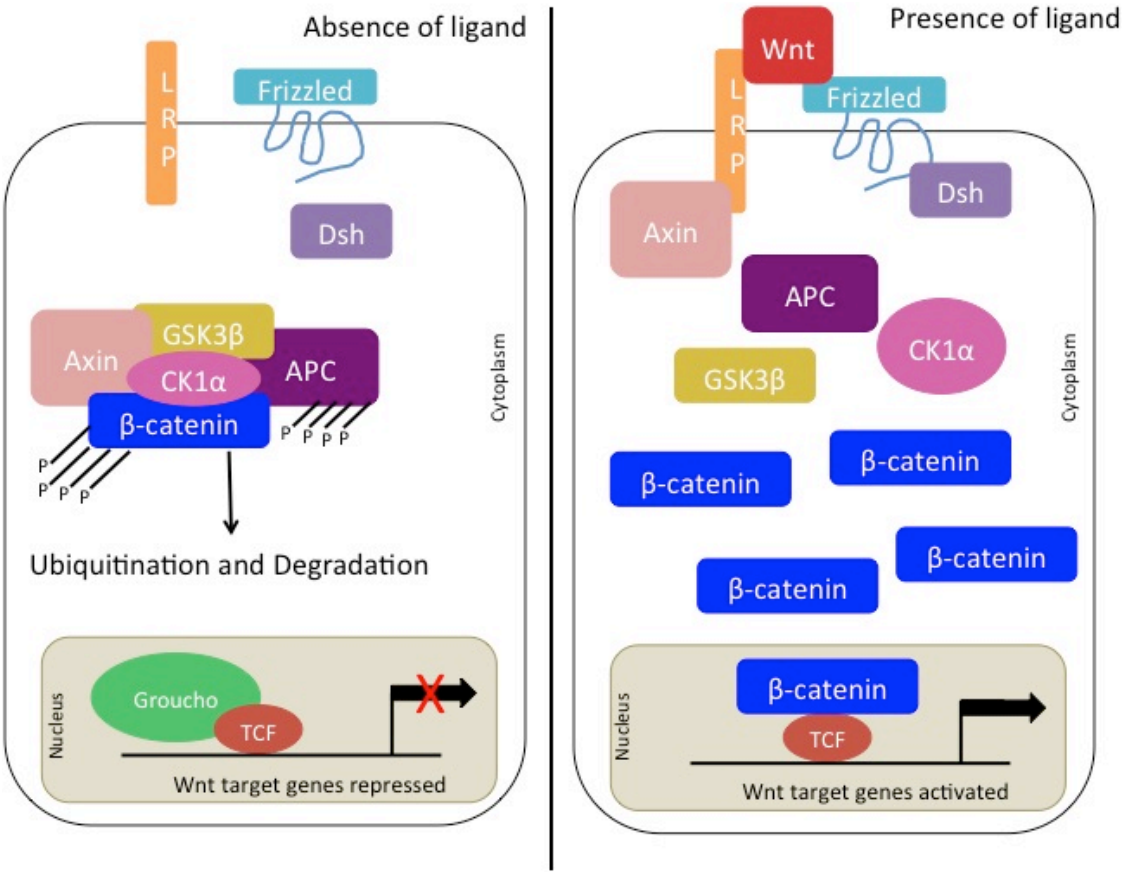

Fig. 31: Schematic of the canonical Wnt / β-catenin signalling pathway in the absence (left) and presence (right) of Wnt ligand.

The loss of APC occurs in the early stages of colorectal cancer and leads to the development of adenomas. Due to genomic instability following the formation of adenomas, subsequent mutations in protooncogenes such as k-ras and other tumour suppressor genes such as TP53 and TGF-β lead to upregulated cell proliferation and downregulated apoptosis, giving the mutated cells a growth advantage. This causes the cancer to progress from the adenoma to the carcinoma stage and can lead to the development of metastases (Rodriguez-Bigas *et al.* 2003, Markowitz & Bertagnolli 2009).

1.1.4 Risk factors and causes

The American Cancer Society distinguishes between two groups of risk factors associated with the development of colorectal cancer, non-modifiable (NM) and modifiable risks. The greatest NM risk factor is age, with 85% of cases being diagnosed in individuals aged 60 or over. Further NM risk factors include a personal or family history of colorectal cancer, diabetes, chronic inflammatory bowel diseases such as Crohn's disease and ulcerative colitis, as well as two know genetic predispositions called familial adenomatous polyposis (FAP) and hereditary non polyposis colorectal cancer (HNPCC or Lynch syndrome), accounting for around five per cent of cases. Modifiable or lifestyle related risk factors include lack of physical activity, obesity, increased consumption of red and processed meat, smoking and high alcohol intake (Cancer Research UK, Huang 2003, American Cancer Society 2011a).

1.1.5 Treatments

Treatment plans for colorectal cancer are assessed depending on the tumour type, size and spread and also on the individual's general health and age. In most cases, early stage cancers can be surgically removed without the need for adjuvant therapy. Later stage tumours, especially in the case of metastasis, often require extensive surgery followed by a combination of chemotherapy, radiation and / or biologically targeted therapies such as monoclonal antibodies. The most commonly used chemotherapies include 5-Fluorouracil, Irinotecan and Oxaliplatin (Cancer Research UK, American Cancer Society 2011a).

1.2 The role of iron in colorectal carcinogenesis

1.2.1 Association and epidemiological studies

Diet is a major lifestyle related risk factor in the development of colorectal cancer. Especially the high consumption of processed and red meat has been found to drive carcinogenesis (Larsson & Wolk 2006, American Cancer Society 2011a, Corpet 2011). This is distinctive when looking at the geographical differences in cancer incidence as shown in figure 32. The maps clearly show that the colorectal cancer burden is significantly higher in economically developed countries in comparison to developing countries.

Studies directly link these high cancer rates to the Western diet which is rich in red meat and processed foods. Several reviews have reported that a daily increase in red meat consumption by 100 g leads to a 17% higher risk of developing colorectal cancer (Larsson & Wolk 2006). Based on this observation, a range of causative hypotheses have been suggested explaining the negative impact of red meat on colonic health.

When cooking meat at high temperatures, heat-induced mutagens and carcinogens namely heterocyclic amines and polycyclic aromatic hydrocarbons are released. Together with the consumption of carcinogenic *N*-nitroso compounds from preserving agents found in processed red meat, they are thought to be linked to colon cancer development. However, these compounds are only consumed in low non-toxic concentrations and are also found in both red and white meat.

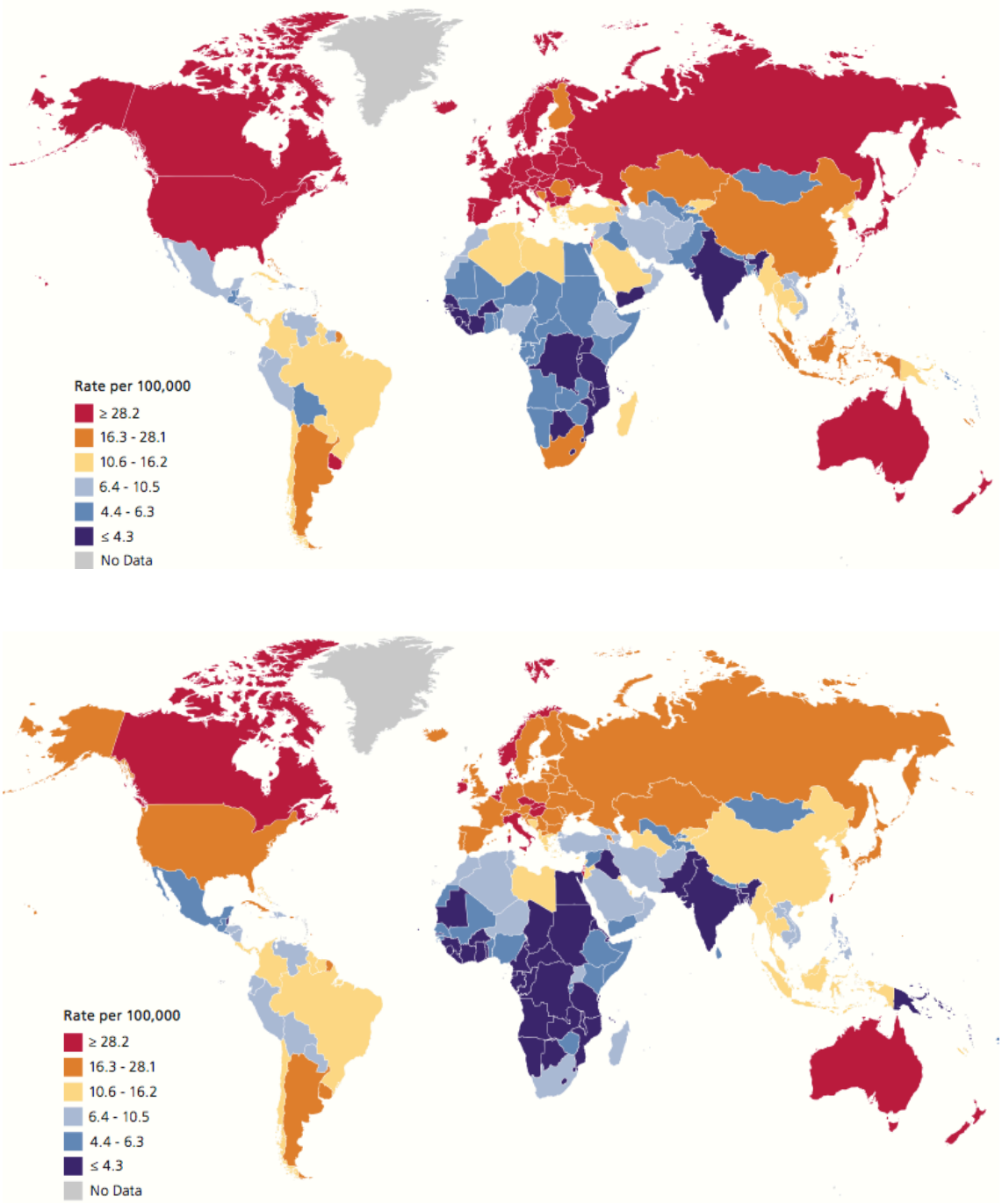

Fig. 32: International variation in age-standardised colorectal cancer incidence rates amongst males (top) and females (bottom) in 2008 (Jemal et al. 2011).

Furthermore, it has been suggested that the high fat content of meat could increase the production of secondary bile acids which can have negative effects on colonic health. However, this hypothesis has not yet been supported by further studies (Larsson & Wolk 2006, Bastide *et al*. 2011, Corpet 2011).

Finally, the most plausible and best-studied hypothesis is that of dietary haem iron as a carcinogen. High levels of haem iron in red meat have been associated with colorectal carcinogenesis as it can cause damage to the colonic mucosa by catalysing the formation of toxic oxygen radicals (Larsson & Wolk 2006, Corpet 2011). This has been supported by several association studies.

A meta-analysis of several cohort studies looking into the effects of haem iron on colonic health published in 2011, looked at the data from over 500,000 individuals. They found a significant and consistent correlation between the amount of red meat consumed and the risk of developing colorectal cancer, with people in the high consume category being 95% more at risk than those in the low consume group (Bastide *et al*. 2011). Also, a beneficial effect was associated with the regular consume of calcium which has been found to greatly decrease iron absorption from the diet (Hallberg *et al*. 1992, Corpet 2011, Jemal *et al*. 2011). This study's results are supported by the findings of the European Prospective Investigations into Cancer and Nutrition which also looked at a cohort of more than 500,000 individuals aged between 27 and 70.

They further found an association between dietary fibre intake from vegetables and fruit in the prevention of colon cancer and there are two hypotheses as to why this might be. Firstly, fibre increases stool weight, reduces transit time and dilutes colonic contents reducing their contact with the intestinal lining. Stimulation of bacterial anaerobic fermentation leads to the production of butyrate which has been found to limit cell proliferation and induce apoptosis in cancer cell lines (Bingham *et al*. 2003). Secondly and more importantly, it has been reported that the compound inositol hexaphosphate or phytic acid which is abundantly found in plants, has the potential to inhibit the formation of toxic reactive oxygen species (ROS) by chelating metals in the lumen with a high affinity for iron (Graf & Eaton 1985).

Besides studies linking iron from the diet to the worldwide incidence of colorectal cancer, others have found a connection between increased body iron stores and cancer. A meta-analysis carried out by Nelson in 2001 combined the data from 33 epidemiological studies out of which 75% supported this association.

Knekt *et al*. (1994) used transferrin saturation as a means to determine body iron stores. They found a significant increase in colorectal cancer incidence in individuals with a transferrin saturation greater than 60%. Moreover, several studies reported that individuals who regularly lowered their body iron stores through blood donation had a significantly lower risk of developing colorectal cancer in comparison to the control group (Merk *et al*. 1990, Edgren *et al*. 2008, Zacharski *et al*. 2008).

This could also explain the gender difference in colorectal cancer incidence based on the fact that men have higher body iron stores than women throughout their lifetime (Merk *et al*. 1990).

Hereditary haemochromatosis has been reported to be a major risk factor in the development of colorectal cancer (Chua *et al.* 2010). Patients with this genetic disease have increased body iron stores due to excessive absorption of dietary iron and a positive association for colonic polyps and colon cancer in heterozygote individuals has been reported (Nelson *et al*. 1995, Huang 2003).

From the evidence presented in this section, a link between colorectal carcinogenesis and iron becomes evident. A study by Kato *et al*. (1999) did not find supporting evidence associating increased body iron stores to colorectal cancer development. They did, however, suggest a link between excessive luminal iron concentration and an increased colorectal cancer risk. The convincing evidence obtained from dietary association studies as well as cellular and animal studies supports these findings.

1.2.2 *In vitro* studies – Cellular models

Iron plays a crucial role in many metabolic processes such as DNA synthesis, cell cycle progression and cell growth. Given their accelerated proliferation in comparison to normal cells, it is not surprising, that tumour cells have been found to have an amplified iron uptake.

This is due to the increased activity of ribonucleotide reductase, an enzyme that drives DNA synthesis and therefore cell growth (Le & Richardson 2004). A study by Brookes *et al*. (2006) reported increased iron staining in colorectal carcinomas compared to normal colonic epithelium (see figure 33).

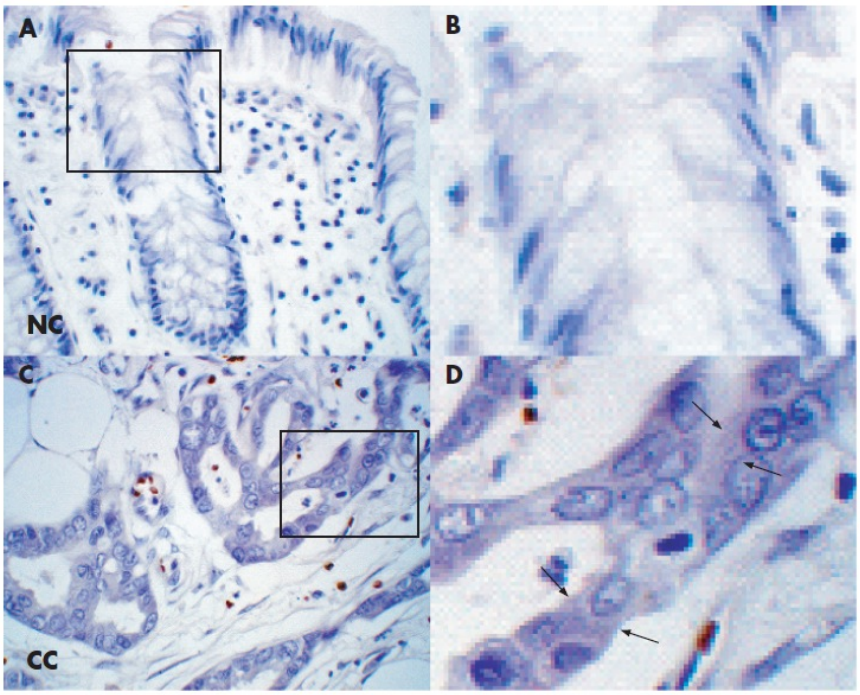

Fig. 33: Perl's Prussian blue staining used to examine colonocyte iron content: (A+B) Colonic epithelium with no detectable staining; (C+D) Colorectal carcinoma with detectable with enhanced staining (Brookes et al. 2006).

Besides that, they also found a marked increase in expression of proteins involved in cellular iron import, namely duodenal cytochrome b (DCYTB), divalent metal transporter 1 (DMT1) and transferrin receptor 1 (TfR1), and a reduction in production of the iron export proteins hephaestin and ferroportin. Loss of the latter was associated with more advanced disease stages, and increased iron loading in CaCo-2 and SW480 cells lead to increased proliferation.

Studying the effects of physiological ferric or ferrous iron on human colon adenocarcinoma HT29 clone 19A cells, Glei *et al.* (2009) found that after treating cells with ferric-nitrilotriacetate or haemoglobin, an increased iron uptake causing oxidative DNA damage in the cells could be observed. Furthermore, the use of quercetin, a plant-derived flavonoid antioxidant, inhibited the DNA damage and they therefore linked increased iron levels in the colon to colorectal carcinogenesis.

As mentioned earlier, the activation of the APC/Wnt/β-catenin signalling pathway plays an important role in the development of colorectal cancer. A study looking at the effects of both inorganic iron and haem iron on Wnt signalling in wild-type and mutant APC cancer cells lines showed that by exposing the mutant APC cells to high levels of iron, it lead to increased Wnt signalling while the wild-type APC cell lines were not affected by elevated iron levels (Brookes *et al*. 2008).

1.2.3 *In vivo* studies – Animal models

There is a vast amount of evidence from animal studies indicating an association between iron and tumour formation. Richmond (1959), as one of the earliest, found that intramuscular injection with iron-dextran lead to sarcoma formation at the administration site in 70% of rats. More recent studies have tried to link increased intake of dietary iron to colorectal carcinogenesis. Pierre *et al*. (2003) looked at the effects of haem iron on rats at the aberrant crypt foci (ACF) stage, a change of the colonic lining that can lead to the development of colon cancer.

Alongside a control group, rats were fed with varying doses of haemoglobin or haemin and a dose-dependent aggravation of the pre-cancerous lesions leading to an increase in ACF size and number was found. A co-administration of calcium and antioxidants inhibited this effect.

Another study found that feeding rats with iron supplements led to increased oxidative damage caused by free radicals in the colon and cecum and also increased abnormal cell growth in the colonic crypts which links iron to the formation of tumours in the colon. Furthermore, rats fed with dietary haem presented with augmented colonic epithelial proliferation and faecal water from such rats was found to be highly cytotoxic (Huang 2003).

An interesting observation was made by Seril *et al*. (2002), who studied the effects of iron on mice with colorectal cancer induced by an inflammatory agent. They showed, that while increased dietary iron levels lead to an increase in tumour formation, augmented systemic iron levels did not cause this effect. These findings are supported by a recent study, which explicitly links the luminal rather than the systemic pool of iron to colorectal carcinogenesis. It showed a significant decrease in tumour burden in a mouse model of intestinal tumourigenesis ($Apc^{min/+}$) when fed an iron deficient diet compared to a control group. A third group of mice was fed an iron deficient diet whilst being systemically replenished using iron dextran. Again, tumour burden was significantly reduced compared to the control cohort, supporting said hypothesis (Radulescu *et al*. 2012).

Taken together with data obtained through dietary association studies in humans and *in vitro* experiments, these findings provide strong support for the hypothesis that the luminal pool of so called “free iron” rather than systemic iron plays a promoting role in colorectal carcinogenesis.

1.3 Toxicity of iron

Looking at the data presented previously, a relationship between colorectal cancer incidence and excess luminal iron is undeniable. However, the question arises as to how iron can be toxic to the human body.

Iron is vital for all organisms, as it plays a crucial role in the active side of many proteins involved in a range of metabolic processes such as oxygen transport via haemoglobin, DNA synthesis, cell cycle progression and growth (Heli *et al.* 2011, Torti & Torti 2013). Examples of such proteins are cytochromes, Fe-S centre-containing proteins, lipoxygenases, cyclooxygenases, and ribonucleotide reductase (Richardson 2002). Iron homeostasis is tightly regulated via intestinal absorption and most iron in the human body is then bound in haem proteins or ferritin, an iron storage protein (Huang 2003).

However, as mentioned before, it is the excess unabsorbed dietary iron that is greatly dangerous due to its potential to mediate the formation of ROS (Richardson 2002, Huang 2003).

Physiological ROS formed because of excess iron include superoxide, hydroxyl radicals, alkoxyl radicals, hydroperoxyl radicals and lipid peroxides (Heli *et al.* 2011). Figure 34 demonstrates the formation of ROS from molecular oxygen in the presence of a transition metal such as iron.

Free radical formation results in lipid, protein and DNA damage causing carcinogenesis-inducing mutations (Heli *et al.* 2011). Further, oxidative stress can lead to necrotic cell death rather than regulated apoptosis causing neighbouring cells to be affected (Halliwell 2011). Finally, ROS can also damage or affect signalling pathways leading to modulated cell growth and tumour promotion and the activation of protooncogenes such as c-FOS, c-JUN and c-myc (Hussain *et al.* 2003).

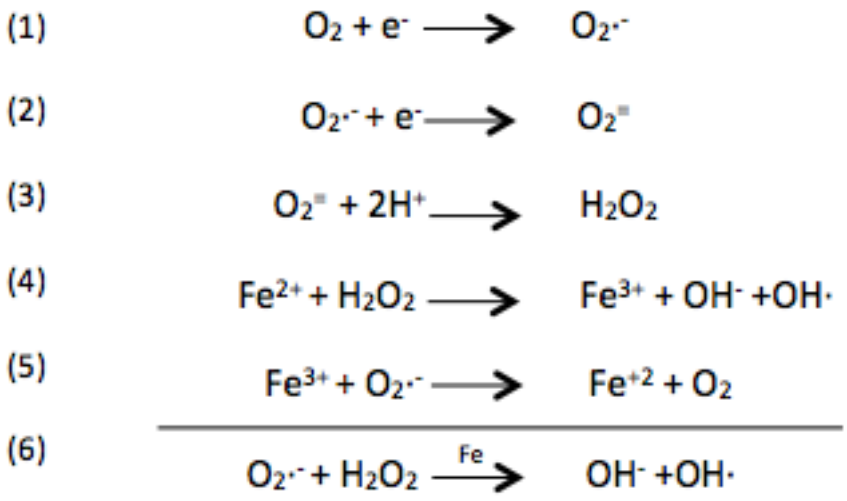

Fig. 34: Redox reactions showing the formation of ROS: (1) Superoxide radical formation; (2) Peroxide ion formation (3) Hydrogen peroxide formation; (4) Hydroxyl radical formation via Fenton-type reaction of ferrous iron with hydrogen peroxide; (5) Reduction of ferric iron by the superoxide anion; (6) Haber-Weiss reaction: Iron-catalyses formation of the hydroxyl radical (Crisponi & Remelli 2008).

1.4 Iron chelation in colorectal cancer therapy

Based on the detrimental effects of unbound iron in carcinogenesis, in recent years, the use of iron chelators to overcome ferrotoxicity in the prevention of cancer has been suggested by several studies. As bound iron is not reactive, it looses its potential to catalyse ROS formation and can therefore not cause any oxidative damage.

The first candidate considered as an iron chelator in cancer therapy was Desferrioxamine, a compound currently used in the treatment of iron overload diseases such as haemochromatosis and β-thalassemia. Several *in vitro*, *in vivo*, and clinical trial studies have found that Desferrioxamine has anti-neoplastic effects against both bone cancer and neuroblastoma. Due to its limitations, such as the inability to permeate cell membranes, recent studies have focused on testing other compound groups such as Thiosemicarbazones and Aroylhydrazones for their cancer preventative properties (Richardson 2002, Heli *et al.* 2011).

While there is a plethora of evidence suggesting the free iron in the colonic lumen to be a major promoter of colorectal carcinogenesis, to date there is no therapy available based on the chelation of this pool of iron.

Orally active chelators that are aimed at the removal of systemic iron have to fulfil several criteria. They have to chelate nontransferrin-bound iron, chelate iron from the liver, heart and endocrine tissues, have low toxicity and have limited access to the brain and foetus (Hider & Zhou 2005).

However, for a chelator that exclusively binds free iron in the colonic lumen, the following properties are desirable:

- Be non-absorbable at any point along the gastrointestinal tract;
- Be non-fermentable or digestible by the intestinal microbiota;
- Bind iron selectively and with adequate binding affinity, removing it from the colon via excretion;
- Chelate iron at a selected point along the digestive tract and,
- Ideally be natural occurring, non-synthetic and safe for human consumption.

These five criteria were chosen for the following reasons. A non-absorbable chelator binds iron within the colon rather than systemic iron. This is important, as we do not want to elevate the risk of anaemia in patients with for example ulcerative colitis and previous research has shown that it is not the systemic pool of iron causing colon cancer (Radulescu *et al*. 2012). If the chelator was fermentable, it could get broken down by the intestinal microbiota, reducing its iron binding capacity and possibly even releasing any bound iron. The chelator must be selective for iron to avoid any removal of essential or beneficial ions such as calcium, which has been proven to have preventative properties against colorectal cancer (Hallberg *et al*. 1992, Corpet 2011, Jemal *et al*. 2011). The chelator needs be active at a point in the gastrointestinal tract after iron absorption has taken place. This way, only the toxic free iron is bound rather than any essential dietary iron. Finally, it is desirable to find a naturally occurring, non-synthetic compound which has already been deemed safe for human consumption in order to streamline clinical trials and accelerate drug development.

Based on these criteria, a group of compounds called alginates were selected to study their iron chelating properties.

1.5 Alginates

1.5.1 Structure and properties

Alginates (or alginic acid) are naturally occurring structural hydrophilic polysaccharides that can be found in marine brown seaweeds (Phaeophyceae). Besides algal sources, several bacterial strains such as *Azotobacter vinelandii* and *Pseudomonas aeruginosa* have been found to produce alginates as capsular polysaccharides (Gacesa 1988, Draget & Taylor 2011).

Alginates extracted from algae are linear binary copolymers made up of unbranched 1,4-linked glycuronans (Draget & Taylor 2011). These residues are β-D-mannuronic (M) acid and its C5 epimer, α-L-guluronic (G) acid. As shown in figure 35, there is only little difference between these uronic acids, however, this causes them to arrange in different chair conformations (Gacesa 1988). The M and G monomers can either be arranged as homopolymeric blocks namely poly(β-D-mannuronate) or poly(α-L-guluronate) blocks or heteropolymeric blocks with an alternating G/M sequence (figure 36) (Haug *et al*. 1974). As shown in figure 37, the packing of the blocks and the orientation of the glycosidic bond have an influence on the overall shape meaning that M-rich regions will form ribbon-like structures whereas G-rich regions form a buckled chain (Gacesa 1988).

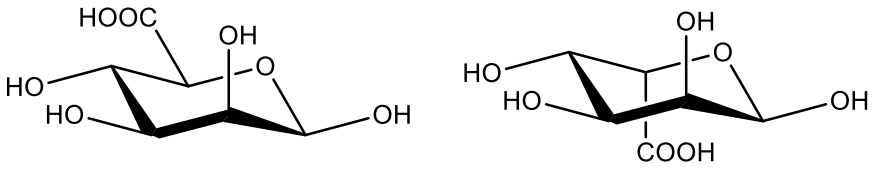

Fig. 35: The alginate monomers D-mannuronic (left) and L-guluronic acid (right) (Gacesa 1988).

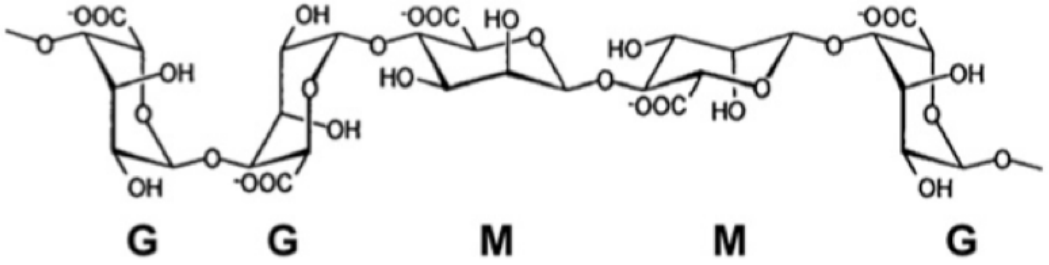

Fig. 36: G/M heteropolymeric block (Draget & Taylor 2011).

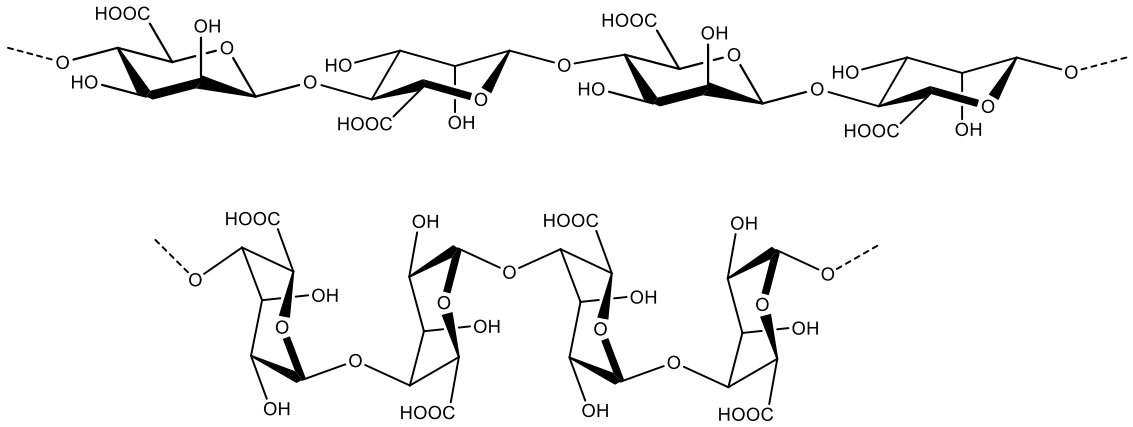

Fig. 37: Ribbon structure of poly(β-D-mannuronate) (top) and buckled chain structure of poly(α-L-guluronate) (bottom) (Gacesa 1988).

Fig. 38: Example block distribution (Draget & Taylor 2011).

All algal alginates are comprised of a mixture of these three block forms (see figure 38). Besides the G/M ratio, the relative proportion of said blocks greatly influences the physiochemical properties of each alginate in solution.

For example high G alginates have a greater binding affinity for calcium than mixed GM and high M alginates, whereas the proportion of heteropolymeric blocks affects the alginates' solubility in acid (Haug *et al*. 1974, Ertesvag & Valla 1998).

1.5.2 Interaction of alginates with multivalent cations

Alginates, in the presence of multivalent cations, such as calcium (Ca^{2+}) ions, have the ability to form thermostable gels.

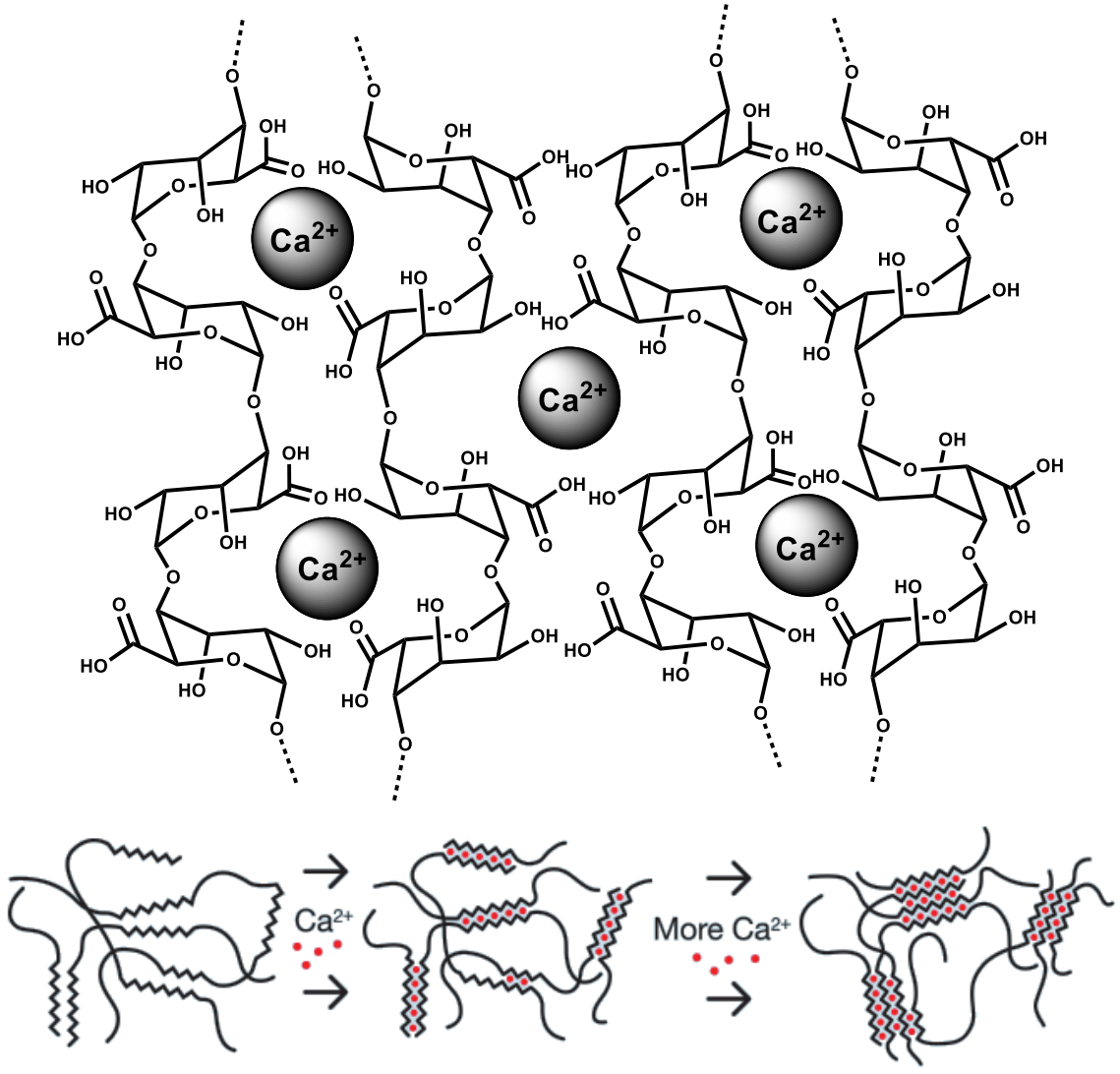

Fig. 39: Gel formation of poly(α-L-guluronate) blocks with Ca^{2+} ions; Top: "egg-box" formation; Bottom: Alginate gelation, (^^^) represents poly-G unit interaction in the presence of Ca^{2+} ions (•) (modified from FMC BioPolymer 2003).

The physical properties of the gel depend on the G/M ratio of the alginate, with G-rich alginates forming strong, inelastic gels. As shown in figure 39, this is due to the regions of poly(α-L-guluronate) forming a so-called “egg-box” support frame trapping the ions within the gaps. With increasing M content the gels become weaker but more plastic (Gacesa 1988).

1.5.3 Pharmaceutical and industrial applications

Because of their gel forming properties, alginates have found a wide range of applications mainly as stabilisers, viscosifiers and gelling agents in the food and drinks industry (Gacesa 1988, Draget & Taylor 2011). Alginates are further used in the pharmaceutical industry in anti-ulcer and reflux medication, emulsion stabilisers, gastro enteric coatings for tablets and wound dressings. Furthermore, they are used as immobilisation agents for cells and enzymes and it has been found that high M alginates have strong immunostimulating properties (Ertesvag & Valla 1998). As most alginates are insoluble in the presence of acid, they are non-degradable in the human body and have been approved by several food safety agencies and the World Health Organisation (WHO) (Gacesa 1988).

1.5.4 Alginates as iron chelators

Based on previous research by the Tselepis group (unpublished data) a range of alginates with different G/M ratios and block compositions was chosen to study their iron chelation properties, namely Protanal LFR 5/60, Protanal RF 6650, Manucol LD, Manucol DH, Manugel GHB and Keltone HVCR KTHVCR (FMC BioPolymer UK Ltd, names abbreviated from here on – see Abbreviations).

These alginates were all stratified in terms of their iron binding potential under physiological relevant conditions. Based on initial experiments, Man DH was chosen as main focus of the research, having had the greatest iron binding capacity under physiological calcium conditions (0.2 mM; see figure 40).

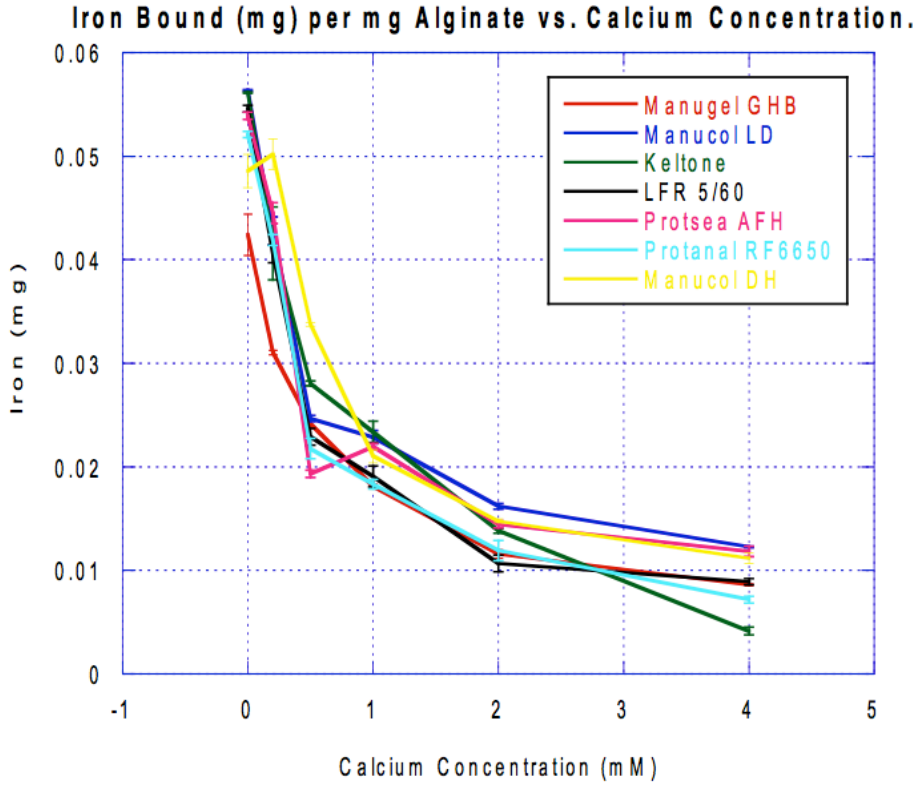

Fig. 40: Iron loss (assessed using the Ferrozine assay) at varying calcium concentrations for the range of alginates (Horniblow 2012).

However, subsequent *in vitro* studies looking at the effects of iron co-incubated with alginates on human colorectal carcinoma RKO cells gave surprising results. As shown in figure 41, rather than reducing the cellular iron content in comparison to an iron only control, co-incubation with 0.3% Man DH significantly increased total iron levels. This result was unexpected and obviously a confounded effect of a supposed iron chelator.

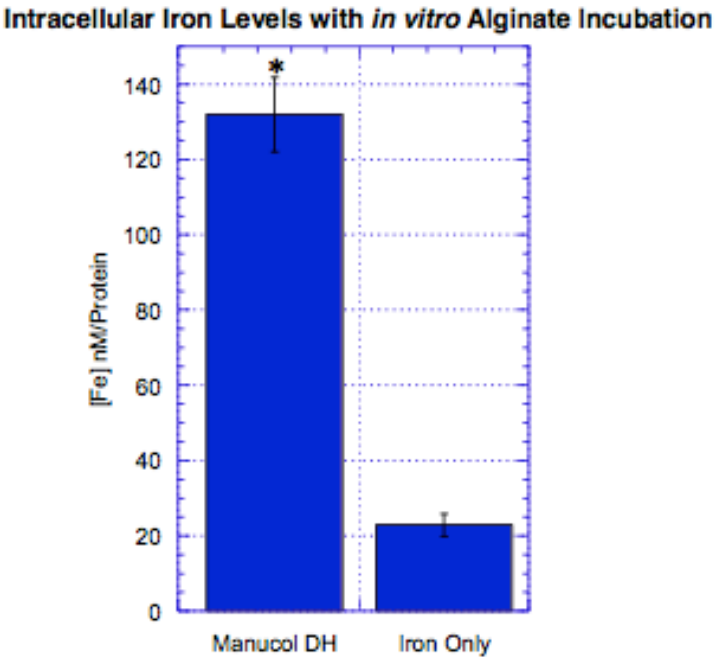

Fig. 41: Analysis of total cellular iron content (assessed using the Ferrozine assay) in human RKO cells incubated with equal concentrations of iron (100 µM $FeSO_4$, 10 µM sodium L-ascorbate) with and without co-incubation with alginate Man DH (0.3% w/v) (Horniblow 2013).

This finding was supported by the outcome of a recent study by Wawer *et al.* (2012) using Man DH to increase the bioavailability of iron in human epithelial colorectal adenocarcinoma CaCo-2 cells. They showed that co-incubating cells with 30 µmol/l ferric ammonium citrate (FAC) and Man DH at 0.1%, 0.5% and 1% (w/v), markedly increased the cells' ferritin expression in comparison to a FAC only control.

1.6 Aims and objectives

Based on the confounding and somewhat surprising iron augmenting effect of Man DH, the aims and objectives of this study were determined.

The first aim was to assess whether the type of iron delivery using iron only or iron with Man DH had any effect on cell phenotype. In order to do this, equal total cellular iron concentrations had to be achieved when incubating human colorectal carcinoma RKO cells with iron only or iron with Man DH. Therefore, cells were stimulated with a constant concentration of iron (100 μM) and varying alginate concentration until an equal level was reached. The total cellular iron content was assessed using the Ferrozine assay. Then, using this predetermined concentration, any changes in the cells' phenotype and therefore viability were measured using the MTT assay.

The second aim was to look at the whole range of alginates to possibly identify a more suitable iron chelator than Man DH. Therefore, MTT assays were performed with all alginates to observe any effects on cell viability. Western blotting was employed to determine the alginates' effect on cellular iron acquisition and therefore on ferritin expression, and finally, dialysis was used to assess the alginates' iron loading capacity.

The third aim was to study the alginates' physiochemical properties and to link them to their iron binding potential. Static and dynamic light scattering was used to measure the alginates' molecular weight and size respectively. Furthermore, circular dichroism was used to determine the G/M ratio of each alginate.

2. METHODS AND MATERIALS

The chemicals and other ingredients mentioned in this section were purchased from Sigma-Aldrich Company Ltd or Fisher Scientific UK Ltd unless stated otherwise. Sterile phosphate buffered saline (PBS) was purchased from the School of Cancer Sciences. The recipes for all buffers / stocks / solutions mentioned in this section can be found in the appendix. All tissue culture relevant procedures were carried out in a sterile laminar flow hood which was cleaned with 70% industrial methylated spirits (IMS) before and after use.

2.1 Tissue Culture

The human colorectal carcinoma RKO cell line was used for all *in vitro* experiments carried out in this study.

2.1.1 Maintaining cell cultures

Adherent cells were routinely cultured in tissue culture flasks in Dulbecco's Modified Eagle's Medium (DMEM) supplemented with 10% fetal calf serum (FCS), 100 units/ml penicillin and 0.1 mg/ml streptomycin in a 37°C incubator with 95% relative humidity and 5% CO_2. They were split regularly whenever they reached between 80-100% confluency (every three to four days). In a sterile hood the growth medium was removed, the cells were washed with 10 ml PBS to remove any residual medium and then 5 to 7.5 ml trypsin (TrypLE Express (1x) – gibco Life Technologies) was added. The cells were incubated for five minutes at 37°C to detach the cells from the flask. To deactivate the trypsin, equal amounts (5-7.5 ml) of 10% DMEM were added.

The solution was transferred into a 15 ml tube and centrifuged for five minutes at 1500 RPM to pellet the cells. The supernatant was decanted and the pellet was fully resuspended with 10 ml 10% DMEM. From this, the appropriate amount for the desired split (e.g. 1 in 10) was transferred into a fresh culture flask and this was made up to a final volume with 10% DMEM.

2.1.2 Plating cells

For experimentation, cells were seeded in 6 well plates at a standard concentration of 1 x 10^5 cells/ml. Therefore, the cells were pelleted and resuspended in 10 ml 10% DMEM as explained above and then the cell density was determined using a haemocytometer. As shown below, the amount of cell suspension needed for 1 ml media / well was calculated and this was made up to a total of 2 ml/well.

$$\left[\frac{1 \times 10^5 \text{ cells / ml}}{(\text{Value 1}) \times 10^4 \text{ cells / ml}}\right] = (\text{Value 2})$$

(Value 2) x Amount of media needed for X plates (ml) = Amount of cell suspension needed for X amount of media (ml)

Example - 40 ml media needed overall:

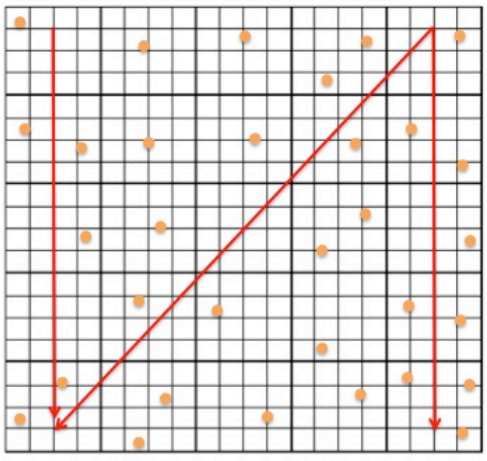

6
9
5
} = 20 cells / 3
= 6.67 cells x 5 grids

→ Cell count: 33.34 x 10^4 cells / ml (Value 1)

$$\left[\frac{1 \times 10^5 \text{ cells / ml}}{33.34 \times 10^4 \text{ cells / ml}}\right] = 0.3 \text{ (Value 2)}$$

0.3 x 20 ml = 6 ml cell suspension in 37.5 ml media

The cells were plated accordingly and were left to grow for 24 hours.

2.1.3 Stimulating cells

Once established, the growth medium was removed and a stimulation medium was added to the cells. For an alginate-loaded medium, the required amount of 10% DMEM was mixed with the appropriate amount of 2% alginate stock. For an iron-loaded medium, the required amount of 10% DMEM was mixed with the appropriate amount of 10 mM iron (Fe) and 1 mM sodium L-ascorbate (Na-asc) stock. For an alginate-Fe loaded medium, appropriate amounts of 2% alginate stock and 10 mM Fe 1 mM Na-asc stock were pre-mixed before adding the required amount of 10% DMEM. The maximum alginate concentration used was 0.3% and a standard final concentration of 100 µM Fe was used for all experiments. Cells were incubated with the stimulation medium for 24 hours. Unless stated otherwise, 6 wells were treated with the same condition for each experiment.

2.1.4 Lysing cells

After the incubation period, the medium was mostly removed with a stripette and any residual medium was removed with a P1000 pipette. The cells were washed twice with 2 ml PBS before adding 150 µl HEPES saline lysis buffer to each well. Using a cell scraper (Corning) the cells were scraped into solution. The cell lysates were transferred into 1.5 ml tubes and either kept on ice or frozen until needed.

To prepare cell lysates for Western blots, the same protocol was used but the plates were kept on ice after removing them from the incubator and 150 µl of RIPA was added for lysing.

2.2 Protein assay

2.2.1 Assay protocol

The Pierce BCA Protein Assay Kit (Thermo Scientific) was used to determine the protein content in cell lysate samples. For a standard calibration, the provided 2 mg/ml bovine serum albumin (BSA) standard was diluted with the appropriate lysis buffer (HEPES or RIPA) to obtain concentrations of 0, 0.5 and 1 mg/ml BSA. The standards were treated alongside the samples and were prepared fresh for every experiment.

If the samples were frozen after lysing, they were fully thawed at room temperature and were then keep on ice. Each sample was well mixed by vortexing for five seconds before pipetting any material. For this assay, 10 µl cell lysate was transferred into a 96 well plate. This was done in triplicate for each sample as shown in figure 42.

Fig. 42: Plating regime (Clker.com 2011)

Following the manufacturers' instructions, reagents A and B were mixed in a 1:50 ratio and 200 µl of this mixture was added to each well. The assay was left to develop for 30 minutes at 37°C before reading the absorbance at λ=550 nm with a plate reader (Victor^2 1420 Multilabel Counter – Wallac).

2.2.2 Data analysis

The data analysis was carried out using Microsoft Excel for Mac 2011. Firstly, the mean was calculated for all standards and the 0 mg/ml standard mean value was subtracted from that. A standard curve was drawn using these values (x-axis – absorbance; y axis – concentration). Then, 0 m/ml standard mean value was subtracted from all sample readings and the amount of protein in µg/µl for each sample was calculated (formula y = x; trend line forced through 0). The mean for all triplicate readings was calculated followed by the amount of protein (µg) in 90 µl of sample. This value was then used to normalise Ferrozine assay data.

2.3 Ferrozine assay

2.3.1 Assay protocol

A Ferrozine assay was used to determine the iron content in cell lysate samples. For a standard calibration, following standards were used: water (used to make up standards), 0 mM (90 µl HEPES lysis buffer, 200 µl 20% trichloroacetic acid (TCA), 600 µl ferrozine), 0.05, 0.1, 0.2, 0.3 and 0.5 mM (200 µl standard stock, 200 µl 20% TCA, 600 µl ferrozine). The standards were treated alongside the samples and were prepared fresh for every experiment.

If the samples were frozen after carrying out the protein assay, they were fully thawed at room temperature first. Each sample was well mixed by vortexing for five seconds before pipetting any material. For this assay, 90 µl cell lysate was transferred to a clean 1.5 ml tube and 200 µl 20% TCA was added.

The samples were mixed well by vortexing for five seconds and were then boiled for five to ten minutes at 100°C in a heat block. After boiling, the samples were centrifuged at 12,000 RPM for five minutes to precipitate the cellular contents. Then, 200 µl of the supernatant was carefully aspirated and transferred into a clean 1.5 ml tube. To this, 600 µl of ferrozine stock was added and the solution was mixed well by vortexing for five seconds. Then, 200 µl of each sample was transferred into a 96 well plate. This was done in triplicate for each sample as shown in figure 42. The absorbance was read at λ=550 nm with a plate reader (Victor^2 1420 Multilabel Counter – Wallac).

2.3.2 Data analysis

The data analysis was carried out using Microsoft Excel for Mac 2011. Firstly, the mean was calculated for all standards and the 0 mM standard mean value was subtracted from that. A standard curve was drawn using these values (x-axis – absorbance; y axis – concentration). Then, the 0 mM standard mean value was subtracted from all sample readings and the amount of Fe in mM for each sample was calculated (formula y = x; trend line forced through 0). The mean for all triplicate readings was calculated and to normalise the data the values for mM Fe were divided by the values for µg protein in 90 µl determined in the protein assay. Finally, an overall mean for each condition in nM, the standard deviation and standard error were determined and the data was plotted in a bar chart. The Student's t-test was used for statistical analysis of each condition in relation to control / Fe only.

2.4 MTT assay – Optimised for 6 well plates

2.4.1 Assay protocol

To study the viability of cells treated with different stimulation media, an MTT assay was performed. This assay was optimised for the use with 6 well plates based on the original protocol for 96 well plates (Van Meerloo *et al.* 2011).

After 21 hours of incubation with the stimulation media, in the hood, 100 µl MTT was added to each well straight into the medium. The plates were gently swirled to ensure sufficient mixing and the assay was left to incubate at 37°C for 3 1/2 hours. The medium was mostly removed with a stripette and any residual medium was removed with a P1000 pipette. To release the dye from the cells, 2 ml dimethyl sulfoxide (DMSO) was added to each well and the cells were scraped into solution using a cell scarper. Then, 200 µl of each sample was transferred into a 96 well plate. This was done in triplicate for each sample as shown in figure 42. The absorbance was read immediately at λ=550 nm with a plate reader (Victor^2 1420 Multilabel Counter – Wallac).

2.4.2 Data analysis

The data analysis was carried out using Microsoft Excel for Mac 2011. Firstly, the mean for all triplicate readings and the overall mean for each condition were calculated. Then, to normalise the data and to obtain the mean fold change for each condition relative to control, all overall means were divided by the overall mean for the control condition (then control = 1).

Finally, the standard deviation and standard error of each mean fold change were determined and the data was plotted in a bar chart. The Student's t-test was used for statistical analysis of each condition in relation to control / Fe only.

2.5 Western blot protocol

2.5.1 Sample preparation

If the samples were frozen after lysing, they were fully thawed on ice before sonicating them for 10 seconds (Soniprep 150 MSE – Sonyo) to further lyse the cells. Using the protein assay (see 2.2) the protein concentration in each sample was determined and the amount needed for 20 µg/µl protein was calculated. This amount was then mixed with 5 µl 5 X SDS sample loading buffer and the samples were boiled in a heat block at 100°C for five minutes.

2.5.2 SDS-PAGE gel

Using the Mini-PROTEAN Tetra handcast system (BIO-RAD), SDS-PAGE gels were prepared fresh. To cast a gel, all bottom gel ingredients were mixed according to table 16 and poured between the glass plates. To achieve an even surface, isopropanol was added drop-wise to cover the gel. After leaving the gel to set, the isopropanol was thoroughly washed off with deionised water (diH_2O).

The top gel ingredients were mixed according to table 16 and poured onto the bottom gel. Immediately, a clean 10 well Mini-PROTEAN comb was pressed into the top gel and this was left to set. The gel was transferred into a Mini-PROTEAN Tetra electrophoresis system filled with 1 X gel running buffer.

After removing the comb, 10 µl PageRuler^{TM} Plus Prestained Protein Ladder (Thermo Scientific) was added to the first well. The amount calculated for 20 µg/µl protein (accounting for the addition of loading buffer) for each sample was added to the appropriate wells. Gels were initially run through the top gel for 15 minutes at 100 V and then were turned up to 180 V through the bottom gel.

Table 16: Ingredients for SDS-PAGE gels

For two gels:	12.5%	Top gel
Ammonium persulfate	spatula end	spatula end
diH_2O	1.9 ml	3.7 ml
Gel buffer (I) or (II)	10 ml (I)	5 ml (II)
Polyacrylamide	8.1 ml	1.3 ml
Tetramethylethylenediamine	60 µl	60 µl

(Polyacrylamide: ProtoGel – GENEFLOW)

2.5.3 Protein transfer

For protein transfer, a Hybond hydrophobic polyvinylidene difluoride (PVDF) membrane (Amersham Hybond-LFP – GE Healthcare) was used. The membrane was cut to the appropriate size and was pre-treated by soaking in methanol (MeOH) for 30 seconds. It was then washed and kept in 1 X transfer buffer until use.

The SDS-PAGE gel was removed from its glass cast and the top gel and any dark lines at the bottom of the gel were cut off. Then, a transfer cassette was assembled as shown in figure 43. By pre-soaking the sponges and filter paper in 1 X transfer buffer and by rolling a pipette over each layer, the formation of air bubbles was avoided.

The transfer sandwich and an ice pack were placed into a transfer tank filled with 1 X transfer buffer. Transfers were run for 90 minutes at 90 V.

2.5.4 Blocking / Incubation with primary antibodies

Following transfer, the membrane was placed in blocking solution (10% milk in Tris buffered saline with Tween 20 (TBST)) for one hour at room temperature with gentle agitation on an orbital shaker. It was then rinsed with 1 X TBST and was cut along the 35 kDa marker with a scalpel (β-actin – 45 kDa; ferritin light chain – 20 kDa). The cuts were placed in individual trays and were incubated with 20 ml of the appropriate primary (probing) antibodies overnight at 4°C on an orbital shaker.

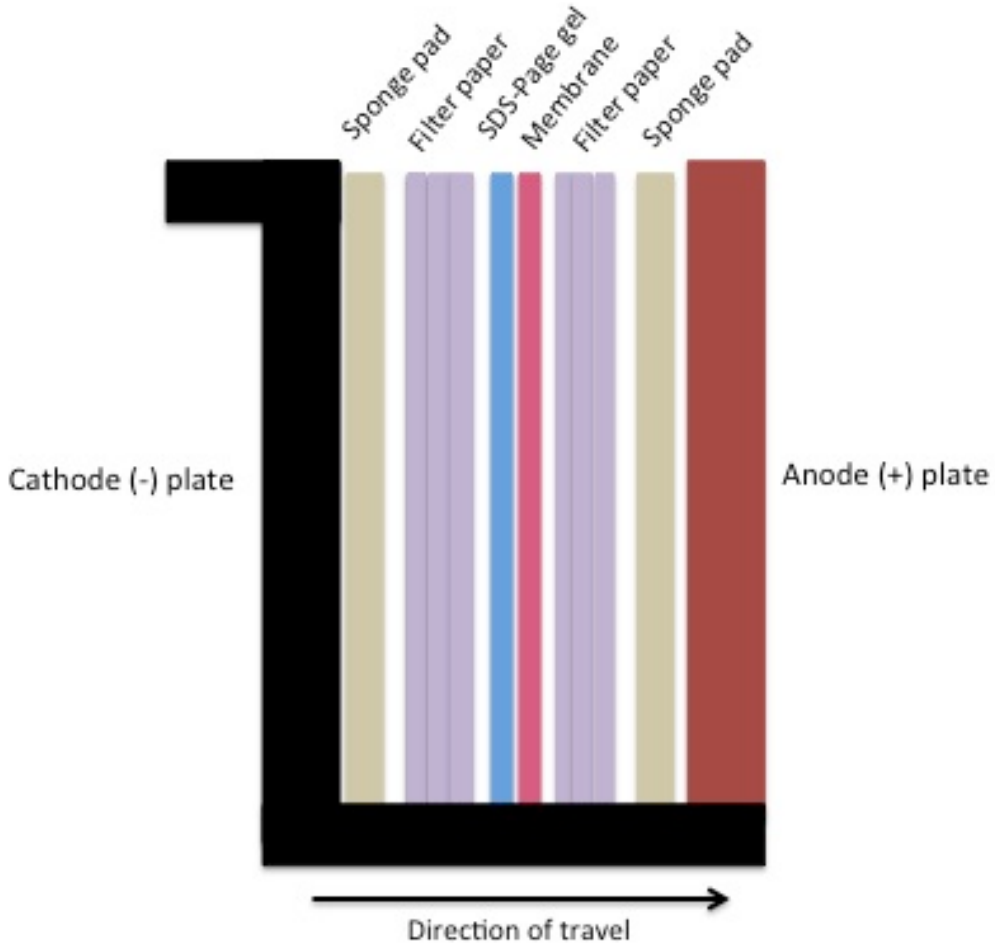

Fig. 43: Western blot transfer sandwich

2.5.5 Washing / Incubation with secondary antibodies

The primary antibodies were rinsed off with 1 X TBST and the membranes were then washed in 20 ml 1 X TBST for 30 minutes, changing the buffer every 10 minutes (three buffer changes). Subsequently, the membranes where incubated with the appropriate secondary peroxidase conjugated antibody for 50 minutes at room temperature on an orbital shaker. Finally, the membranes were washed again as explained before.

2.5.6 Blot development

The Amersham ECL Western Blotting Detection Reagents kit (GE Healthcare) was used to develop the blots. According to the manufacturers' instructions, the reagents were mixed in a 1:1 ratio and kept protected from light until use. The paired membranes together with 5 ml detection reagent were sealed in a plastic bag and the reagents were gently rubbed over the sealed membranes for one minute. The bags were cut open and the reagents were drained before placing the membranes in a clean developing cassette (Amersham Hypercassette – GE Healthcare). In a dark room, a developing film (Amersham Hyperfilm MP – GE Healthcare) was placed on the membranes. Films were developed after one and five minutes and 24 hours for the best result.

2.5.7 Blot analysis

The data analysis was carried out using LI-COR Image Studio Lite and Microsoft Excel for Mac 2011. All ferritin bands were normalised to a β-actin control and the data was plotted in a bar chart. The Student's t-test was used for statistical analysis of each condition in relation to control / Fe only.

2.6 Alginate Dialysis

To study the iron loading capacity of each alginate, dialysis experiments in different Fe loading media were carried out.

2.6.1 Sample preparation

A dialysis tubing cellulose membrane from Sigma-Aldrich with a typical molecular weight cut-off around 14,000 (average flat width 33mm) was used for these experiments. It was cut into strips with the appropriate length to hold 10 ml of sample. To remove contaminants, the membrane strips were washed in 700 ml diH_2O for 30 minutes. Any excess water was stripped from the membranes before clipping the bottom to form a bag. Then, 10 ml of 0.3% alginate solution was added and the top of the bag was clipped tightly to avoid any volume change. This was done in triplicate for all alginates. The bags were placed in diH_2O until all samples were prepared to allow for them to be incubated at the same time.

2.6.2 Buffer preparation

The bags were placed in individual beakers (three bags per alginate / beaker) filled with 400 ml of the dialysing medium. Dialysis was carried out in different buffer conditions as shown in table 17. According to the required Fe final concentration, the appropriate amount of 100 mM Fe stock and 10 mM Na-asc stock was added to the buffer (at the same time to the avoid oxidation).

Table 17: Dialysis buffer conditions

Dialysing medium	Supplements	
	FCS final concentration	Fe final concentration
diH_2O	-	100 µM
Colourless DMEM	-	100 µM
Colourless DMEM	10%	100 µM
Colourless DMEM	10%	200 µM

2.6.3 Dialysis

The bags were incubated in the supplemented dialysis buffer for 1.5 hours at 37°C on a shake plate. The bags were also stirred every 20 minutes to ensure that all samples were evenly exposed to the medium. After the incubation period, the bags were rinsed twice with 100 ml diH_2O. A 1 ml sample (prewash) was taken from each bag before washing them in 400 ml diH_2O for 1.5 hours at 37°C on a shake plate. Another 1 ml sample (washed) was taking after the washing period.

2.6.4 Ferrozine Assay

The Ferrozine assay was used to assess the iron content in the prewash and washed samples. Therefore, 200 µl of each alginate sample was mixed with 600 µl ferrozine stock. Calibration standards were also prepared (see 2.3.1). Then, 200 µl of each sample was transferred into a 96 well plate. This was done in triplicate for each sample as shown in figure 42. The absorbance was read at λ=550 nm with a plate reader (Victor^2 1420 Multilabel Counter – Wallac). Using the values obtained for the standards, the iron content for each sample was calculated (see 2.3.2).

2.7 Phenol-sulphuric acid (PSA) assay

The PSA assay was carried out in order to accurately determine the carbohydrate (alginate) content in the SLS / DLS samples. The assay was optimised based on the original protocol by Dubois *et al.* (1956).

For a standard calibration, following standards were used: SLS / DLS water, 0.015, 0.0125, 0.005 and 0.0025% alginate. The standards were treated alongside the samples.

For this assay, 2 ml of 0.002% alginate solution was accurately transferred into a glass vial and 50 µl of 80% phenol in water were added. Then, 5 ml concentrated sulphuric acid was added rapidly as a constant stream against the liquid surface using a 5 ml pipette. For reliable results this process needed to be performed identically for all samples. For this reason, one measurement for each standard and duplicate measurements for all alginate samples were carried out to minimise any error. The solutions were allowed to stand to cool down for 10 minutes, then shaken vigorously and subsequently incubated in a waterbath at 37°C for 20 minutes. To read the absorbance, 200 µl of each sample was transferred into a 96 well plate. This was done in triplicate for each sample as shown in figure 42. The absorbance was read at λ=490 nm with a plate reader (Victor^2 1420 Multilabel Counter – Wallac). Using the values obtained for the standards, the carbohydrate content for each sample was calculated (as explained under 2.2.2). Alginate concentrations were limited to no greater than 0.015% as above this upper limit, UV absorbance saturation was observed.

2.8 Dynamic (DLS) and static light scattering (SLS)

To determine the size and molecular weight (MW) of each alginate, DLS and SLS measurements were recorded on a Malvern Zetasizer Nano ZS using a 1 cm path length, quartz cuvette. The measurements were carried out on the prepared SLS /DLS samples (see appendix) and 4:1, 3:1, 2:1, 1:1 and 1:2 dilutions. The measurements were taken going from the highest to lowest concentration and the following settings were used for the measurements:

- Refractive increment: dn/dc = 0.15 mg/ml
- Refractive index: chitosan
- Scattering standard: toluene
- Solvent: SLS / DLS water
- Shape connection mode: small molecule
- Temperature: 21°C
- Sample volume: 1 ml in quartz cuvette

Between each measurement, the cuvette was thoroughly cleaned by rinsing with diH_2O and then with acetone. Any residual liquid was removed with a filter tip pipette and the cuvette was left to dry before adding the next sample.

The Malvern Zetasizer software was used to analyse the data.

2.9 Circular dichroism (CD)

To determine the G/M ratio of each alginate, CD spectra measurements were recorded on a Jasco J-810 CD spectropolarimeter using a 1 cm path length, blackened quartz cuvette. The measurements were carried out using 0.075% alginate solutions and the following settings:

- Start: 300 nm
- End: 190 nm
- Speed: 200 nm/min
- Band width: 1 nm
- Data pitch: 0.2 nm
- Scanning mode: continuous
- Accumulations: 6
- Response: 1 sec
- Sample: 1.5 ml 0.075% alginate
- Blank: CD water

Three scans averaged for each alginate were taken. Between each measurement, the cuvette was thoroughly cleaned by rinsing with diH_2O and then with acetone. Any residual liquid was removed with a filter tip pipette and the cuvette was left to dry before adding the next sample.

Microsoft Excel for Mac 2011 was used to produce graphs in order to compare the individual measurements.

3. RESULTS

Statistical significance was calculated by use of the Student's t-test. All analyses were carried out using Microsoft Excel for Mac 2011. Differences were considered to be significant at $p \leq 0.05$. (*) Denotes statistical significance compared to control, $p \leq 0.05$. (+) Denotes statistical significance compared to Fe 100 µM only value, $p \leq 0.05$. Error bars represent ± SEM. Each figure represents data from one experiment unless stated otherwise. The number of replicates performed in each experiments is indicated as *n* and is provided in the figure captions.

Unless stated otherwise, a standard Fe concentration of 100 µM (100 µM $FeSO_4$ + 10 µM Na-asc) was used in all experiments. Alginate concentrations given in the following are (w/v) values.

3.1 *In vitro* experiments with alginates

3.1.1 Iron level studies with Man DH only

Previous experiments in the Tselepis group, found that Man DH had an iron augmenting rather than a chelating effect on *in vitro*. Therefore, the first aim of this study was to assess whether the type of iron delivery using Fe only or Fe with Man DH had any effect on cell phenotype. In order to do this, equal total cellular iron concentrations had to be achieved when incubating cells with both conditions. Cells were stimulated with a constant concentration of 100 µM Fe and varying Man DH concentration until an equal level was reached. The total cellular iron content was assessed using the Ferrozine assay.

Cells were stimulated with Fe only and Fe with Man DH at 0.09%, 0.1% and 0.2%. As shown in figure 44 (a), whilst a Man DH concentration of 0.09% ($p = 0.004$) was too low, there was no statistical difference between Fe only and Fe with Man DH at 0.1% and 0.2%. However, an equal iron level did not appear to be reached at these concentrations. Due to the difference between Fe only and Fe with Man DH 0.1% being smaller ($p = 0.059$) than for Fe with Man DH 0.2% ($p = 0.239$), the experiment was repeated with values closer to Man DH 0.1%.

Cells were stimulated with Fe only and Fe with Man DH at 0.12%, 0.13%, 0.14% and 0.15%. As shown in figure 44 (b), Fe with Man DH 0.14% ($p = 0.168$) was the only condition that was statistically not different to Fe only, meaning that equal cellular iron levels were achieved at this concentration. Therefore, this value was used in cell viability studies.

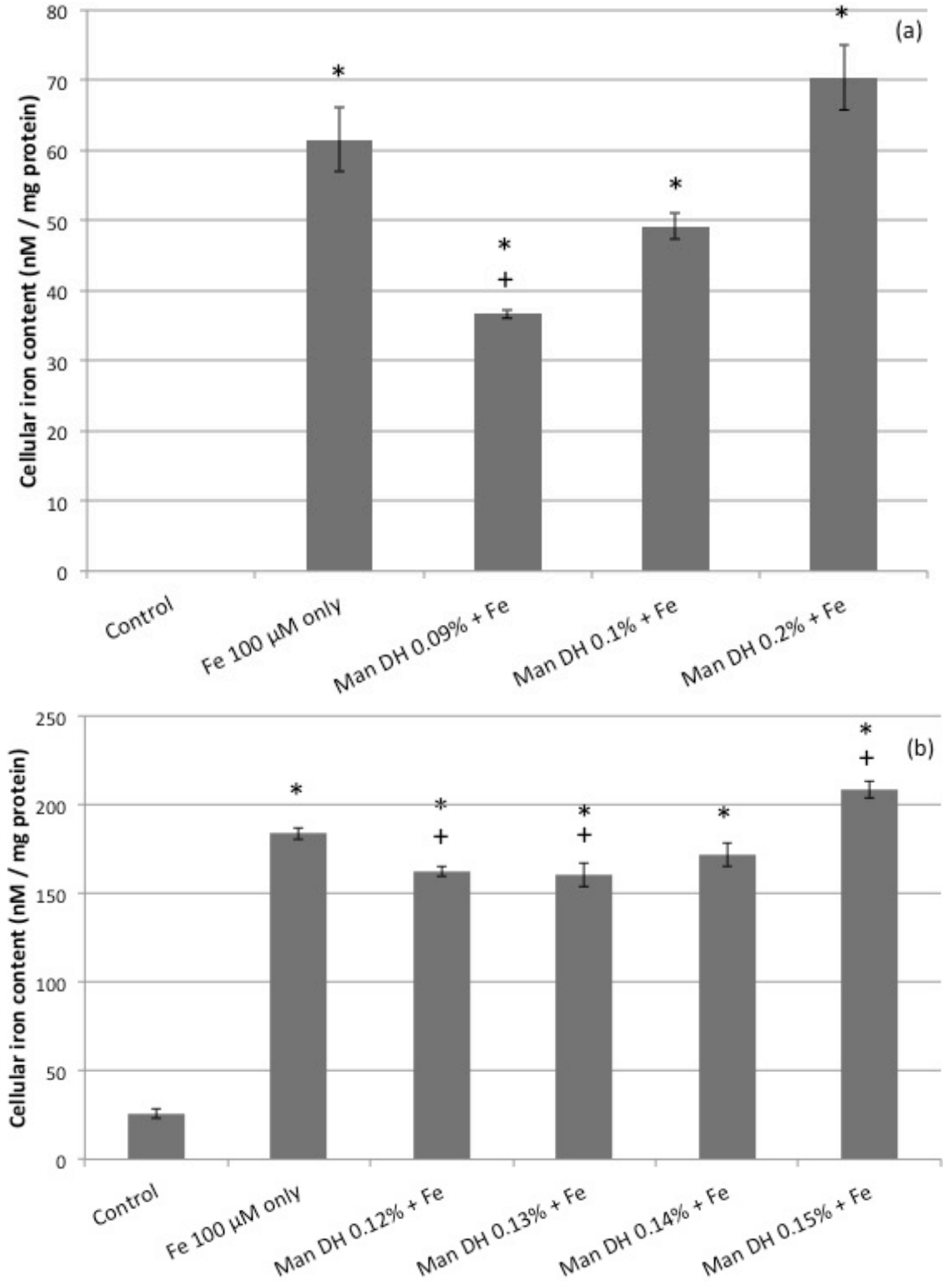

Fig. 44: Total cellular iron levels as determined using the Ferrozine assay for RKO cells stimulated with Fe only and (a) Fe with Man DH at 0.09%, 0.1% and 0.2%; (b) Fe with Man DH at 0.12%, 0.13%, 0.14% and 0.15%. (*) Denotes statistical significance compared to control, $p \leq 0.05$. (+) Denotes statistical significance compared to Fe 100 µM only value, $p \leq 0.05$. Data represent the mean ± SEM (n = 6).

3.1.2 Cell viability studies with Man DH only

The predetermined Man DH concentration of 0.14% was subsequently used to study any phenotypic changes caused by iron delivery using Fe only or Fe co-incubated with Man DH. Any changes in the cells' viability were measured using the MTT assay.

RKO cells were stimulated with Fe only and Man DH at 0.14% with and without Fe. As shown in figure 45, no significant effect on cell viability was observed comparing Man DH with and without Fe to both, control or Fe only. Furthermore, Fe only increased viability by around 12%, but this effect was not statistical compared to control.

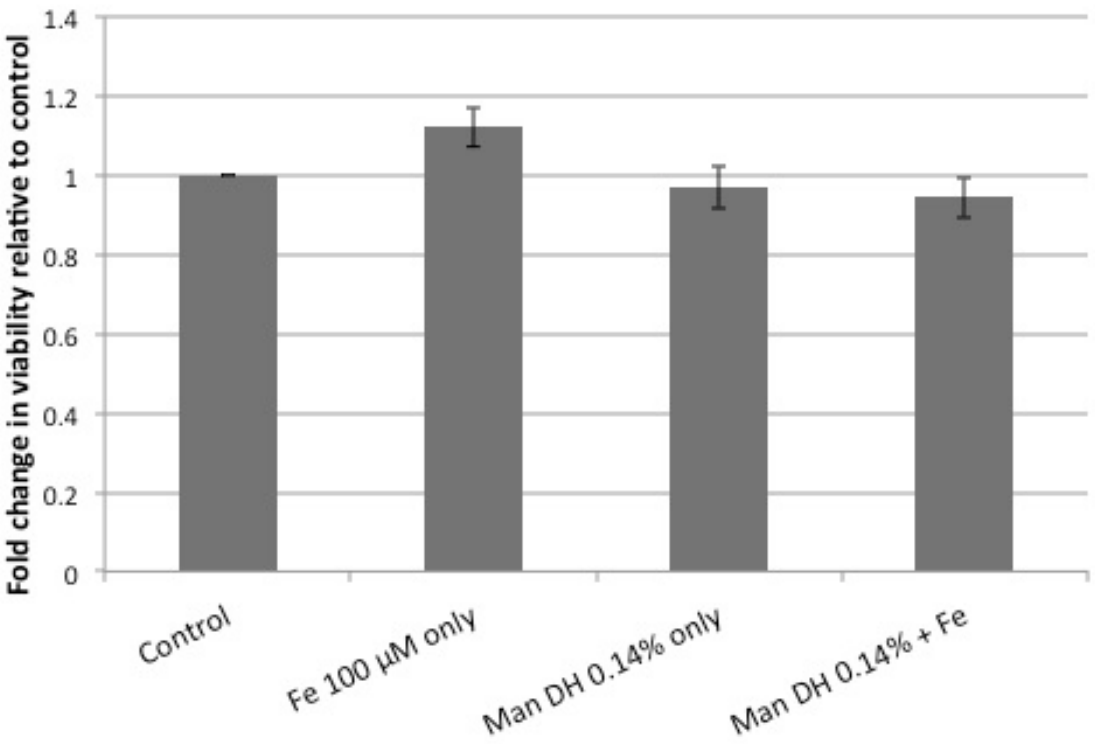

Fig. 45: Cellular viability as determined using the MTT assay for RKO cells stimulated with Fe only and Man DH at 0.14% with and without Fe. Data represent the mean fold change relative to control from four experiments ± SEM (n = 6).

3.1.3 Cell viability studies with the range of alginates

Based on the observations made in the experiments using Man DH only, the second aim of this study was to look at the whole range of alginates to possibly identify a more suitable iron chelator than Man DH. To assess the alginates' effect on cells, several MTT assays were performed.

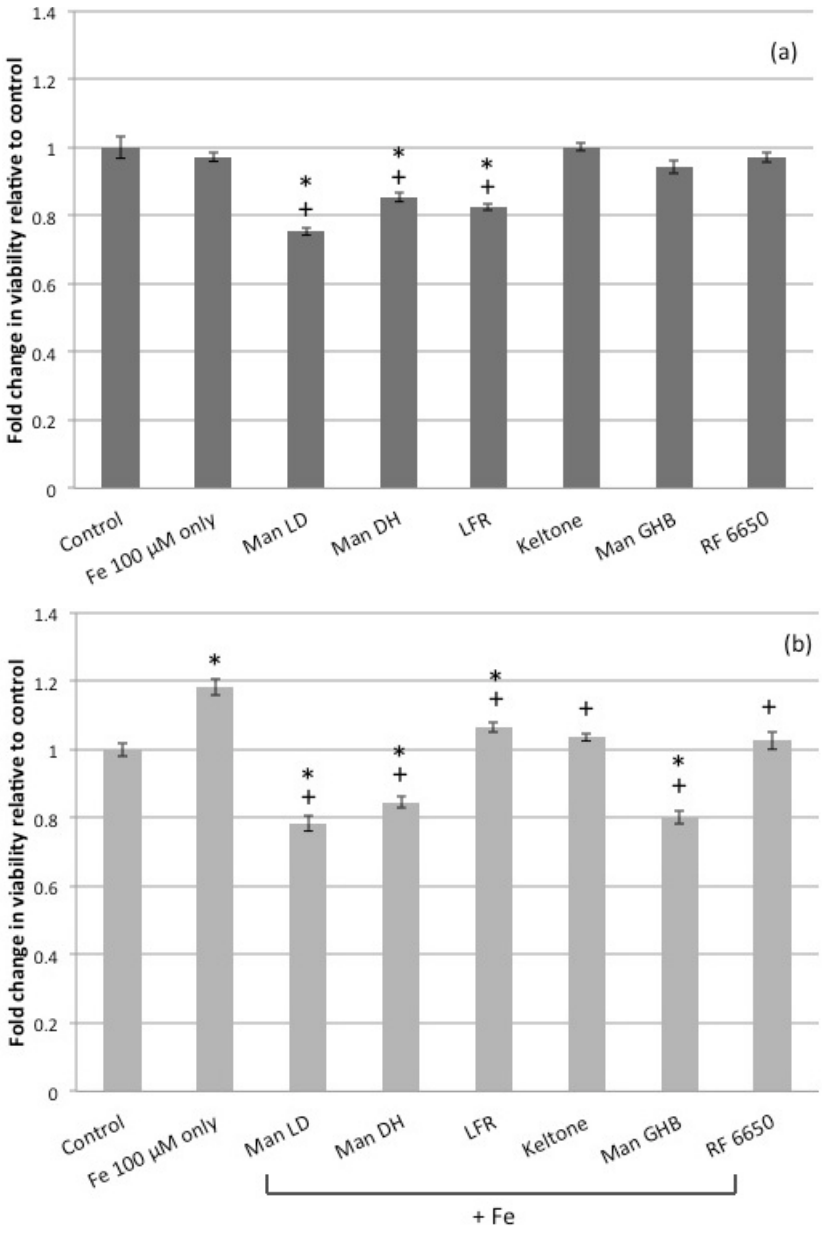

Fig. 46: Cellular viability as determined using the MTT assay for RKO cells stimulated with Fe only and all alginates at 0.14% (a) without and (b) with Fe. (*) Denotes statistical significance compared to control, $p \leq 0.05$. (+) Denotes statistical significance compared to Fe 100 µM only value, $p \leq 0.05$. Data represent the mean fold change relative to control ± SEM (n = 6).

To assess the effect of the alginates alone on cells, RKO cells were stimulated with Fe only and all alginates at 0.14% without Fe. Figure 46 (a) shows that Man LD (25%), Man DH (14%) and LFR (17%) significantly decreased cell viability relative to the control. This decrease was also significant compared to Fe only.

To assess the effect of alginates in combination with Fe, RKO cells were stimulated with Fe only and all alginates at 0.14% with Fe. Figure 46 (b) shows that Man LD (22%), Man DH (15%) and Man GHB (20%) significantly decreased cell viability relative to the control. This decrease was also significant compared to Fe only.

Given the results from the comparative MTT, it was decided to repeat the assay with Man LD and Man DH only. Therefore, RKO cells were stimulated with Fe only and Man LD / DH with and without iron. As shown in figure 47, there was a significant decrease in viability in cells stimulated with Man LD with (18%) and without (19%) Fe. Man DH with (6%) and without (3%) also decreased viability in relation to control, however this was not statistical.

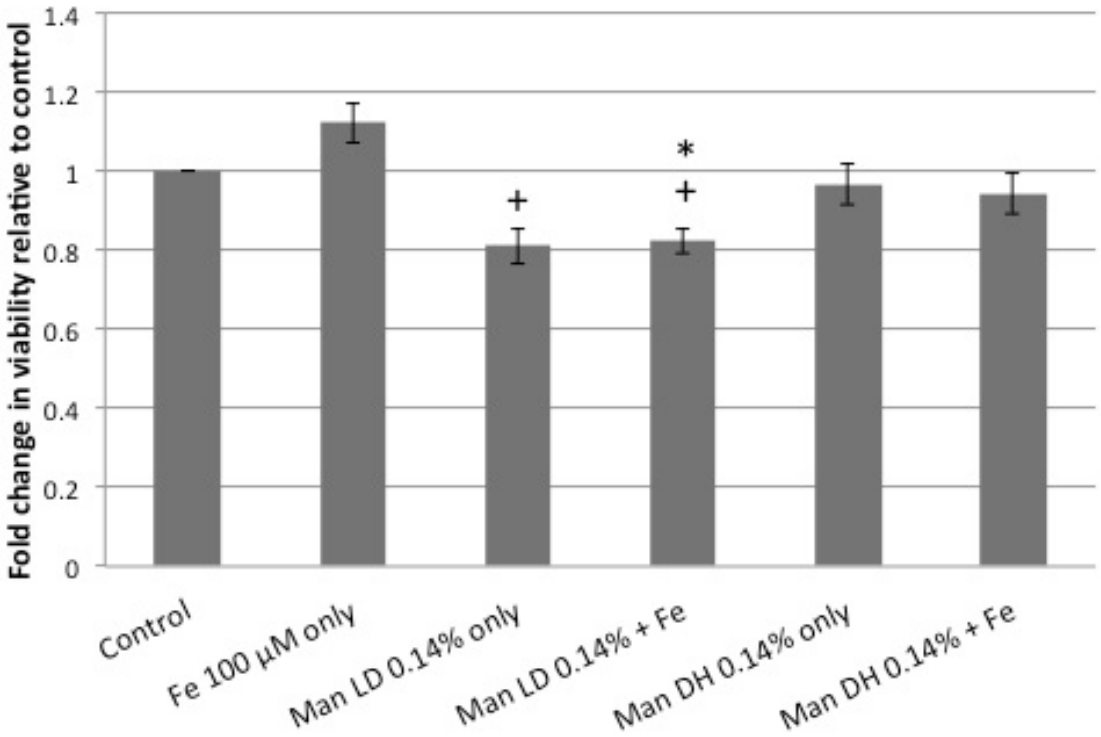

Fig. 47: Cellular viability as determined using the MTT assay for RKO cells stimulated with Fe only and Man LD / DH at 0.14% with and without Fe. (*) Denotes statistical significance compared to control, p ≤ 0.05. (+) Denotes statistical significance compared to Fe 100 µM only value, p ≤ 0.05. Data represent the mean fold change relative to control from four experiments ± SEM (n = 6).

3.1.4 Cellular iron acquisition

In the final part of the cellular studies, Western blotting was employed to determine the alginates' effect on cellular iron acquisition and therefore on ferritin expression.

To assess the effect of alginates in combination with Fe, RKO cells were stimulated with Fe only and all alginates at 0.3% with Fe. As shown in figure 48 (a) and (b), there was great variation in ferritin expression over the range of alginates and Man LD was the only one showing a statistical decrease compared to Fe only (p = 0.03) and no difference relative to control (p = 0.17).

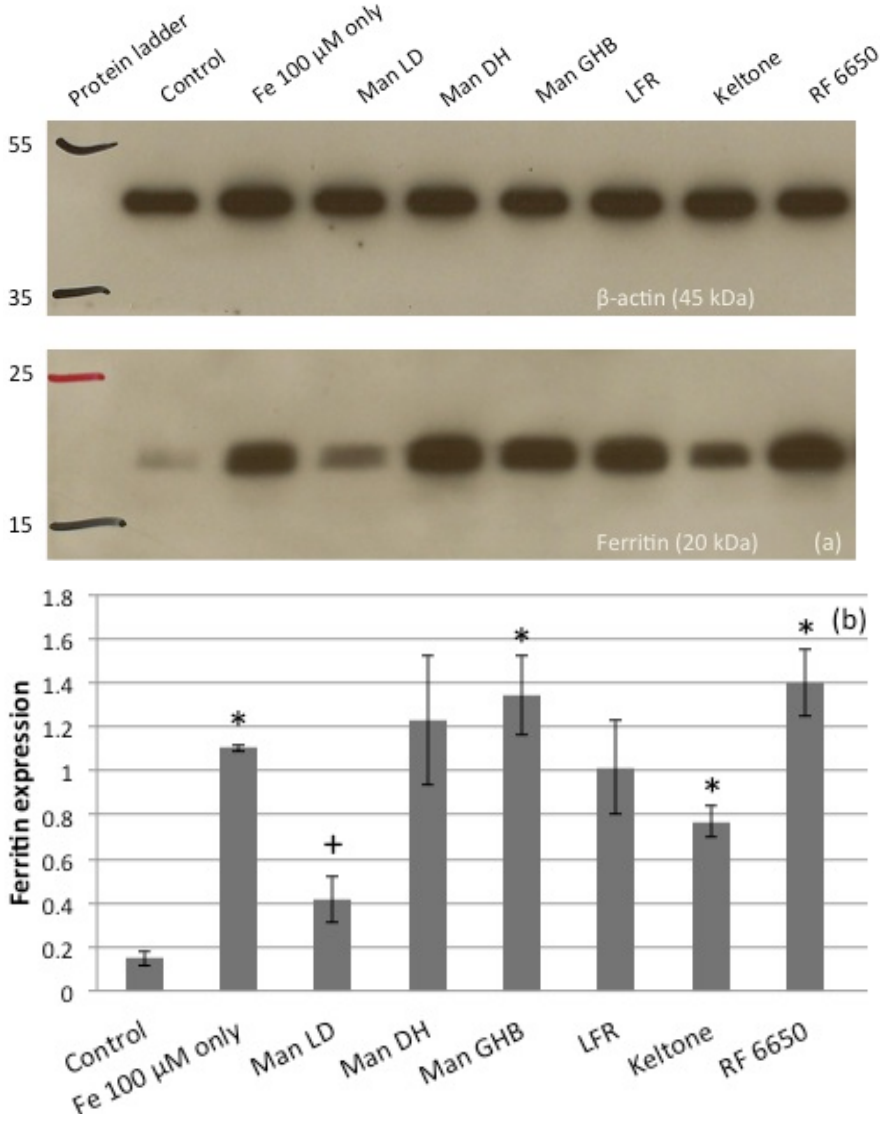

Fig. 48: Cellular ferritin expression as assessed by Western blotting for RKO cells stimulated with Fe only and all alginates at 0.3% with Fe. (a) Western blot showing bands for β-actin and ferritin expression; (b) Graph showing ferritin expression normalised by β-actin. (*) Denotes statistical significance compared to control, $p \leq 0.05$. (+) Denotes statistical significance compared to Fe 100 µM only value, $p \leq 0.05$. Data represent the mean from three experiments ± SEM (n = 3).

Given the results from the comparative Western blot, it was decided to repeat the experiment with Man LD only. Therefore, RKO cells were stimulated with Fe only and Fe with Man LD at 0.14% and 0.3%. As shown in figure 49 (a) and (b), no ferritin was expressed in both the 0.14% ($p = 0.0036$) and 0.3% ($p = 0.04$) Man LD samples and this was statistically significant in relation to Fe only.

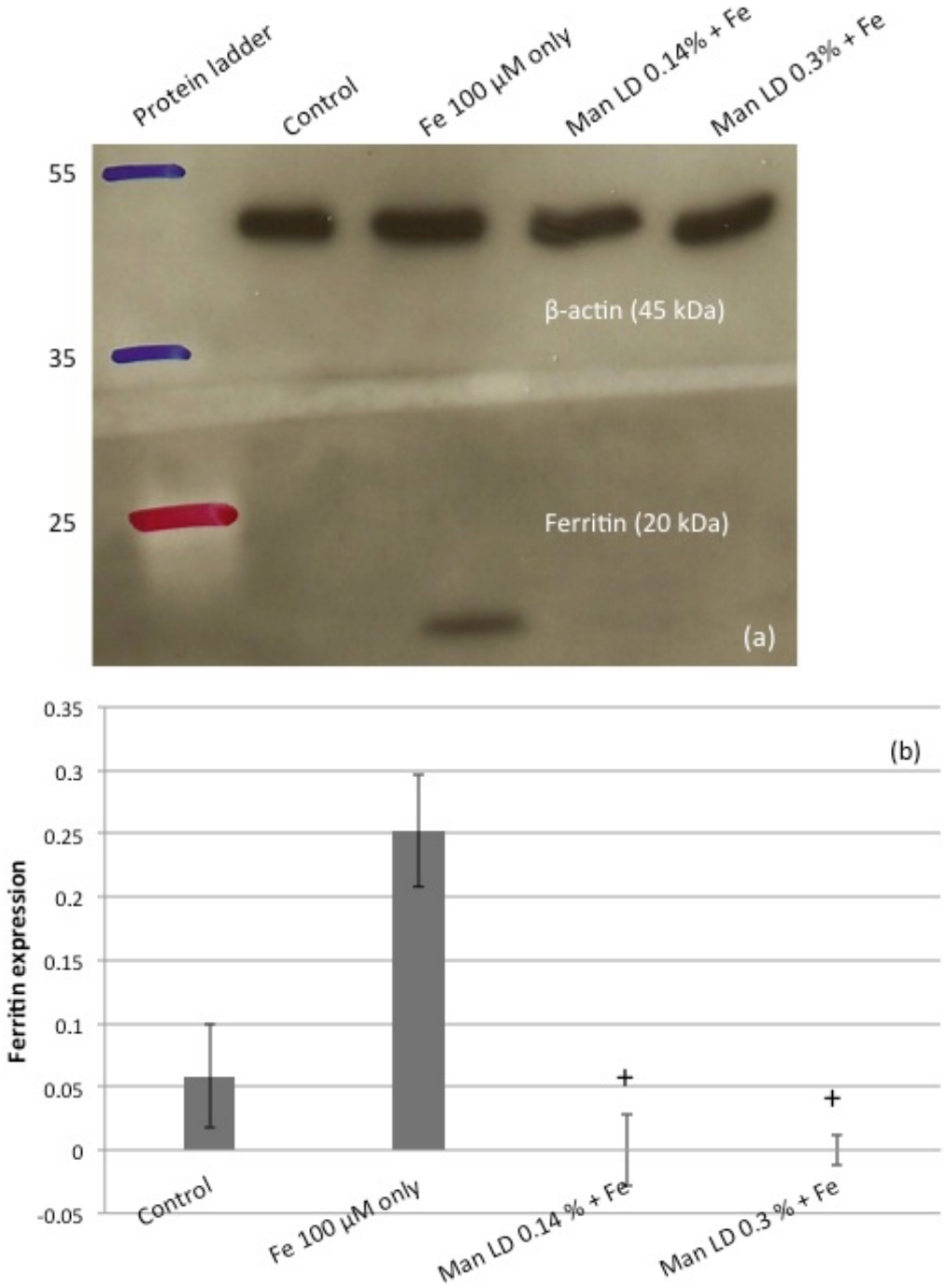

Fig. 49: Cellular ferritin expression as assessed by Western blotting for RKO cells stimulated with Fe only and Man LD 0.14% and 0.3% with Fe. (a) Western blot showing bands for β-actin and ferritin expression; (b) Graph showing ferritin expression normalised by β-actin. (+) Denotes statistical significance compared to Fe 100 µM only value, $p \leq 0.05$. Data represent the mean from three experiments ± SEM (n = 3).

3.1.5 Alginate iron loading capacity

In order to assess the alginates' iron loading capacity, the alginates were dialysed in different Fe containing media. The Ferrozine assay was then used to determine the amount of Fe bound by the alginates pre- and post-wash.

As shown in figure 50 (a-c), all alginates at 0.3% were incubated in triplicate with 10 µM $FeSO_4$ and 10 µM Na-asc in diH_2O, colourless DMEM and 10% FCS colourless DMEM. To assess iron binding at colonic luminal iron concentrations, in a further experiment (figure 50 (d)), alginates were dialysed in 10% FCS colourless DMEM supplemented with 20 µM $FeSO_4$ and 20 µM Na-asc.

No statistical analysis could be performed on these results due to the lack of a control / Fe only condition and also as these experiments have been performed only once in triplicates.

In the condition resembling *in vitro* iron concentrations, the iron binding capacity of all alginates was never greater than 0.004 nM Fe. In diH_2O, however, the iron binding capacity was dramatically increased with peak Fe concentrations of around 35 nM.

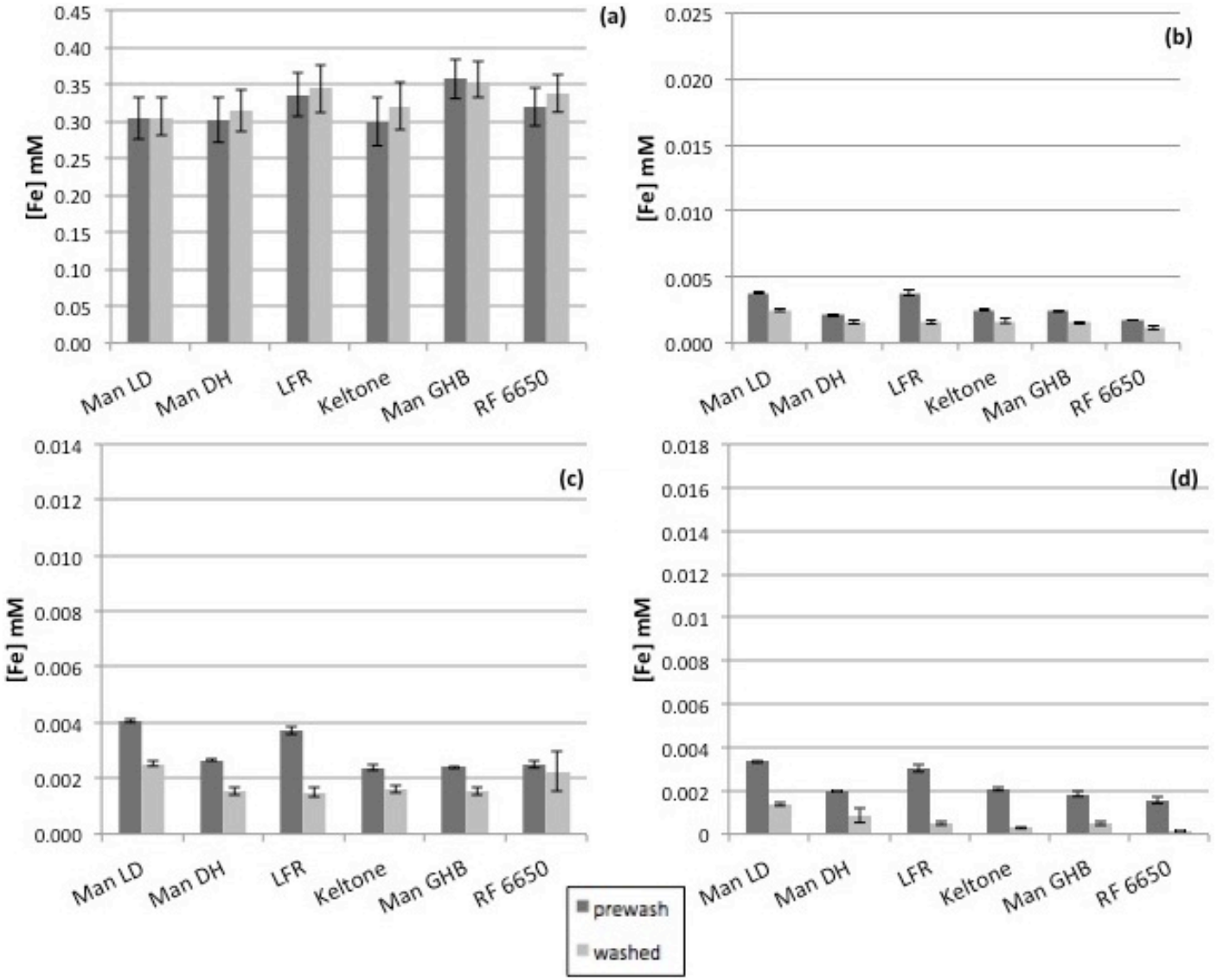

Fig. 50: Alginate iron loading capacity as assessed by dialysis and Ferrozine assay. Alginates at 0.3% were stimulated with 100 µM $FeSO_4$ 10 µM Na-asc in different dialysis media: (a) diH_2O (b) colourless DMEM (c) 10% FCS colourless DMEM; (d) Alginates at 0.3% stimulated with 200 µM $FeSO_4$ 20 µM Na-asc in 10% FCS colourless DMEM. Dialysis for 1 ½ h followed by 1 ½ h wash in diH_2O; 37°C on a shake plate. Data represent the mean ± SEM (n = 3).

3.2 Physiochemical properties of alginates

The *in vitro* studies showed that the alginates have different effects on cell viability and cellular iron acquisition as well as different iron loading capacity. To understand the underlying basis of their iron binding properties and to identify the characteristics that allow for a suitable colonic luminal iron chelator, the final aim of this study was to assess the physiochemical properties of all alginates.

3.2.1 Alginate size in solution

To assess the alginates' size in solution, DLS measurements were performed. The data obtained is presented as size distribution by volume. Due to lack of sample, no data was obtained from Man GHB. Table 18 gives the exact values obtained for each peak shown in figure 51 and also gives a ranking of the alginates by size.

Table 18: DLS values obtained for each peak and ranking of alginates according to their size (1 = largest, 5 = smallest alginate); d.nm = Diameter (nm).

Alginate	**Peak 1 (d.nm) / % Volume**		**Peak 2 (d.nm) / % Volume**		**Peak 3 (d.nm) / % Volume**		**Ranking**
Manucol DH	420.9	16.4	24.82	83.6	0	0	1
Keltone	717.7	2.9	15.58	97.1	0	0	2
Manucol LD	361.6	1.0	10.76	99.0	0	0	3
LFR 5/60	360.4	0.3	8.864	99.7	0	0	4
RF 6650	599.1	1.7	27.71	8.5	7.525	89.8	5

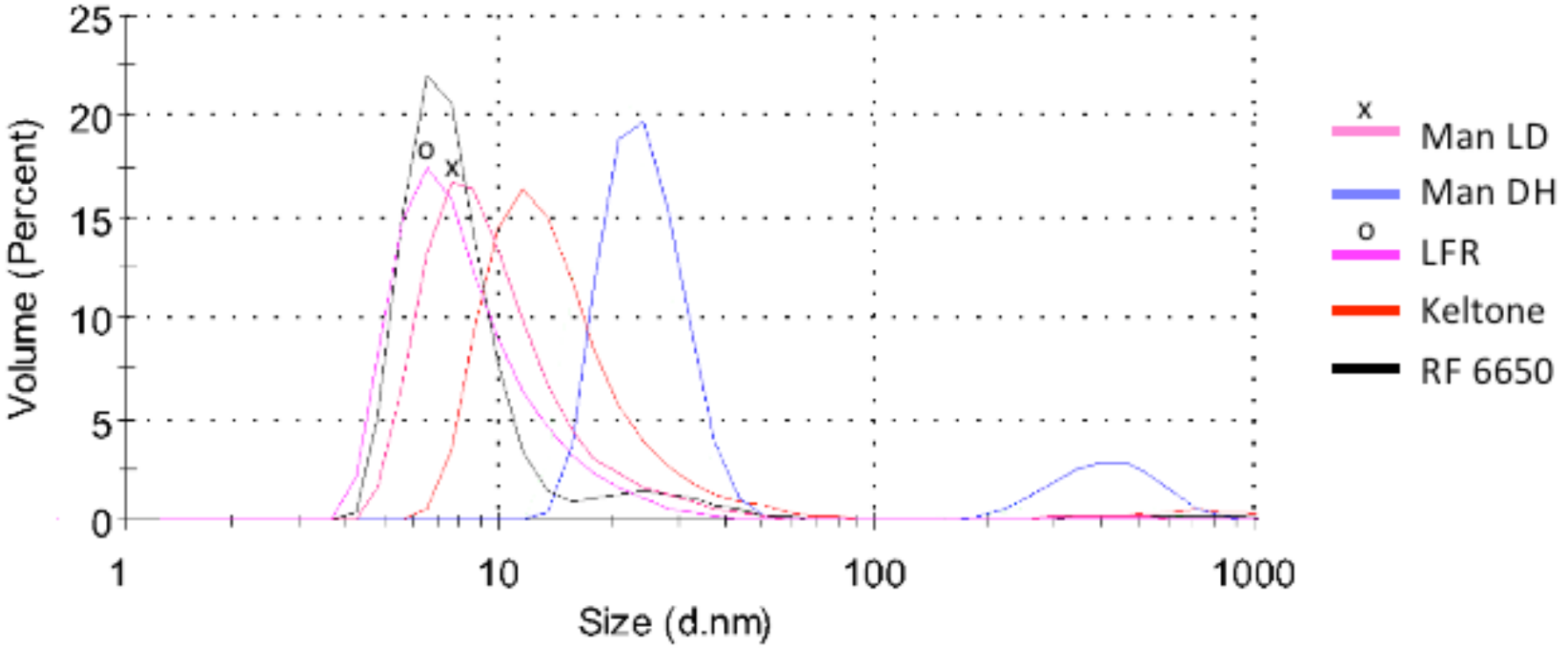

Fig. 51: DLS of alginate samples. Graph shows the particles' size distribution by volume; d.nm = Diameter (nm).

3.2.2 PSA and molecular weight determination

To assess the alginates' MW, SLS measurements were performed. Prior to this, the PSA assay was used to determine the carbohydrate concentration in the alginates samples.

Consistent PSA assay results were obtained for Man LD, Man DH and LFR and therefore SLS measurements could only be performed these alginates. The data gathered from this are presented in table 19.

Table 19: Carbohydrate concentration in alginate samples as assessed using the PSA assay. Alginate MW determined using SLS.

Alginate	Carbohydrate content (g/l)	Molecular weight (kDa)
Manucol LD	1.92 g/l	47.4 + / - 1.77
Manucol DH	1.88 g/l	131 + /- 6.29
LFR 5/60	2.10 g/l	34.3 +/- 2.36

Figure 52 (a-c) shows the Debye plots for all three alginates obtained from the Malvern Zetasizer Nano ZS. According to the information obtained from the machine, good quality data was collected for these measurements.

The data obtained for intensity describes the intensity of scattering of the solution caused by the particles.

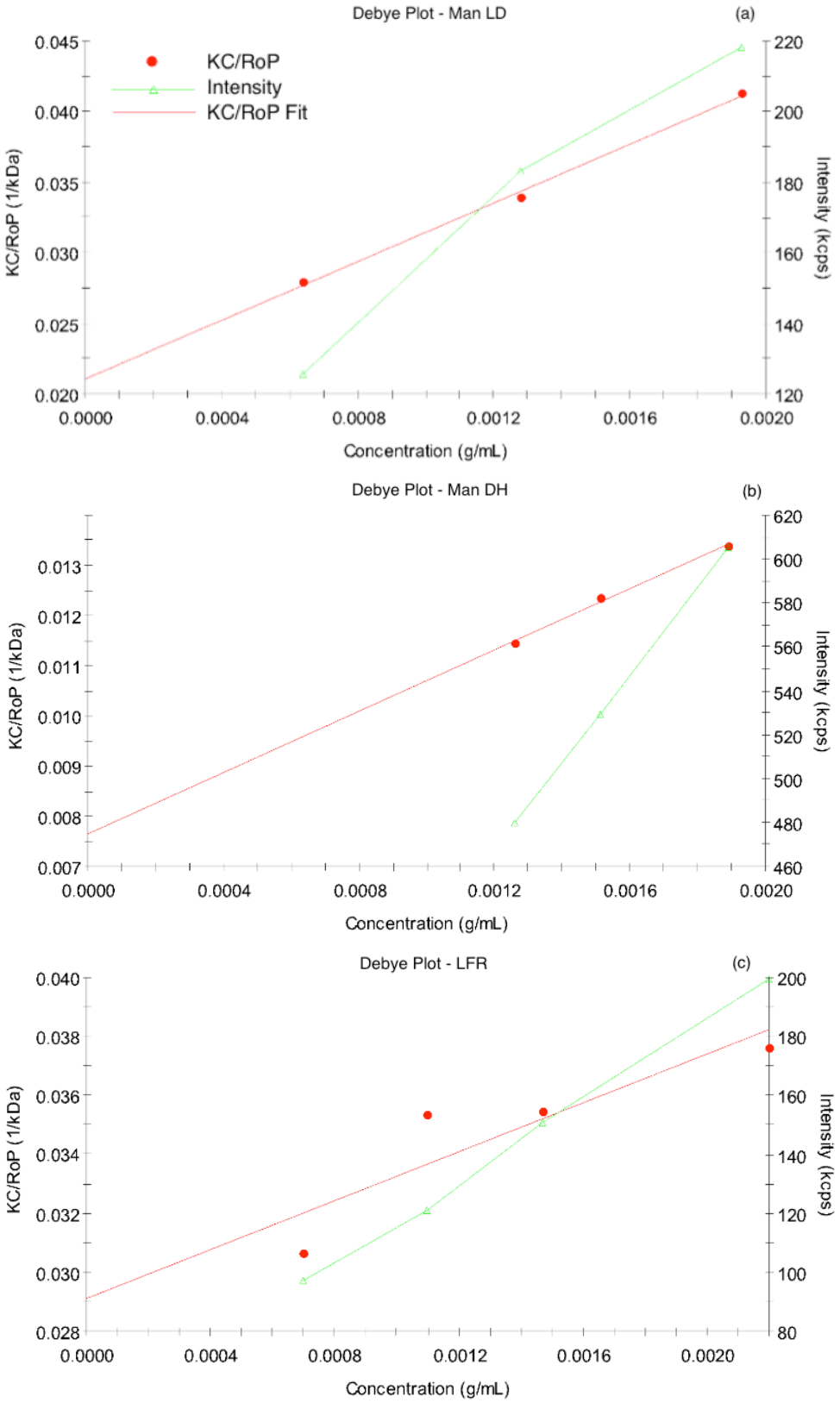

Fig. 52: Debye plots obtained for Man LD, Man DH and LFR using the Malvern Zetasizer Nano ZS. Intensity (kcps) describes the intensity of scattering of the solution caused by the particles; Concentration (g/ml) describes the alginate concentration in solution. KC/RoP (1/kDa) is the intercept which is proportional to 1/MW.

3.2.3 Guluronic acid content

To assess the alginates' G content, CD measurements were performed. Figure 53 (a) shows the CD spectrum obtained for all alginates. The exact CD readings measured at 210 nm and a ranking of the alginates by their G content are given in table 20.

Table 20: Exact CD (mdeg) readings at 210 nm obtained for each alginate and ranking of alginates according to their G content (1 = highest G, 6 = lowest G).

Alginate	**CD (mdeg) at 210 nm**	**Ranking**
LFR 5/60	-92,9375	1
GHB	-84,8443	2
RF 6650	-84,8114	3
Keltone	-59,2908	4
Manucol DH	-57,8315	5
Manucol LD	-53,1083	6

Figure 53 (b) and (c) show the absorbance and HT (V) spectra obtained for all alginates.

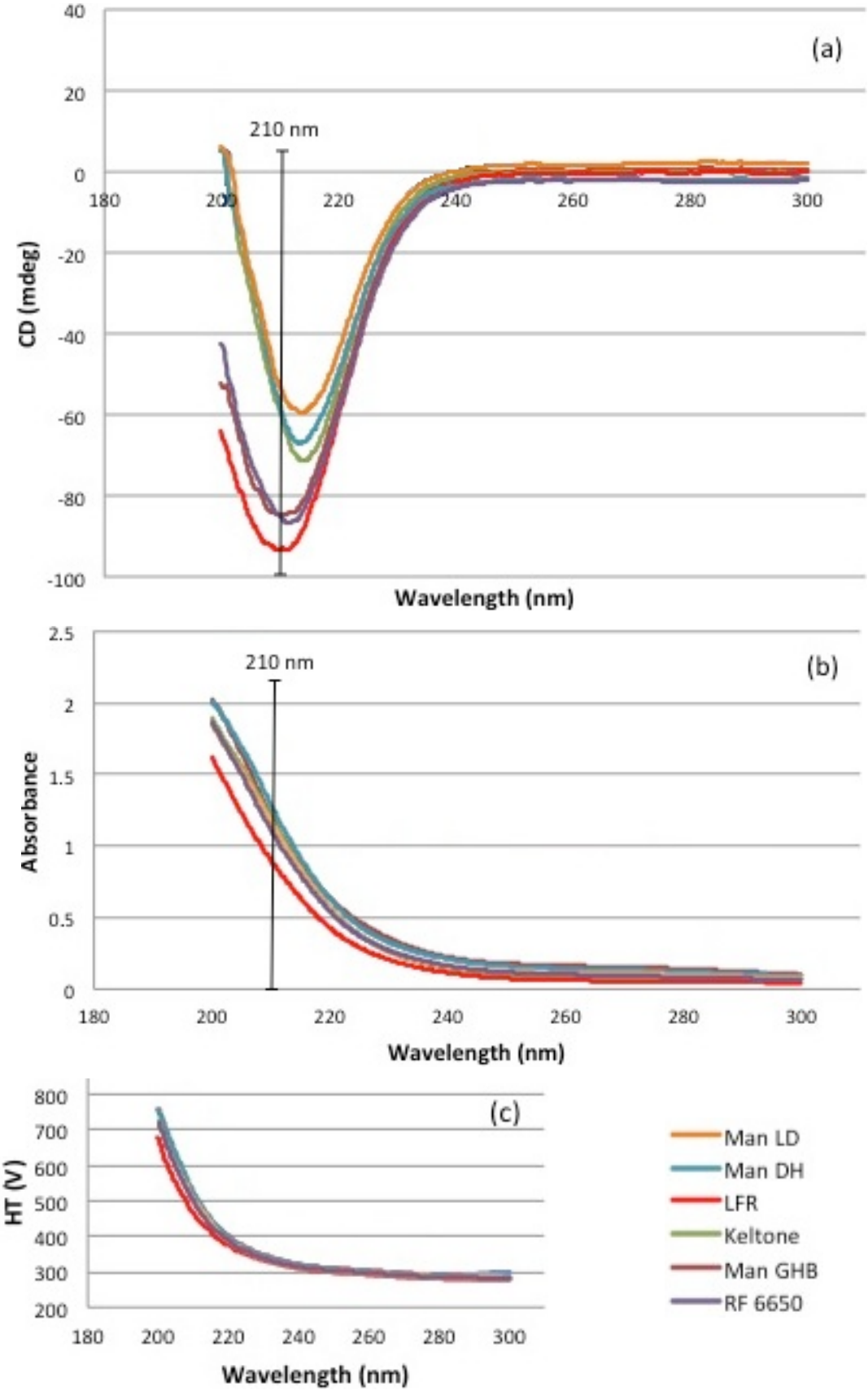

Fig. 53: Graphs showing (a) CD, (b) absorbance and (c) HT (V) spectra obtained for all alginates.

4. DISCUSSION

Previous cellular data in the group indicated that even though Man DH had the highest iron binding capacity under physiological conditions, it significantly augmented total cellular iron levels within an *in vitro* setting in comparison to a iron only control (see figure 40 and 41). This is a confounding and somewhat surprising effect, making it unsuitable as an iron chelator. However, what remained unknown was whether alginate-bound iron within cells is inert or whether it can exert phenotypical changes similar to iron alone. Therefore, one of the aims of this study was to determine whether the type of iron delivery using Fe only or Fe co-incubated with Man DH had any effect on cell phenotype.

In order to carry out these experiments, first it was necessary to achieve equal total cellular iron concentrations for both conditions. As shown in figure 44 (b), at a Man DH concentration of 0.14% co-incubated with 100 µM Fe, an equal level was reached compared to Fe only, and therefore this value was used in the subsequent cell viability studies.

The question behind the cell viability studies with Man DH was even though the measurement for total cellular iron suggests that there are equal amounts of iron present in the cells, what effect does it have on the cell phenotype when the iron is delivered by an alginate. It was hypothesised, that when cells load the same amount of iron according to the Ferrozine assay, then they should be just as viable with and without alginate.

However, the preferred effect for an iron chelator would be that the alginate binds the iron but does not release it into the cells, which would decrease viability.

As shown in figure 45, at the predetermined Man DH concentration of 0.14% with and without Fe, no change was observed. Given that cancer cells have a higher requirement for iron in order to proliferate, it was expected that with increased iron availability, the cell viability would increase accordingly. However, Fe only did not have a statistical effect on cell viability compared to control. These results show that Man DH with and without Fe does neither increase nor decrease cellular viability.

Whilst not unexpected, this effect is not desirable for an iron chelator, and therefore the decision was made to expand the cell viability studies onto all alginates available, in order to find a stronger more suitable chelator.

The aim of this comparative viability experiment was to find an alginate that could decrease cell viability, at the same concentration at which Man DH had no effect. The data obtained from this experiment was used more to find an alginate that shows a trend to have the ability to reduce cell viability rather than to make a definite conclusion about the effect that alginates have on cells. This was based on the fact that the MTT assay appeared to have several limitations. Firstly, the values obtained could not be normalised and therefore the measured viability was strongly dependent on the amount of cells in each well.

Even though, thorough cell counting and accurate plating techniques were applied, there still might have been variations between wells and especially experiments. Another factor that could have an impact on the outcome of the MTT assay is the quality of the cell line, which might vary from split to split or be depended on the number of passages (e.g. more or less susceptible to iron uptake with later passages).

For example, as can be seen in figure 46 (a) and (b), Man DH decreased cell viability by around 15% which was statistically significant compared to both control and Fe only. However, these graphs represent data from only one experiment with six replicates for each condition, whereas the data from the previous graph (figure 45) came from four independent experiments. The same discrepancy can be seen for Fe only. While no effect could be observed in the first experiment (alginates without Fe, figure 46 (a)), in the second experiment Fe only increased cell viability by 18% ($p = 0.0003$). Therefore, in this case, it was more important to look at the data in relation to control rather than Fe only, as this value was normalised and set as 1.

As shown in figure 46 (a), in the first experiment without Fe, Man LD (25%), Man DH (18%) and LFR (17%) significantly decreased viability compared to control. In the second experiment, besides Man LD (22%) and Man DH (15%), Man GHB decreased viability by 20%. While the results for Man GHB and LFR were not consistent for both experiments, they were consistent for Man LD and Man DH.

With an average decrease in viability by about 23.5%, Man LD seemed to have the most negative effect on cells out of the range of alginates. To confirm these findings, the next step was to repeat the MTT assay, comparing only Man LD and Man DH.

The results presented in figure 47 came from four independent experiments and provides sufficient evidence to reinforce the previous finding (figure 45) that Man DH in fact has no impact on cellular viability and further support the data from the comparative MTT showing that Man LD has a negative effect on cells with a fold change of about 18%.

To assess the effect of alginates' on cellular iron uptake, Western blotting was used to determine levels of ferritin expression in cells. Ferritin is a highly conserved storage protein for intracellular iron and research has found a positive association between ferritin overexpression and increasing iron supply and import (Cairo *et al.* 1985). Ferritin consists of two parts, the heavy and light chain subunits, which if put together form an iron storage cavity holding up to 4500 iron (III) atoms per ferritin molecule. While the heavy chain subunit catalyses the oxidation of iron from the ferrous to the ferric form, the light chain subunit is mainly responsible for long-term iron storage (Harrison & Arosio 1996). Therefore, in this study, Western blot analysis of ferritin light chain expression was used.

In comparison to the Ferrozine assay, which was used to measure the total cellular iron concentration including iron loosely bound to the cell surface, ferritin expression can be used to measure only the intracellular iron content and therefore gives a more accurate representation of the cellular iron uptake in the absence and presence of alginates.

As shown in figure 48, there was a statistical difference between Fe only ($p = 0.01$) and control proving the point that with increased iron availability, ferritin expression is amplified. Looking at both figure 48 and 49, it is explicit, that out of the range of alginates, Man LD was the only one showing no statistical difference to control but to Fe only, which means that Man LD significantly decreased ferritin expression and therefore lowered cellular iron uptake.

Looking at the other alginates, Man GHB and RF 6650 in fact seemed to increase ferritin synthesis, while Man DH and LFR had no effect compared to Fe only. Besides Man LD, Keltone was the only alginate that seemed to have a negative effect on iron uptake, but this finding was not statistical.

To assess the alginates' iron binding potential under conditions resembling *in vitro* iron concentrations, dialysis in different iron-loaded media was used. Both the samples' iron content before and after washing the bags in diH_2O was determined, however, the real iron binding capacity is only represented by the post-wash data.

When looking at the results shown in figure 50 (a), it is apparent that the alginates' iron binding capacity was more than seven times higher when dialysed in diH_2O than in any of the other conditions. Dialysis in diH_2O shows how much iron the alginates could bind in the absence of other divalent cations especially calcium. In both, the phenol red liquid DMEM used for tissue culture and the colourless DMEM powder, calcium is present at a concentration of 0.2 g/l (Sigma-Aldrich), which could have a negative effect on the alginates' iron binding affinity. Furthermore, other weak chelators present in the media and FCS could interfere with the alginates' binding potential. Therefore, the results shown in figure 50 (a) do not represent the actual iron binding capacity under *in vitro* conditions.

Looking at the alginates in the conditions resembling *in vitro* iron concentrations (figure 50 (b-c)), it appears as though Man LD had the greatest iron loading capacity, while the other alginates all seem to have similarly low potential.

Based on the data gathered in the cell studies and iron loading dialysis, it became apparent that there must be underlying differences in their structure and composition causing the alginates to have these distinctive effects in *in vitro* conditions. Therefore, the last aim of this thesis was to characterise the physical and chemical properties of all alginates in order to link them to their iron binding capacity in solution. In the following, the techniques used, the results obtained and their limitations are discussed.

Dynamic light scattering is a routine physiochemical method used for the characterisation of polymers in aqueous solutions. As described by Strand *et al.* (1982), it is a quick and easy was to determine the particle size of alginates. The technique is based on the Rayleigh theory which infers a proportional relationship between the size of a particle and the intensity of light scattered by this particle. This means, that the larger a particle, the more light it scatters and therefore the smaller the particle the less light it scatters. DLS can therefore be used to determine the particle size of polymers and was used in this study to obtain sizing for all alginates (Indian Academy of Sciences).

Because of lack of sample, no data could be obtained for Man GHB. As shown in figure 51, one can see that the alginates all have different sizes to one another and also that they are more or less polydispersed in solution. This means that within each alginate sample there are different sizes leading to a non-uniform size distribution which is represented in peaks on the graph. Each of the alginates has two peaks except for RF 6650, which has three peaks meaning that it is even more polydispersed than the others. One can see that with increasing size, the peaks are shifted to the right on the graph indicating more particles with greater diameters. Therefore, the alginates can be divided into three groups: small alginates (RF 6650, LFR, Man LD), medium alginates (Keltone) and large alginates (Man DH).

Based on the same principle as DLS, static light scattering can be used to determine the molecular weight of macromolecules such as polymers or proteins.

The technique is commonly used for the determination of MW in alginates and the preparation of samples used in this study was based on a reliable protocol by Strand *et al.* (1982).

SLS data was only gathered for Man LD, Man DH and LFR. Due to time constrains, inconsistent results from the PSA assay and poor quality data, it was not possible to obtain results for the other alginates.

The MWs obtained for Man LD (47.4 kDa) and LFR (34.3 kDa) were based on high quality data and were found to be consistent with literature. The MW previously reported for Man LD was around 40 kDa (FAO Corporate Document Repository) and for LFR around 34.7 kDa (manufacturer's information FMC BioPolymers). The data for Man DH (131 kDa) on the other hand was not consisted between different measurements. Nevertheless, the MW values obtained were always greater than of Man LD and LFR suggesting that Man DH has a higher MW than the other two alginates. This finding is also consistent with literature suggesting a MW of around 97 kDa (Chan *et al.* 2009). The SLS results strongly tie in with the sizes obtained from DLS, with LFR being the smallest, Man LD the second smallest and Man DH being the largest alginate.

While SLS is a very useful technique when trying to determine the MW of small polymers such as Man LD or LFR, there are difficulties with obtaining high quality data when the polymers are bigger such as Man DH.

In the case of the latter, the samples produce too much scattering resulting in poor quality data with low correlation between the measurements. Another problem with using SLS for the characterisation of alginates is their polydispersity in solution, which was confirmed by DLS. Too many different particle sizes give confounding results in the machine and lead to low quality data. Furthermore, there can be problems due to contamination of the sample with dust or other aggregates (Strand *et al.* 1982). Even if the samples are filtered, when transferring them into the machine, contamination with airborne particles cannot be ruled out. Therefore, in order to characterise the other alginates, the technique would require further optimisation.

Circular dichroism is a method that is used to study the structure and composition of polymers. In 1975, Morris *et al.* validated it for the use with alginates in particular for the determination of the relative G content of alginates. Both uronic acids have chiral carbon atoms, C4 and C5, which allow them to be studied using CD spectroscopy. Positive bands are associated with D-uronic acids (M units) whereas poly-G units cause negative bands. However, as can be seen in figure 53, the signal produced by the G units at around 210 nm is very strong and shadows any signal from the M units. This is why, for this thesis, CD was exclusively used to determine the alginates G content.

Looking at the CD spectra in figure 53, one can see that the alginates can be separated into two distinct groups, low-G alginates (Man LD, Man DH and Keltone) and high-G alginates (RF 6650, Man GHB and LFR). Out of these groups, LFR had the highest G content and Man LD the lowest G content.

A drawback when using CD is that due to the intensity of the signal produced by the G units in an alginate sample, CD cannot be used to determine the M content of a sample. Also, rather than providing actual values for G content, the information is limited and only gives an implication of relative differences in G content between alginates. However, the relative G content of a sample does give information about the amount of M units in an alginate and therefore it cannot be said that an alginate is for example high M based on its low G content. To complement and confirm the results obtained from CD, NMR spectroscopy could be used to determine the definitive G/M composition of each alginate (Gacesa 1988).

Combining the results from the physiochemical analysis, it is possible to conclude that Man DH had low iron binding capacity, no statistical effect on cell viability and ferritin expression, it was the largest alginate with a high MW of 131 kDa (literature around 97 kDa) and it had the second lowest G content. These findings are consistent with literature which describes Man DH as a high M alginate with a M/G ratio of 1.56 and a G content of 35% (Liew *et al.* 2006, Chan *et al.* 2009).

LFR had the same *in vitro* effects as Man DH, low iron binding capacity, it was the second smallest alginate with a low MW of 34.3 kDa (literature around 34.7kDa) and it had the highest G content which is supported by the manufacturer's information stating that LFR has a G content of 65-75% (FMC BioPolymers).

Man GHB had low iron binding capacity, no marked effect on cell viability but it caused a small increase in ferritin expression. There is no sizing or MW data available for Man GHB and it had the second highest G content. Again, this was confirmed by findings in the literature reporting a G content of around 63% (Chan *et al.* 2009).

RF 6650 had the same *in vitro* effects as Man GHB, had low iron binding capacity and it was the smallest alginate with the third highest G content. The G content was nearly identical to that of Man GHB which is supported by Walewijk *et al.* (2008) who found that RF 6650 had a G content of 63%.

Keltone had low iron binding capacity, had no effect on cell viability, caused a small but not statistical decrease in ferritin expression and it was the second largest alginate with the third lowest G content. Ma *et al.* (2007) determined the G content of Keltone to be 60% which ties in with the ranking of this alginate and the data found in literature found for other alginates.

Man LD had the highest iron binding capacity, was the only alginate to significantly reduce cellular viability and ferritin expression, it was the third smallest alginate with a low MW of 47.4 kDa (literature around 40kDa) and it had the lowest G content. In the literature, Man LD is described as a high M alginate with a M/G ratio of 0.41 and only 30% G (FAO Corporate Document Repository).

These are preliminary results and caution has to be taken when drawing conclusions. Nevertheless, when looking at Man LD in comparison to the other alginates, it becomes apparent that it must be a combination of both G content and size / MW that affects the alginates' iron binding capacity and their effect on cells. For example, Man DH has a very similar G content to Man LD, but is much larger whereas LFR is smaller than Man LD but has a much higher G content. Both alginates have a low iron binding capacity. Another example supporting this structure-function relationship is RF 6650 and Man GHB. These alginates have the same *in vitro* effects, low iron binding capacity and nearly identical G content which was supported by literature.

There are several explanations why high G content in alginates makes them unsuitable as iron chelators. Firstly, poly-G units have a high binding affinity for calcium and preferably bind calcium over iron (Gacesa 1988). It is therefore not surprising, that all high G alginates were found to have no or little effect on RKO cells and low iron loading capacity in dialysis performed using DMEM. M rich alginates on the other hand, have a lower binding affinity for calcium and M blocks have even been found to have a higher binding affinity for iron than G blocks (Perez-Moral *et al.* 2013).

Secondly, poly-G alginates are restricted by their buckled chain conformation which changes into the so-called "egg-box" structure to form microcrystalline junctions with divalent cations. In comparison to that, high M alginates have a ribbon-like structure making them less restricted in their conformation (Gacesa 1988, Perez-Moral *et al.* 2013).

However, not just G content but also size seemed to have an effect on the alginates' behaviour *in vitro* (especially looking at Man DH and Man LD). Ma *et al.* (2008), found that the higher the MW and therefore the larger the alginate the more constraint is its confirmation, which significantly lowers its iron binding capacity.

The work presented in this thesis provides preliminary evidence for a structure-function correlation between the alginates' physiochemical properties and their iron binding potential. Nevertheless, further testing is needed to assess and validate these findings in order to obtain a list of the most desirable criteria for an alginate as iron chelator.

Man DH and Man LD are extracted from the same algal source which is split into different fractions during the manufacturing process. They both have the same G/M ratio but Man DH is the bigger fraction while Man LD is the smaller fraction of the same algae (manufacturer's information, FMC BioPolymers). This has been supported by the data gathered in this study, showing that Man DH and Man LD had very similar G content with Man DH being the largest and Man LD being the second smallest alginate out of the range. Insightful future investigations to prove the hypothesis of small, low G alginates being better iron chelators than large, high G alginates could include the following experiment. Man DH could be digested into smaller fragments to achieve a more similar size to Man LD. If the hypothesis is correct, then these digests should have comparable iron loading properties to Man LD and therefore reduce viability and ferritin expression *in vitro*.

In conclusion, this study provides an initial yet enlightening investigation into the chemical, physical and *in vitro* properties of the alginates. The data obtained indicates that there are distinct and apparent differences warranting further investigation into correlations between alginate composition and iron binding capacity, both *in vitro* and *in vivo.* The hypothesis emerging from these prospective results indicates that a low G (potentially high M) alginate with a small size and low molecular weight might serve as the best iron chelator for a potential therapy in the prevention of colorectal cancer.

5. APPENDIX – Recipes for Section 2

In the following the recipes for all buffers / stocks / solutions referred to in the Methods and Materials section can be found. They were made up using the purest diH_2O (18.2) to ensure that there were no contaminants (e.g. iron) in the water.

The chemicals and other ingredients mentioned here were purchased from Sigma-Aldrich Company Ltd or Fisher Scientific UK Ltd unless stated otherwise. Sterile PBS was purchased from the School of Cancer Sciences.

All tissue culture relevant stocks were prepared in a sterile laminar flow hood which was cleaned with 70% IMS before and after use.

Growth and stimulation media

Supplemented 10% FCS growth medium

For a standard 10% FCS growth medium, DMEM purchased from Sigma-Aldrich was supplemented with 50 ml filter sterilised (0.2 µm) FCS (Biosera or PAA Laboratories GmbH) and 5 ml of penicillin-streptomycin solution (100 units/ml penicillin and 0.1 mg/ml streptomycin). The medium was kept and 4°C and was brought to 37°C in a waterbath before use.

2% Alginate stocks

For a 2% alginate stock, 0.8 g alginate was dissolved in 40 ml diH_2O. Given the viscosity of alginates in solution, it was not possible to filter sterilise the stocks before adding them to cells. Therefore, before weighting out the alginate powder, the scales, spatula and weighting boats were cleaned with 70% IMS to achieve semi-sterile conditions. Immediately after weighting out 0.8 g of alginate, the weighting boat was transferred into a sterile hood. To aid the alginates dissolve, diH_2O was warmed up to 37°C in a waterbath before filter sterilising 40 ml into individual tubes in the hood.

The alginate powder was then added to the warm sterile diH_2O and mixed immediately by shaking. The stocks were left in a 37°C incubator until the alginates were fully dissolved. The stocks were kept up to four weeks at 4°C. Before use, the alginate stocks were warmed up to 37°C in a waterbath.

10 mM Fe 1mM Na-asc stock

For a 10 mM ferrous sulphate heptahydrate (Fe) and 1 mM Na-asc stock, 0.108 g Fe was added to 40 ml diH_2O and mixed thoroughly. Immediately after dissolving the Fe, 0.008 g Na-asc was added to prevent oxidation. In the hood, the solution was sterilised using a 0.2 µm syringe filter. This stock was made fresh for each experiment.

Lysis buffers

HEPES saline lysis buffer

HEPES saline lysis buffer was prepared by dissolving 0.566 g (10 mM) HEPES and 1.8 g (0.9% w/v) sodium chloride (NaCl) in 150 ml diH_2O. The pH was adjusted to 7.4 with 0.1 M sodium hydroxide (NaOH). The buffer was made up to a final volume of 200 ml and was stored at 4°C.

RIPA lysis buffer

RIPA lysis buffer was prepared by mixing 1 ml NP-40 detergent (IGEPAL), 0.5 g sodium deoxycholate and 0.1 g sodium dodecyl sulphate (SDS) in 100 ml diH_2O. The solution was split into 5 ml aliquots and stored at -20°C. For use, 6% v/v protease inhibitors was added (Protease inhibitor cocktail tablets, complete EDTA-free – Roche).

Assay stocks / standards

Ferrozine stock

For a 10 mM ferrozine stock, 0.91 g (0.23 M) Na-asc, 0.089 g (10 mM) 3-(2-pyridyl)-5,6-diphenyl-1,2,4-triazine-4',4''-disulfonic acid sodium salt (ferrozine) and 13.78 g (2 M) sodium acetate were dissolved in 122 ml diH_2O. The stock was thoroughly mixed and stored protected from light at 4°C.

20% TCA stock

For a 20% (w/v) stock, 20 g trichloroacetic acid was dissolved in 100 ml diH_2O. The stock was stored at 4°C.

MTT stock

For a 12 mM MTT stock, 50 mg of 3-(4,5-dimethylthiazol-2-yl)-2,5-diphenyltetrazolium bromide (MTT) was added to 10 ml sterile PBS in a hood. The solution was mixed thoroughly before sterilising with a 0.2 µM syringe filter. The stock was made fresh for each experiment and was protected from light if not used immediately.

Western blot

SDS-PAGE protein loading buffer

For a 5 X stock, 50 ml 1 M Tris-HCl (pH 6.8), 100 ml glycerol, 1 g bromophenol blue and 30 g SDS were mixed and the solution was made up to 250 ml with diH_2O. This stock was stored at room temperature. For a 5 X working solution (reducing buffer), 400 µl of stock were mixed with 100 µl β-mercaptoethanol. The working solution was stored at 4°C. In case the solution changed from blue to orange or yellow, a drop of 5 M NaOH was added to adjust the pH.

Gel buffer (I)

Gel buffer (I) was prepared by dissolving 45.45 g (0.75 M) Tris and 1 g (0.2% w/v) SDS in 400ml diH_2O. The pH was adjusted to 8.8 with hydrochloric acid (HCl) and the buffer was made up to a final volume of 500 ml.

Gel buffer (II)

Gel buffer (II) was prepared by dissolving 15.15 g (0.25 M) Tris and 1 g (0.2% w/v) SDS in 400 ml diH_2O. The pH was adjusted to 6.8 with HCl and the buffer was made up to a final volume of 500 ml.

Gel running buffer

For a 10 X stock, 30 g (248 mM) Trisma Base, 144 g (1.92 M) glycine and 10 g (1% w/v) SDS were dissolved in 900 ml diH_2O. The pH was adjusted to 8.3 with HCl and the buffer was made up to a final volume of one litre For running SDS-PAGE gels, the buffer was diluted to 1 X by mixing 100 ml 10 X stock with 900 ml diH_2O.

Transfer buffer

For a 10 X stock, 30.28 g (248 mM) Trisma Base, 144 g (1.92 M) glycine and 1 g (0.1% w/v) SDS were dissolved in diH_2O for a final volume of one litre. Before use, this stock was diluted to 1 X by mixing 100 ml 10 X stock, 200 ml MeOH and 700 ml diH_2O.

TBST

For a 10 X stock, 200 ml 1 M Tris (pH 8.0), 175.5 g NaCl and 10 ml Tween 20 were mixed with diH_2O for a final volume of two litres. Before use, the buffer was diluted to 1 X by mixing 100 ml 10 X stock with 900 ml diH_2O.

All Western blot related buffers were stored at room temperature.

Blocking solution – 10% TBST milk

The blocking solution was prepared by mixing 5 g non-fat, dried milk powder (Marvel) with 50 ml 1 X TBST buffer. This was prepared fresh every time.

Antibodies in 5% TBST milk

For each membrane, 20 ml of antibodies in 5% TBST milk was prepared. Therefore, 1 g non-fat, dried milk powder (Marvel) was mixed with 20 ml 1 X TBST buffer. To this the appropriate antibodies were added:

- Primary antibodies (Abcam) – 1:5000 dilution (4 µl in 20 ml)
    - Ferritin light-chain – rabbit
    - β-actin – mouse

- Secondary antibodies (Jackson Laboratories) – 1:10000 (2 µl in 20 ml)
    - Peroxidase-conjugated AffiniPure Goat Anti-Rabbit IgG (H + L)
    - Peroxidase-conjugated AffiniPure Goat Anti-Mouse IgG (H + L)

Antibodies were prepared fresh for each experiment.

Dialysis

0.3% Alginate stocks

For a 0.3% alginate stock, 0.12 g alginate was dissolved in 40 ml diH_2O. The stocks were left in a 37°C incubator until the alginates were fully dissolved. The stocks were made fresh for each dialysis experiment.

Colourless DMEM + / - 10% FCS

For three litres of colourless DMEM, 30 g powdered medium was added to 2.5 l diH_2O (15-20°C). The solution was stirred to dissolve the powder before adding 11.1 g sodium bicarbonate. Whilst stirring, the pH of the medium was adjusted to 7.4 (+/- 0.1) with 1 M NaOH. FCS-free medium was made up to the final volume of three litres. For a 10% FCS medium, 300 ml FCS were added before adjusting the pH.

100 mM Fe and 10 mM Na-asc stocks

For a 100 mM Fe stock, 1.08 g Fe were added to 40 ml diH_2O and mixed thoroughly. For a 10 mM Na-asc stock, 0.08 g Na-asc were added to 40 ml diH_2O and mixed thoroughly. Both stocks were prepared immediately before use to prevent oxidation of the Fe stock.

PSA assay

80% Phenol in water

For an 80% (w/v) phenol in water solution, 16 g of phenol was added to 20 ml of diH_2O. The solution was shaken well to mix the contents before use.

Alginate standards

For the PSA assay, standards were needed for all alginates. Therefore, 0.3% alginate stocks were prepared by dissolving 0.12 g alginate in 40 ml diH_2O substituted with one drop of toluene. This stock was diluted for the standards as follows:

- Standard 1 - 0.015% 1 ml in 19 ml
- Standard 2 - 0.0125% 0.83 ml in 19.17 ml
- Standard 3 - 0.005% 0.33 ml in 19.67 ml
- Standard 4 - 0.0025% 0.17 ml in 19.83 ml

SLS / DLS and CD

SLS / DLS water

The protocol for preparing SLS / DLS water and samples was modified from Strand *et al.* (1982). For the SLS / DLS water, 0.149 g (0.001 M) ethylenediaminetetraacetic acid (EDTA) and 2.1 g (0.09 M) NaCl were dissolved in 400 ml diH_2O substituted with two drops of toluene. In a hood, the water was filtered through a 0.2 µm syringe filter into sterile tubes free from dust and other contaminants. The water was stored at room temperature.

SLS / DLS alginate samples

For each alginate, an upper limit concentration of 2 g/l (0.2%) was prepared. Therefore, 0.08 g alginate were dissolved in 40 ml SLS / DLS water. The samples were incubated at 37°C until the alginates were fully dissolved and the solutions were then clarified by centrifugation for two hours at 200,000 g. In a hood, the supernatant was aspirated and filtered through a 0.2 µm syringe filter into a sterile tube free from dust and other contaminants. The samples were stored at room temperature.

SLS /DLS sample dilutions

For the PSA assay, the samples were diluted in SLS / DLS water 1:10 for a final concentration of 0.002% alginate.

Following the PSA assay, the samples were diluted with filtered SLS / DLS water in a ratio of 4:1, 3:1, 2:1, 1:1 and 1:2 to use in SLS measurements. To exclude dust and other contaminants this was carried out in a hood using filter tips and sterile tubes.

CD water and alginate samples

For the CD water, 0.149 g (0.001 M) EDTA was dissolved in 400 ml diH_2O. For a 0.075% alginate solution, 0.03 g alginate was dissolved in 20 ml CD water. The stocks were incubated at 37°C until the alginates were fully dissolved and were then stored at 4°C.

6. REFERENCES

American Cancer Society. (2009) *Colon and Rectum Cancer Staging 7th Edition*. Atlanta: American Cancer Society.

American Cancer Society. (2011a) *Colorectal Cancer Facts & Figures 2011-2013*. Atlanta: American Cancer Society.

American Cancer Society. (2011b) *Global Cancer Facts & Figures 2nd Edition*. Atlanta: American Cancer Society.

Bastide, N.M., Pierre, F.H.F. and Corpet, D.E. (2011) Heme Iron from Meat and Risk of Colorectal Cancer: A Meta-analysis and a Review of the Mechanisms Involved. *Cancer Prevention Research*. 4, 177-184.

Bienz, M. and Clevers, H. (2000). Linking colorectal cancer to Wnt signaling. *Cell*. *103*, 311–320.

Bingham, S.A., Day, N.E., Luben, R., Ferrari, P., Slimani, N., Norat, T., Clavel-Chapelon, F., Kesse, E., Nieters, A., Boeing, H., Tjønneland, A., Overvad, K., Martinez, C., Dorronsoro, M., Gonzalez, C.A., Key, T.J., Trichopoulou, A., Naska, A., Vineis, P., Tumino, R., Krogh, V., Bueno-de-Mesquita, H.B., Peeters, P.H., Berglund, G., Hallmans, G., Lund, E., Skeie, G., Kaaks, R. and Riboli, E. (2003) Dietary fibre in food and protection against colorectal cancer in the European Prospective Investigation into Cancer and Nutrition (EPIC): an observational study. *The Lancet*. 361 (9368), 1496-1501.

Brookes, M.J., Hughes, S., Turner, F.E., Reynolds, G., Sharma, N, Ismail, T., Berx, G., McKie, A.T., Hotchin, N. Anderson G.J., Iqbal T. and Tselepis C. (2006) Modulation of iron transport proteins in human colorectal carcinogenesis. *Gut*. 55, 1449-1460.

Brookes, M.J., Boult, J., Roberts, K., Cooper, B.T., Hotchin, N.A., Matthews, G., Iqbal T. and Tselepis C. (2008) A role for iron in Wnt signalling. *Oncogene*. 27, 966-975.

Cairo, G., Bardella, L., Schiaffonati, L., Arosio, P., Levi, S. and Bernelli-Zazzera, A. (1985) Multiple mechanisms of iron induced ferritin synthesis in HeLa cells. *Biochemical and Biophysical Research Communications*. 133, 314-321.

Cancer Research UK (no date) *Bowel cancer (colorectal cancer).* [Online]. Available from: http://www.cancerresearchuk.org/cancer-help/type/bowel-cancer/ [Accessed on 12th July 2013].

Chan, E.-S., Lee, B.-B., Ravindra, P. and Poncelet, D. (2009) Prediction models for shape and size of ca-alginate macrobeads produced through extrusion–dripping method. *Journal of Colloid and Interface Science.* 338, 63-72.

Chua, A.C.G., Klopcic, B., Lawrance, I.C., Olynyk, J.K. and Trinder, D. (2010) Iron: An emerging factor in colorectal carcinogenesis. *World Journal of Gastroenterology*. 16 (6), 663-672.

Clker.com (2011) *Eppi Lysat clip art.* [Online]. Available from: http://www.clker.com/clipart-eppi-lysat.html [Accessed on 30th June 2013].

Corpet, D.E. (2011) Red meat and colon cancer: Should we become vegetarians, or can we make meat safer? *Meat Science*. 89, 310-316.

Crisponi, G. and Remelli, M. (2008) Iron chelating agents for the treatment of iron overload. *Coordination Chemistry Reviews.* 252 (11), 1225-1240.

Draget, K.I. and Taylor C. (2011) Chemical, physical and biological properties of alginates and their biomedical implications. *Food Hydrocolloids*. 25, 251-256.

Duboius, M., Gilles, K.A., Hamilton, J.K., Rebers, P.A. and Smith F. (1956) Colorimetric Method for Determination of Sugars and Related Substances. *Analytical Chemistry*. 28 (3), 350–356.

Edgren, G., Reilly, M., Hjalgrim, H., Tran, T.N., Rostgaard, K., Adami, J., Titlestad, K., Shanwell, A., Melbye, M. and Nyre, O. (2008). Donation frequency, iron loss, and risk of cancer among blood donors. *Journal of the National Cancer Institute*. 100, 572–579.

Ertesvag, H. and Valla, S. (1998) Biosynthesis and applications of alginates. *Polymer Degradation and Stability*. 59, 85-91.

FAO Corporate Document Repository. (no date) *3) ALGIN --- A BROWN SEAWEED POLYSACCHARIDE*. [Online]. Available from: http://www.fao.org/docrep/field/003/AB730E/AB730E04.htm [Accessed on 13th July 2013].

FMC BioPolymers (2003) *Alginates.* [Online]. Available from: http://www.fmcbiopolymer.com/Portals/Pharm/Content/Docs/Alginates.pdf [Accessed on 13th July 2013].

Gacesa, P. (1988) Alginates. *Carbohydrate Polymers*. 8, 161-182.

Glei, M., Latunde-Dada, G.O., Klinder, A., Becker, T.W., Hermann, U., Voigt, K. and Pool-Zobel, B.L. (2002) Iron-overload induces oxidative DNA damage in the human colon carcinoma cell line HT29 clone 19A. *Mutation Research*. 519 (1-2),151-61.

Graf, E. and Eaton, J.W. (1985) Dietary Suppression of Colonic Cancer - Fiber or Phytate? *Cancer.* 56, 717-718.

Gunderson, L.L., Jessup, J.M., Sargent, D.J., Greene F.L and Stewart, A.K. (2010) Revised TN Categorization for Colon Cancer Based on National Survival Outcomes Data. *Journal of Clinical Oncology*. 28 (2), 264-271.

Hallberg, L., Rossander-Hultén, L., Brune, M. and Gleerup, A. (1992) Calcium and iron absorption: mechanism of action and nutritional importance. *European Journal of Clinical Nutrition.* 46 (5), 317-327.

Halliwell, B. (2011) Free Radicals and other reactive species in Disease. *Encyclopedia of Life Sciences*. 2011, 1-7.

Harrison, P.M. and Arosio, P. (1996) The ferritins: molecular properties, iron storage function and cellular regulation. *Biochimica et Biophysica Acta*. 1275, 161-203.

Haug, A., Larsen, B. and Smidrod, O. (1974) Uronic acid sequence in alginate from different sources. *Carbohydrate Research*. 32, 217-225.

Heli, H., Mirtorabi, S. and Karimian, K. (2011) Advances in iron chelation: an update. *Expert Opinion on Therapeutic Patents*. 21(6), 819-856.

Hider, R.C. and Zhou, T. (2005) The Design of Orally Active Iron Chelators. *Annals of the New York Academy of Sciences.* 1054, 141-154.

Horniblow, R.D. (2012) *Iron-Chelation Properties of Alginates and other Non-absorbable Ligands for Removal of Excess Iron from the Large Bowel*. School of Cancer Sciences First Year Report (unpublished data).

Horniblow, R.D. (2013) *Iron-chelation Properties of Alginates for the Improvement of Colonic Health*. School of Cancer Sciences Second Year Report (unpublished data).

Huang, X. (2003) Iron overload and its association with cancer risk in humans: evidence for iron as a carcinogenic metal. *Mutation Research*. 533, 153-171.

Hussain, S.P., Hofseth, L.J. and Harris, C.C. (2003) Radical causes of cancer. *Nature Reviews Cancer*. 3 (4), 276-285.

Indian Academy of Sciences. (no date) *Chapter 7 – Light Scattering.* [Online]. Available from: http://www.ias.ac.in/initiat/sci_ed/resources/chemistry/LightScat.pdf [Accessed on 10th July 2013].

Jemal, A., Bray, F., Center, M.M., Ferlay, J., Ward, E. and Forman, D. (2011) Global Cancer Statistics. *CA – A Cancer Journal for Clinicians*. 61 (2), 69-90.

Kato, I., Dnistrian, A.M., Schwartz, M., Toniolo, P., Koenig, K., Shore, R.E., Zeleniuch-Jacquotte, A., Akhmedkhanov, A. and Riboli, E. (1999) Iron intake, body iron stores and colorectal cancer risk in women: a nested case-control study*. International Journal of Cancer.* 80 (5), 693-698.

Knekt, P., Reunanen, A., Takkunen, H., Aromaa, A., Heliövaara, M. and Hakulinen, T. (1994) Body iron stores and risk of cancer. *International Journal of Cancer.* 56 (3), 379-382.

Larsson, S.C. and Wolk, A. (2006) Meat consumption and risk of colorectal cancer: A meta-analysis of prospective studies. *International Journal of Cancer*. 119, 2657–2664.

Le, N.T.V and Richardson, D.R. (2004) Iron chelators with high antiproliferative activity up-regulate the expression of a growth inhibitory and metastasis suppressor gene- a link between iron metabolism and proliferation. *Blood.* 104, 2967-2975.

Liew, C.V., Chan, L.W., Ching, A.L. and Heng, P.W.S. (2006) Evaluation of sodium alginate as drug release modifier in matrix tablets. *International Journal of Pharmaceutics.* 309, 25-37.

Ma, H.-l., Qi, X.-r., Maitani, Y. and Nagai, T. (2007) Preparation and characterization of superparamagnetic iron oxide nanoparticles stabilized by alginate. *International Journal of Pharmaceutics.* 333, 177-186.

Markowitz, S.D. and Bertagnolli, M.M. (2009) Molecular Basis of Colorectal Cancer. *New England Journal of Medicine.* 361 (25), 2449-2460.

Merk, K., Mattsson, B., Mattsson, A., Holm, G., Gullbring, B. and Björkholm, M. (1990) The Incidence of Cancer among Blood Donors. *International Journal of Epidemiology.* 19 (3), 505-509.

Morris, E.R., Rees, D.A., Sanderson, G.R. and Thom, D. (1975) Conformation and Circular Dichroism of Uronic Acid Residues in Glycosides and Polysaccharides. *Journal of the Chemical Society, Perkin Transactions.* 2, 1418-1425.

Nelson, R.L., Davis, F.G., Persky, V. and Becker, E. (1995) Risk of neoplastic and other diseases among people with heterozygosity for hereditary hemochromatosis. *Cancer.* 76 (5), 875-879.

Nelson, R.L. (2001) Iron and Colorectal Cancer Risk: Human Studies. *Nutrition Reviews*. 59 (5), 140-148.

Perez-Moral, N., Gonzalez, M.C. and Parker, R. (2013) Preparation of iron-loaded alginate gel beads and their release characteristics under simulated gastrointestinal conditions. *Food Hydrocolloids*. 31, 114-120.

Pierre, F., Tache, S., Petit, C.R., Van Der Meer, R. and Corpet, D.E. (2003) Meat and cancer: haemoglobin and haemin in a low-calcium diet promote colorectal carcinogenesis at the aberrant crypt stage in rats. *Carcinogenesis*. 24, 1683-1690.

Radulescu, S., Brookes, M.J., Salgueiro, P., Ridgway, R.A., McGhee, E., Anderson, K., Ford, S.J., Stones, D.H., Iqbal, T.H., Tselepis, C. and Sansom, O.J. (2012) Luminal Iron Levels Govern Intestinal Tumorigenesis after Apc Loss In Vivo. *Cell Reports*. 2, 270-282.

Richardson, D.R. (2002) Iron chelators as therapeutic agents for the treatment of cancer. *Critical Reviews in Oncology Hematology*. 42, 267-281.

Richmond, H. G. (1959) Induction Of Sarcoma In The Rat By Iron-Dextran Complex. *The British Medical Journal.* 1 (5127), 947-949.

Rodriguez-Bigas, M.A., Lin, E.H. and Crane, C.H. (2003) *Genetic Pathways in Colorectal Cancer.* In: Kufe, D.W., Pollock, R.E., Weichselbaum, R.R., *et al*., (eds.) Holland-Frei Cancer Medicine. 6th edition. Hamilton (ON): BC Decker Inc. [Online]. Available from: http://www.ncbi.nlm.nih.gov/books/NBK12839/ [Accessed on 28th August 2013].

Seril, D.N., Liao, J., Ho, K.L., Warsi, A., Yang, C.S. and Yang, G.Y. (2002) Dietary iron supplementation enhances DSS-induced colitis and associated colorectal carcinoma development in mice. *Digestive Diseases and Science.* 47, 1266-1278.

Strand, K.A., Boe, A., Dalberg, P.S., Sikkeland, T. and Smidsroed, O. (1982) Dynamic and Static Light Scattering on Aqueous Solutions of Sodium Alginate. *Macromolecules.* (15), 570-579

Torti, S.V. and Torti, F.M (2013) Iron and cancer: more ore to me mined. *Nature Reviews Cancer*. 13, 342-355.

Van Meerloo, J., Kaspers, G.J. and Cloos, J. (2011) Cell sensitivity assays: the MTT assay. *Methods in Molecular Biology*. 731, 237-245.

Walewijk, A., Cooper-White, J.J. and Dunstan, D.E. (2008) Adhesion measurements between alginate gel surfaces via texture analysis. *Food Hydrocolloids*. 22, 91-96.

Wawer, A.A., Sharp, P.A., Perez-Moral, N. and Fairweather-Tait, S. (2012) Evidence for an Enhancing Effect of Alginate on Iron Availability in Caco-2 Cells. *Journal of Agricultural and Food Chemistry*. 60, 11318-11322.

Zacharski, L.R., Chow, B.K., Howes, P.S., Shamayeva, G., Baron, J.A., Dalman, R.L., Malenka, D.J., Ozaki, C.K. and Lavori, P.W. (2008) Decreased cancer risk after iron reduction in patients with peripheral arterial disease: results from a randomized trial. *Journal of the National Cancer Institute.* 100, 996–1002.